

An-Najah National University
Faculty of Graduate studies

**Performance Study of Inner Tracker (ITK) in
ATLAS at the Large Hadron Collider (LHC)
at CERN**

By
Tasnim Abdallah

Supervisor
Dr. Ahmed Bassalat

**This Thesis is Submitted in Partial Fulfillment of the Requirements
for the Degree of Master in Physics, Faculty of Graduate Studies,
An-Najah National University, Nablus, Palestine
2018**

**Performance Study of Inner Tracker (ITK) in ATLAS at the Large
Hadron Collider (LHC) at CERN**

**By
Tasnim Abdallah**

This thesis was defended successfully on 22/4/2018 and approved by:

Defense Committee Members

Signature

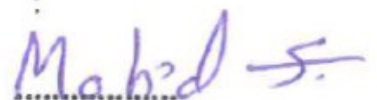
- Dr. Ahmed Bassalat /Supervisor



- Dr. Jamal Ghabboun /External Examiner



- Dr. Mohammed Abu-Jafar /Internal Examiner



Acknowledgements

This thesis was performed in the framework of ATLAS-LAL group, Orsay, France. Special and great thanks to a An-Najah National University represented by the administrative and professors especially my supervisor Dr. Ahmed Bassalat who worked hard to provide me with this opportunity.

A warm thanks to every one in LAL group, especially Prof. Achille Stocchi, the director of LAL group.

My deepest thanks to the ATLAS leader group, Lydia Fayard, who went beyond her job to help me in every aspect during my time at LAL.

I would like to express my gratitude to my supervisor and instructor Dr. Ahmed Bassalat for his invaluable support and unlimited help and guidance during this work.

The biggest thanks to the colleagues and supervisors in ATLAS-LAL group, especially Dr. David Rousseau and Dr. Dimitris Varouchas for their unlimited help and support, this work can not be achieved without both of you.

Dedication

In the beginning, thanks to Allah who helped me to be here today. This thesis is dedicated to my grandfather soul, who always had faith in me and was my biggest supporter. To my parents, my sisters and brother, for being there for me and encouraging me at the toughest times. My friends, All of love and respects to them, thank you for your endless support. A warm thank to every one who taught me since I was a child until now. Thanks to every one who made a contribution in Tasnim's personality.

الإقرار

أنا الموقع أدناه مقدم الرسالة التي تحمل العنوان:

دراسة أداء المتتبع الداخلي للكاشف أطلس الموجود في مصادم الهدرونات الكبير التابع للمنظمة

الأوروبية للأبحاث النووية

Performance Study of Inner Tracker (ITK) in ATLAS at the Large

Hadron Collider (LHC) at CERN

أقر بأن ما اشتملت عليه هذه الرسالة إنما هي نتاج جهدي الخاص باستثناء ما تمت الإشارة إليه حيثما

ورد, وأن الرسالة ككل أو أي جزء منها لم يقدم من قبل لنيل أية درجة أو بحث علمي لدى أية

مؤسسة تعليمية أو بحثية أخرى.

Declaration

The work provided in this thesis unless otherwise references, is the researcher's own work, and has not been submitted elsewhere for any other degree or qualification.

Student's name:

اسم الطالب: تسنيم عبد الله

Signature:

التوقيع: Tasnim

Date:

التاريخ: ٢٩ / ٥ / ١٨

Contents

Acknowledgements	iii
Dedication	iv
Declaration	vi
Table of contents	vii
List of Figures	viii
List of Tables	xv
Abstract	xv
Thesis Flow chart	xvii
Chapter One: Introduction	1
Chapter Two: The ATLAS Experiment	8
2.1 Overview	8
2.2 ATLAS Coordinates Systems and Parameters	9
2.3 ATLAS Sub-detectors	12
2.3.1 Moun System of ATLAS	14
2.3.2 The Calorimeter System in ATLAS	15
2.3.3 The Inner Detector of ATLAS (ID)	16
2.3.4 Pixel Detector in The Current ID (after adding the Insertable B Layer (IBL))	18

Chapter Three: Inner Tracker (ITK)	22
3.1 Overview	22
3.2 Tracking Performance	24
3.3 Tracking In Dense Environment (TIDE) in ITK . . .	30
3.3.1 Jet Transverse Momentum (p_T) Study	32
3.3.2 Jet Pseudorapidity (η) Study	37
3.3.3 Jet Angular Distance (ΔR) Study	41
3.3.4 Displaced Vertices Study	49
 Chapter Four: ITK Pixel Modules	 55
4.1 Overview	55
4.2 Sensors	57
4.3 Pile-up Study	67
 Chapter Five: Conclusion	 76
 References	 78
 List of Symbols and Abbreviations	 82

List of Figures

1	Process of accelerating in LHC.	2
2	The standard model of particle physics.	3
3	Upgrades in LHC during the years [6].	6
4	ATLAS detector.	8
5	ATLAS coordinates.	9
6	ATLAS parameters, in the transverse plane in the right and in longitudinal plane in the left.	10
7	Schematic graph of traveling particles in order of η	12
8	Left: Angular coordinates in ATLAS. Right: Cones around jets.	12
9	Layout of ATLAS detector.	13
10	Particle identification through sub-detectors of ATLAS. . . .	14
11	Left: Electron-hole pair formation in the inner detector of ATLAS. Right: Trajectory of a charged particle leaving hits through different layers of the inner detector.	17
12	The inner detector of ATLAS.	18
13	Schematic diagram for pixel detector.	20
14	Left: The ATLAS IBL detector prior to the insertion [23]. . .	21
15	ATLAS Inner Tracker (ITK) layout, red lines are strips and blue lines are pixels.	24
16	New reach in pseudorapidity η of ITK.	25

17	The trajectory of charged particles in a magnetic field, left plot indicates that the radius is increasing with momentum while the right figure shows how R can be calculated.	27
18	Reconstructed tracks associated to groups of hits.	28
19	Types of vertices.	29
20	Blue circles are the hits in the ITK, blue lines associated to the reconstructed tracks while the red lines associated to the truth particles tracks.	29
21	The track reconstruction efficiency as a function of truth jet p_T within all jets in the ITK for different ranges of truth jet η	34
22	The track reconstruction efficiency as a function of truth jet p_T within all jets in the ITK for different ranges of truth jet η (ATLAS simulation, 2016) [34].	35
23	The bad match rate as a function of truth jet p_T within all jets in the ITK.	36
24	The bad match rate as a function of truth jet p_T within jets coming only from Z' in the ITK.	37
25	The track reconstruction efficiency as a function of truth jet η within jets in the ITK for different ranges of truth jet p_T	39
26	The track reconstruction efficiency as a function of truth jet η within jets in the ITK for different ranges of truth jet p_T (ATLAS simulation, 2016) [34].	40
27	The bad match rate as a function of truth jet η within all jets in the ITK.	41

28	The bad match rate as a function of truth jet η within jets coming only from Z' in the ITK.	42
29	The track reconstruction efficiency as a function of truth jet ΔR for b-jets in the ITK.	44
30	The track reconstruction efficiency as a function of truth jet ΔR for light jets in the ITK.	45
31	The track reconstruction efficiency as a function of truth jet ΔR for different ranges of truth jet η , for b-jets in the ITK (ATLAS simulation, 2016) [34].	46
32	The track reconstruction efficiency as a function of truth jet ΔR for different ranges of truth jet η , for light jets in the ITK (ATLAS simulation, 2016) [34].	47
33	The bad match rate for b jet as a function of ΔR within jets in the ITK.	48
34	The bad match rate for b jet as a function of ΔR within jets in the ITK.	49
35	The bad match rate for b jet as a function of ΔR within jets that are coming only from Z' in the ITK.	50
36	Schematic diagram of Displaced tracks.	51
37	Track reconstruction efficiency for leptons decaying from b-hadron as a function of truth production radius of the b-hadron within jets in the ITK for different ranges of truth jet η	52

38	Track reconstruction efficiency for hadrons decaying from b-hadron as a function of truth production radius of the b-hadron within jets in the ITK for different ranges of truth jet η	53
39	Track reconstruction efficiency for leptons decaying from b-hadron as a function of truth production radius of the b-hadron within jets in the ITK for different ranges of truth jet η (ATLAS simulation, 2016) [34].	53
40	Track reconstruction efficiency for hadrons decaying from b-hadron as a function of truth production radius of the b-hadron within jets in the ITK for different ranges of truth jet η (ATLAS simulation, 2016) [34].	54
41	The bad match rate for hadrons decaying from b-hadron as a function of truth production radius of b-hadron within jets in the ITK.	55
42	ITK pixel module.	56
43	Extended and inclined ITK.	57
44	More hit modules can be obtained in the inclined ITK at low incident angle.	58
45	Sketch of the two hybrid pixel technologies, that will be used in the ITK of ATLAS [40].	59

46	The pixel module size is $50 \times 50 \mu\text{m}^2$ in the left figure while it is $50 \times 250 \mu\text{m}^2$ in the right figure, X^2 is smaller in the left one, which means that the resolution is better when the pixel size is smaller.	60
47	The track reconstruction efficiency within jets as a function of truth jet p_T in the ITK for two samples with $50 \times 50 \mu\text{m}^2$ pixel size and $25 \times 100 \mu\text{m}^2$ pixel size.	62
48	The bad match rate within jets as a function of truth jet p_T in the ITK for two samples with $50 \times 50 \mu\text{m}^2$ pixel size and $25 \times 100 \mu\text{m}^2$ pixel size.	62
49	The track reconstruction efficiency within jets as a function of truth jet η in the ITK for two samples with $50 \times 50 \mu\text{m}^2$ pixel size and $25 \times 100 \mu\text{m}^2$ pixel size.	63
50	The bad match rate within jets as a function of truth jet η in the ITK for two samples with $50 \times 50 \mu\text{m}^2$ pixel size and $25 \times 100 \mu\text{m}^2$ pixel size.	64
51	The track reconstruction efficiency within jets as a function of the ΔR for b jets in the ITK for two samples with $50 \times 50 \mu\text{m}^2$ pixel size and $25 \times 100 \mu\text{m}^2$ pixel size.	65
52	The track reconstruction efficiency within jets as a function of the ΔR for light jets in the ITK for two samples with $50 \times 50 \mu\text{m}^2$ pixel size and $25 \times 100 \mu\text{m}^2$ pixel size.	66

53	The track reconstruction efficiency within jets as a function of truth production radius for hadron in the ITK for $50 \times 50 \mu\text{m}^2$ and $25 \times 100 \mu\text{m}^2$ sensors samples.	67
54	The track reconstruction efficiency within jets as a function of truth production radius for lepton in the ITK for two samples with $50 \times 50 \mu\text{m}^2$ pixel size and $25 \times 100 \mu\text{m}^2$ pixel size.	68
55	The track reconstruction efficiency within jets as a function of truth jet p_T in the ITK for four different samples that have a pixel size $50 \times 50 \mu\text{m}^2$ with four different values of μ . . .	70
56	The bad match rate within jets as a function of truth jet p_T in the ITK for four different samples that have a pixel size $50 \times 50 \mu\text{m}^2$ with four different values of μ	71
57	The track reconstruction efficiency within jets as a function of truth jet η in the ITK for four different samples that have a pixel size $50 \times 50 \mu\text{m}^2$ with four different values of μ . . .	72
58	The bad match rate within jets as a function of truth jet η in the ITK for four different samples that have a pixel size $50 \times 50 \mu\text{m}^2$ with four different values of μ	72
59	The track reconstruction efficiency within jets as a function of the ΔR for b jets in the ITK for four different samples that have a pixel size $50 \times 50 \mu\text{m}^2$ with four different values of μ . . .	74

60	The track reconstruction efficiency within jets as a function of the ΔR for light jets in the ITK for four different samples that have a pixel size $50 \times 50 \mu\text{m}^2$ with four different values of μ	75
61	The track reconstruction efficiency within jets as a function of truth production radius for hadron in the ITK for four different samples that have a pixel size $50 \times 50 \mu\text{m}^2$ with four different values of μ	76
62	The track reconstruction efficiency within jets as a function of truth production radius for lepton in the ITK for four different samples that have a pixel size $50 \times 50 \mu\text{m}^2$ with four different values of μ	76

List of Tables

1	η -representations as a function of θ , as eq 2.	11
2	Difference between pixel without IBL and pixel with IBL [22, 23].	21

Performance Study of Inner Tracker (ITK) in ATLAS at the Large Hadron Collider (LHC) at CERN

By

Tasnim Abdallah

Supervisor

Dr. Ahmed Bassalat

Abstract

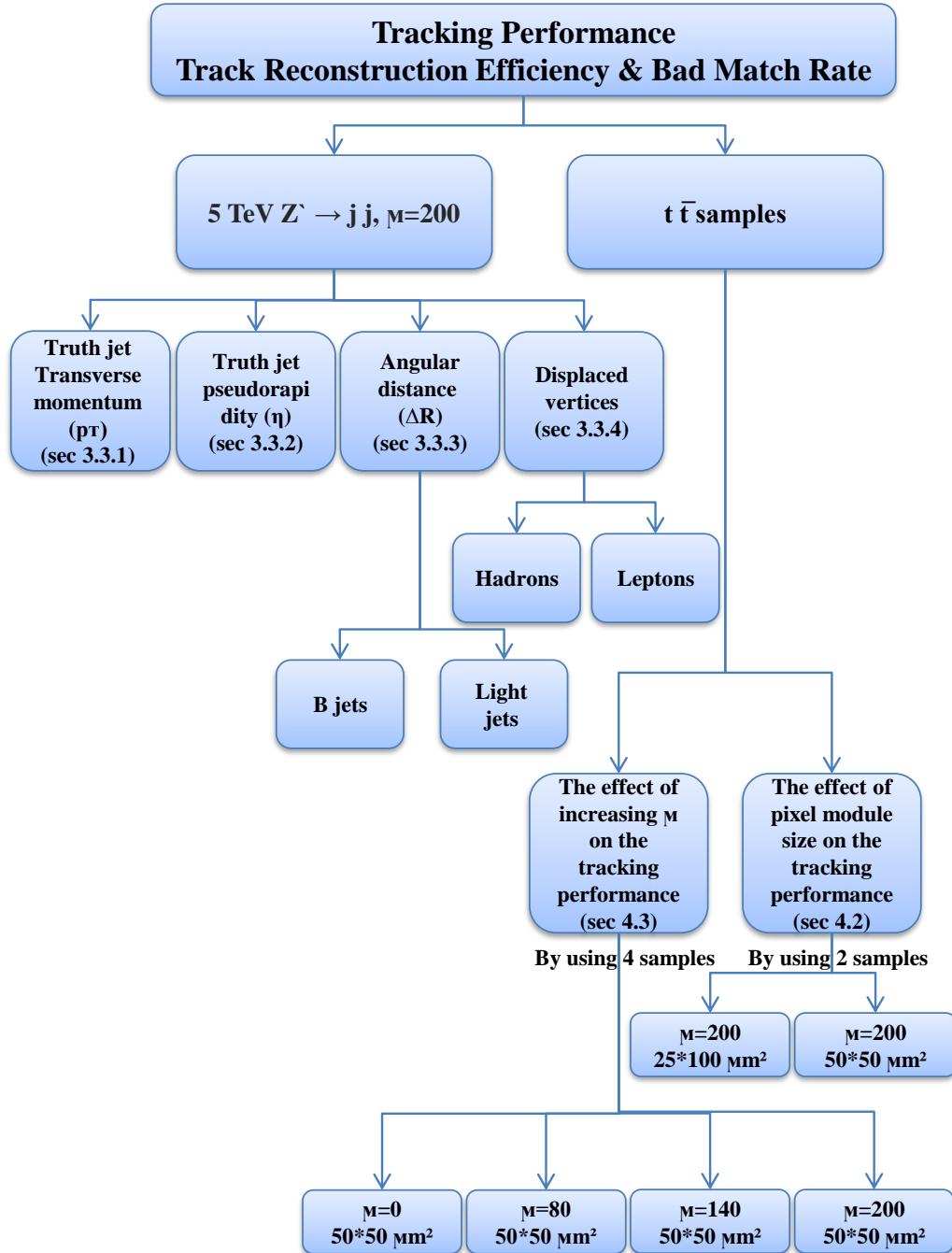
ATLAS is one of the main general-purpose detector in LHC, it will be upgraded in 2023-2025 (which is called phase II). The major upgrade will be for the inner detector, it will be replaced by the new inner tracker (ITK). At that time the stage of high luminosity LHC (HL-LHC) will start with luminosity five times more than the luminosity in run 2 (nowadays), which creates a hope for a substantial advancement in the understanding of physics phenomena related to high-energy physics. The layout of ITK will cover a pseudorapidity (η) up to 4, while the current inner detector covers a pseudorapidity up to $|\eta| = 2.5$.

In this thesis the track reconstruction efficiency (ϵ) and the fake rate as a function of different variables is studied in the ITK of ATLAS, including particles travel in the forward region with a values of $2.5 < |\eta| < 4$.

Tracking reconstruction efficiency (ϵ) as a function of several variables for two different samples is compared and decided which is better to use a modules of pixel size $50 \times 50 \mu\text{m}^2$ or $25 \times 100 \mu\text{m}^2$, this study is done with high pile-up, where the average number of proton-proton interactions per bunch crossing (μ) is around 200.

The tracking reconstruction efficiency also is studied, as the value of μ is increased, this allows to study the robustness of the track reconstruction efficiency with respect to high pile-up.

Thesis Flow chart



Chapter One

Introduction

The Large Hadron Collider (LHC) at the European Organization for Nuclear Research (CERN) near Geneva in Switzerland, is the most powerful, strongest, largest and highest energy accelerator in the world.

In LHC, as shown in figure 1, two beams of hadrons (protons or lead ions) are being accelerated through many accelerating structures, starting from linear accelerator (*Linac*2, 3, 4), followed by PS Booster (*PSB*) and Proton Synchrotron (*PS*), followed by Super Proton Synchrotron (*SPS*), into two superconducting rings of 27 km circumference to obtain the maximum center of mass energy 14 TeV in run 2 (nowadays), with a speed up to 99.99% of the speed of light. Each beam contains around 2808 bunches of particles with 10^{11} particle in each bunch. The accelerated beams undergo a head-on collision in four main positions around the accelerator rings, where the two rings intersect. These positions are the locations of four large detectors experiments to detect and measure particles produced from the collisions.

These experiments are:

- i. ATLAS A Toroidal LHC ApparatuS, a detailed description of ATLAS is presented in chapter .
- ii. CMS Compact Muon Solenoid experiment, is a general purpose detector studying the standard model, physics beyond the standard model, extra dimension and dark matter.

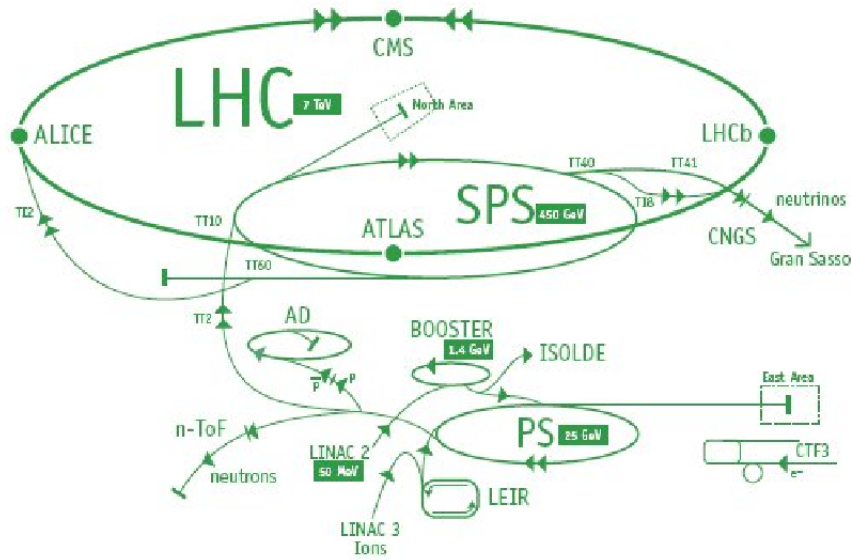


Figure 1: Process of accelerating in LHC.

- iii. ALICE A Large Ion Collider Experiment, is a specialized experiment searches for quark gluon plasma forms of matter via lead ions (pb) collisions.
- iv. LHCb Large Hadron Collider beauty experiment, focuses on discovering the slightly difference between matter and antimatter by studying b quark particles.

LHC experiments and others verified the existence of the main elements in the standard model of particle physics and proved that it is a successful theory in physics describing the elementary particles of matter and how they interact with each other. The standard model as shown in figure 2 states the existence of two families of elementary particles; Fermions and Bosons.

In Fermions there are six quarks and six leptons. Each pair of leptons

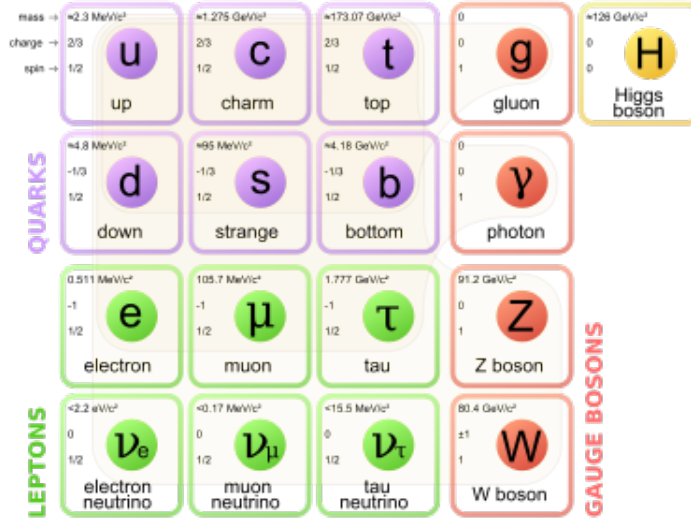


Figure 2: The standard model of particle physics.

or quarks is called a generation. Thus, there are three generations of each type of Fermions; the lightest and most stable particles make up the first generation, whereas the heavier and less stable particles belong to the second and third generations. The first generation of quarks contains up (u) and down (d) quarks, followed by the charm (c) and strange (s) quarks in second generation, the top (t) and bottom (b) quarks in third generation. While the first generation of leptons contains electron (e) and electron neutrino (ν_e), followed by the muon (μ) and muon neutrino (ν_μ) in second generation, the tau (τ) and tau neutrino (ν_τ) in third generation.

In Bosons there are five elements, including Higgs boson (H) which gives the mass to all other elementary particles, there are four force carriers; gluons (g) which is the strong force carrier, photon (γ) which is the electromagnetic force carrier and the weak force carriers; W and Z bosons.

But until now the picture is not complete, since standard model does not answer all of the questions around us, such as; searching for Higgs bosons with different masses and describing the gravity. Thus, physicists are searching for physics beyond the standard model that will lead us to better understanding of our universe. Thus, ATLAS and other experiments are important for that.

ATLAS is the largest experiment in LHC and one of the two general purpose-detectors. The main physics goals of the ATLAS collaboration are the studying of new physics phenomenas at the TeV scale, in order to improve our understanding of the Higgs boson, supersymmetry (SUSY), dark matter, top quark, extra dimensions, mini black holes and other purposes.

ATLAS comes in three main sub-detectors; the inner detector (ID), which is the inner most sub-detector followed by the calorimetry system, and at the outer layer of ATLAS there is a muon detector system.

The inner detector of ATLAS, which is based on silicon and immersed in a 2 T solenoidal magnetic field [1], acts as the tracking and vertexing system for charged particles [2, 3]. As a particle passes through the different layers of the inner detector, it leaves an electrical signals on pixel modules known as a hits. These hits can be identified by detecting their interaction with material at discrete points along the particle path, which means losing energy by the ionizing atoms in the ID in order to analyze the momentum for them.

Since the start of operation of the LHC, September 2008, many upgrades

have been scheduled and planned, as shown in figure 3. At phase II, 2023 – 2025, the luminosity¹ is expected to increase up to $5 \times 10^{34} \text{ cm}^{-2} \cdot \text{s}^{-1}$ as shown in figure 3, with pile-up²(μ) = 200 per 25 ns, and integrated luminosity³ up to 300 fb^{-1} by 2026 which is the year of High Luminosity LHC (HL-LHC). The higher luminosity means more data can be gathered. That will help us to detect rare process at a more sensitive levels which have not been seen before. For example, the HL-LHC will produce up to 15 million Higgs bosons per year by 2025, compared to the 1.2 million produced in 2011 and 2012. Thus, more precise information about properties of Higgs boson that we look forward to know will be accessible, such as; the spin and the different quantum numbers. Rare Higgs production, like Higgs which produced associated with top quark and anti top quark. Rare decay modes, including the Higgs boson decaying to two muons ($H \rightarrow \mu\mu$) and the Higgs boson decaying to a Z boson and a photon ($H \rightarrow Z\gamma$), which has a production rate of 0.022% and 0.15%, respectively [4, 5].

For that, in ATLAS there are many upgrades that are in line to be upgraded at phase II , 2023 – 2025, starting from the replacement of current inner detector by the Inner TracKer detector (ITK), which is the main work for this thesis, up to upgrades in both calorimeters and trigger systems.

The inner detector in ATLAS was made to operate at peak luminosity

¹The luminosity can be defined as the number of events detected per unit of area and unit of time.

²The pile up is the average number of pp interactions per bunch crossing.

³The integrated luminosity is the integral of luminosity over the time.

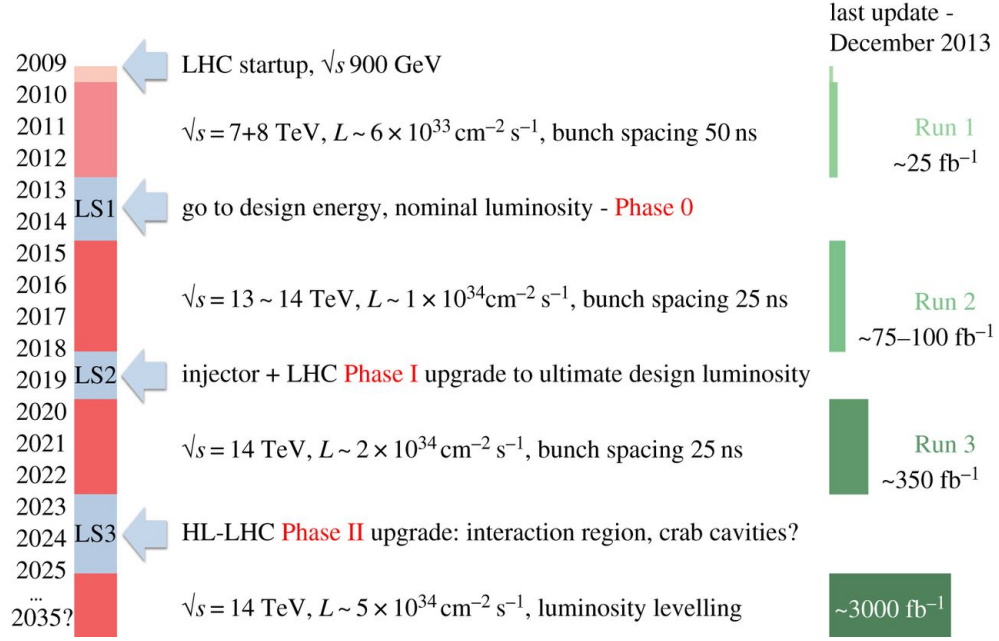


Figure 3: Upgrades in LHC during the years [6].

$10^{34} \text{ cm}^{-2} \text{ s}^{-1}$ for 10 years. After that it will lose its performance sensitivity by the increasing high dose of radiation day after day. In this time the replacement of the inner detector by the Inner Tracker (ITK) is a crucial and needed upgrade in phase II (LS3) 2023 – 2025, since it has the ability to cope with high particle densities, high pile-up and the increase of hard radiation [7].

ITK have the same purposes of inner detector, which is represented by tracking, vertexing the particles and as a result we can analyze the momentum for a charged particles in a more accurate results, especially in; b-tagging and lepton identification. ITK is also a full silicon detector, which is immersed in a 2 T solenoidal field like the current inner detector.

This thesis focuses on the detailed analysis of the performance of the future ITK by studying the track reconstruction efficiency and the fake

rate. The work of this thesis was performed at LAL, in the framework of ATLAS-LAL group. At the beginning of 2017, full monte-carlo simulation (GEANT4) of the new detector was available. The work of this thesis evaluates the track reconstruction efficiency and the fake rate for Tracking In Dense Environment (TIDE) in the ITK.

The track reconstruction efficiency ϵ and the fake rate as a function of different variables is studied in the ITK of ATLAS, including particles travel in the forward region with value of $2.5 < |\eta| < 4$. The effect of pixel module size on the tracking efficiency as a function of different variables also is studied by taking two samples with a pixel module size $50 \times 50 \mu\text{m}^2$ and $25 \times 100 \mu\text{m}^2$ with $\mu = 200$ for both. The tracking reconstruction efficiency as the value of μ increased is also studied in order to see the effect of changing μ on the tracking efficiency as a function of different variable, this allows to study the robustness of the track reconstruction efficiency with respect to high pile-up.

Chapter Two

The ATLAS Experiment

2.1 Overview

ATLAS is one of four main experiments in the LHC, as in figure 4, it is built around the LHC beam pipe, 100 m under ground in Switzerland with a length 45 m, width 32 m, height 35 m and approximately it has a weight around 7000 tones . Thus, ATLAS is cosidered as the largest-volume detector ever found for particle physics. ATLAS collaboration is also a very large group, it has more than 3000 scientist and engineers from 174 universities from different 38 countries around the world [8].

ATLAS aims to solve the nature's ambiguity, to answer the question why

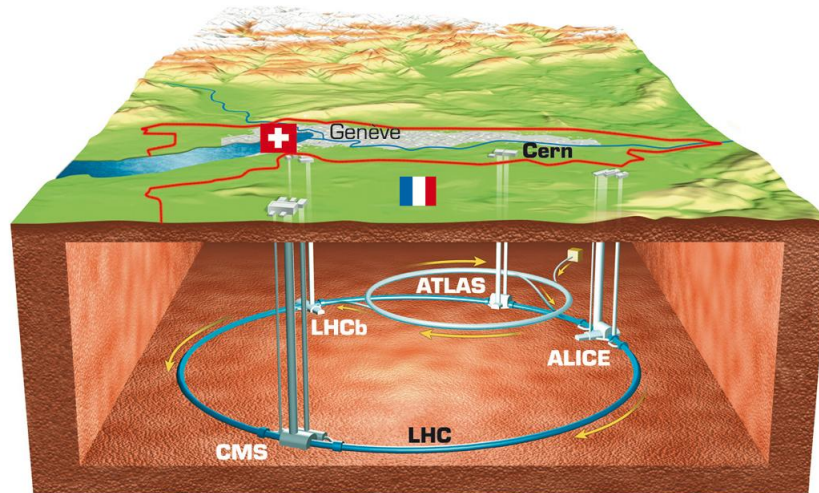


Figure 4: ATLAS detector.

the universe is like that today?, through examining a matter deeply and

going into several important topics in high-energy physics from Higgs boson, dark matter, extra dimension and many others.

2.2 ATLAS Coordinates Systems and Parameters

ATLAS uses a right-handed coordinate system with its origin at the nominal interaction point in the centre of the detector, the cartesian coordinates as shown in figure 5 are:

- i. $z - axis$ is the direction parallel to the beam axis.
- ii. $x - axis$ is the direction perpendicular to the $z - axis$, toward the centre of LHC.
- iii. $y - axis$ is the direction perpendicular to both $x - axis$ and $z - axis$.

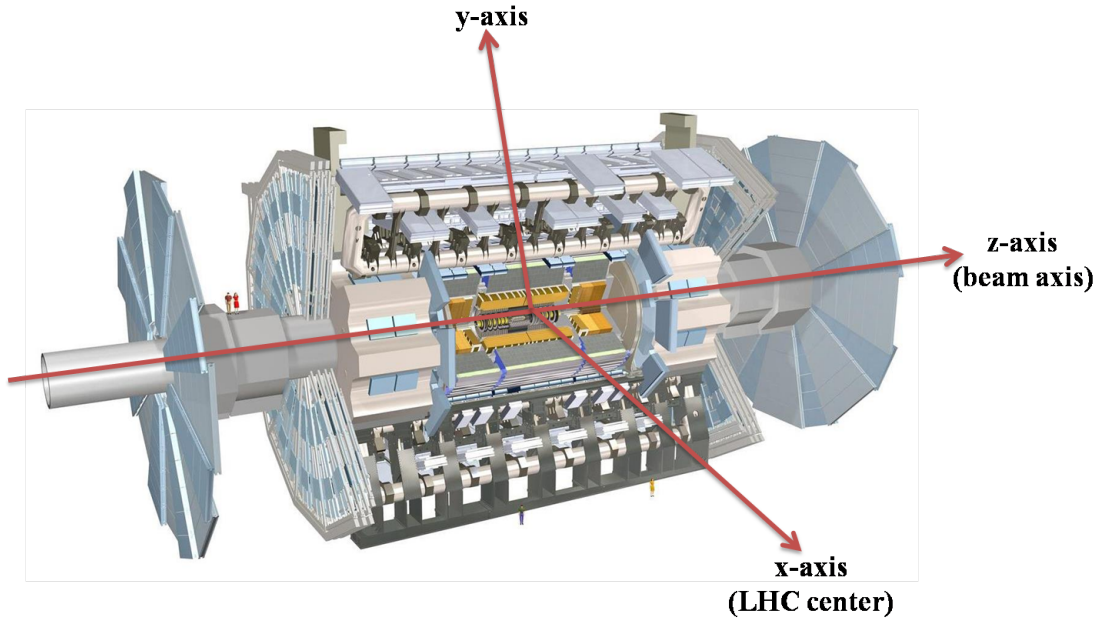


Figure 5: ATLAS coordinates.

Due to the fact that ATLAS detector has cylindrical shape and cylindrical symmetry, the cylindrical coordinate (r, ϕ, z) is very useful to be used. r is defined as $\sqrt{x^2 + y^2}$, while the azimuthal angle ϕ is the angle with the x - $axis$ in the transverse $(x - y)$ plane as shown in figure 6, where $\phi = \tan^{-1}(\frac{y}{x})$, it has a values between $-\pi$ and π .

The charged particle helical trajectory can be defined by a set of 5

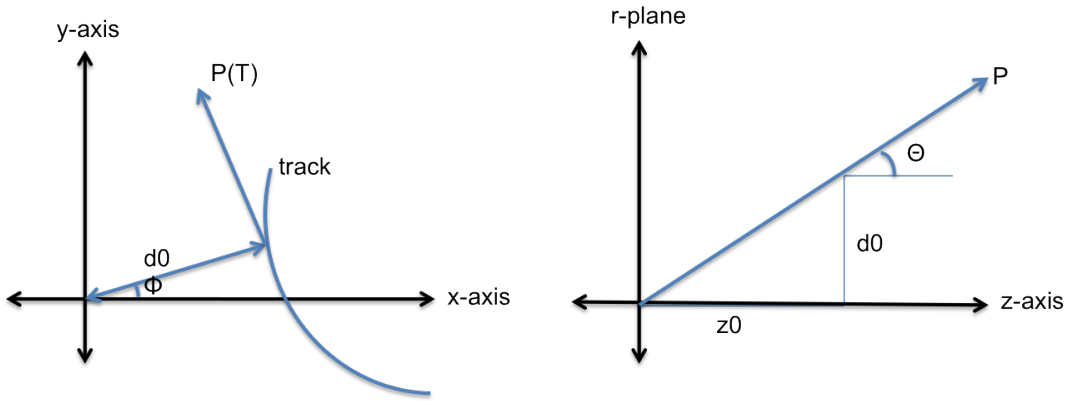


Figure 6: ATLAS parameters, in the transverse plane in the right and in longitudinal plane in the left.

parameters,

$$P = (\phi, \theta, d_o, z_o, \frac{q}{p_T}) \quad (1)$$

They are called "perigee parameters", these parameters follow the standard ATLAS definition. ϕ was defined above, while the others are [9]:

- i. Polar angle θ is the angle with respect to the z - $axis$ in the longitudinal $(r - z)$ plane as shown in figure 6, where $\theta = \cos^{-1}(\frac{z}{r})$, it has a values between 0 and π .
- ii. Transverse impact parameter d_0 is the distance of the closet approach of the trajectory to the origin of the detector in the $x - y$ plane.

- iii. Longitudinal impact parameter z_0 is defined as the value of z of the point on the track that determines d_o .
- iv. $\frac{q}{p_T}$ is the charge of the particle over the transverse momentum, which is defined as the momentum perpendicular to the LHC beam axis as shown in figure 6. $p_T = \sqrt{p_x^2 + p_y^2}$, where p_x is the x-component for the momentum (p) and p_y is the y-component for the momentum.

The best presentation for the angle θ is pseudorapidity η

$$\eta = -\log\left(\tan\left(\frac{\theta}{2}\right)\right) \quad (2)$$

In table 1 and figure 7, different values of η depending on θ :

Another parameter can be defined is the angular distance ΔR , which

Table 1: η -representations as a function of θ , as eq 2.

θ	η	θ	η
0°	∞	180°	$-\infty$
0.1°	7.04	179.9°	-7.04
0.5°	5.43	179.5°	-5.43
1°	4.74	179°	-4.74
5°	3.13	5°	-3.13
10°	2.44	170°	-2.44
45°	0.88	135°	-0.88
90°	0	100°	-0.175

represents how close are two particles or two jets from each other, as shown in figure 8.

Jets can be defined as a narrow and approximately conical bundles of the particles produced by the hadronization of quarks and gluons in a high-energy physics experiment, as shown in figure 8.

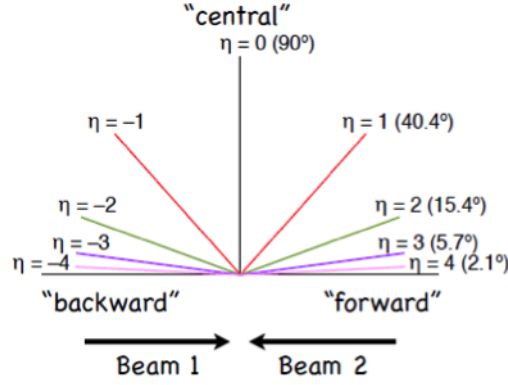


Figure 7: Schematic graph of traveling particles in order of η .

$$\Delta R = \sqrt{(\Delta\eta)^2 + (\Delta\Phi)^2} \quad (3)$$

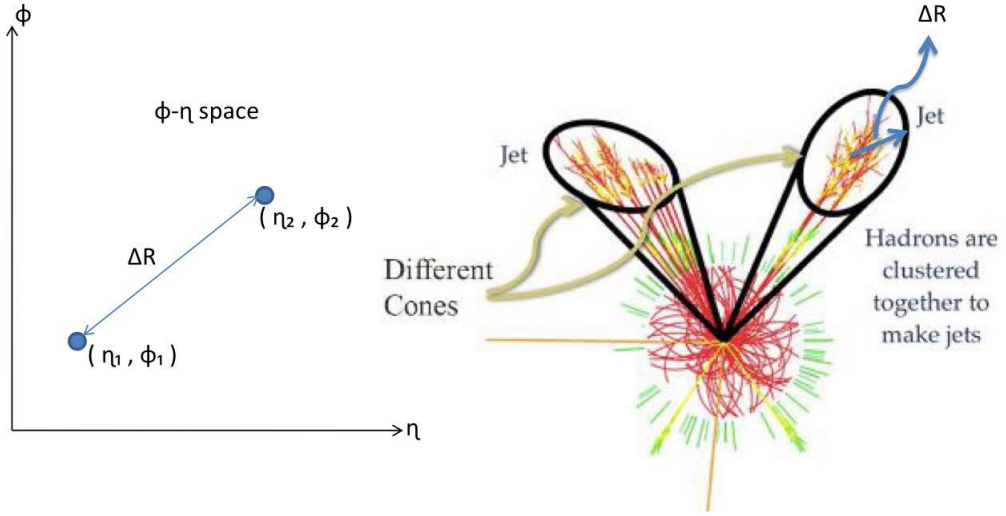


Figure 8: Left: Angular coordinates in ATLAS. Right: Cones around jets.

2.3 ATLAS Sub-detectors

ATLAS is composed of many concentric sub-detectors around the center of collision, as shown in figure 9. These sub-detectors record the path, momentum and energy so we can identify the different types of produced

particles.

These sub detectors from the outside to the inside are:

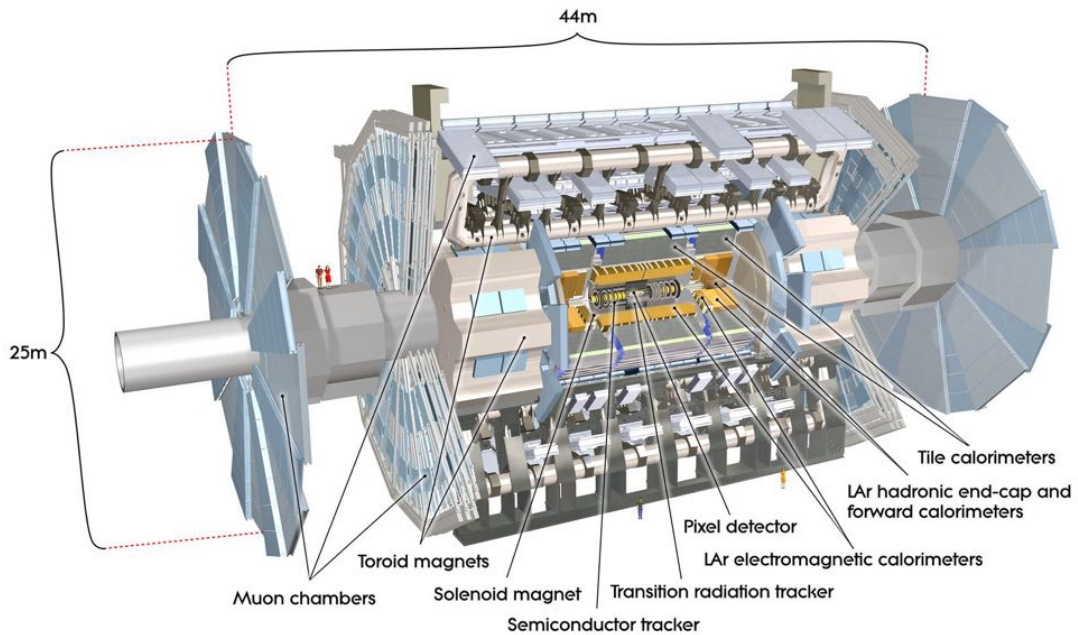


Figure 9: Layout of ATLAS detector.

- i. Muon spectrometer, it is used to identify muons and measure the momentum for them (sec 2.3.1).
- ii. Calorimeters, it is used to measure the energy carried by different particles (sec 2.3.2).
- iii. Inner detector, it is used to measure the momentum of each charged particle (sec 2.3.3).

The charged particles are bent by a magnetic field, their trajectories is measured by the inner detector. After that, calorimeters will stop particles and measure their energy and missing transverse energy by absorbing the particle's energy and transforming it into an electrical signal.

Calorimeters can stop most known particles from electrons, photons and hadrons except muons and neutrinos as shown in figure 10, in addition we can see that Muons can be identified in the outermost muon spectrometer.

Neutrino unseen by detectors, so we can just detect it by observing

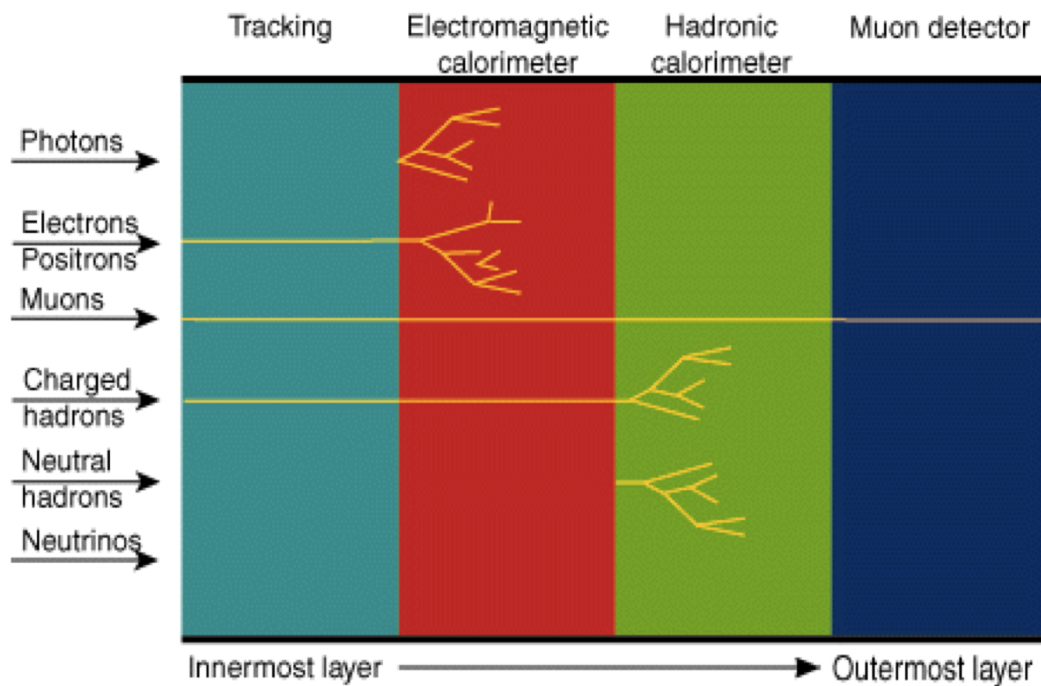


Figure 10: Particle identification through sub-detectors of ATLAS.

the missing transverse energy by applying the conservation law for momentum and energy at the center of mass; before collision we have zero momentum perpendicular to beam axis, so after collision we must have also zero net momentum perpendicular to beam axis. If we add up momenta of all visible particles, the result will not be zero and this might be momentum carried away by a neutrino.

2.3.1 Muon System of ATLAS

At the outer layer of ATLAS detector as shown in figure 9, there is a muon detector system, which uses a 4T toroid magnetic field in order to curve the path for the charged particles.

Muon is a very massive particle, it has a mass of $105.6583745 \text{ MeV}/c^2$ [10]. Thus, they are undetected by the inner detector and the calorimeters, since they can not be stopped in them as in figure 10. Thus, Muon system is a tracking device used to identify just muons and measure the momentum for them by measuring the trajectories of muons that enter the muon sub-detector.

The muon sub-detector covers pseudorapidity η up to 2.7.

2.3.2 The Calorimeter System in ATLAS

As shown in figure 9, in the middle region of ATLAS detector between the inner detector and the muon chamber there is a calorimeter systems. The calorimeters will stop the most known particles except muons and neutrinos before reaching the muon chamber, and measure the particle's energy and missing transverse energy by absorbing the energy and transforming it into an electrical signal.

The calorimeter system can be categorized into two types:

- i. electromagnetic calorimeters measure the energy of photons and electrons as they interact with the electrically charged particles in matter, as shown in figure 10.

- ii. Hadronic calorimeters measure the energy of hadrons, such as: protons and neutrons as they interact with atomic nuclei, as shown in figure 10.

The calorimeter system covers pseudorapidity η up to 4.9. So most of travelled particles will be covered by the calorimeters.

2.3.3 The Inner Detector of ATLAS (ID)

The closest sub-detector to the collision point is the inner detector, as shown in figure 9. The inner detector is based on silicon modules and immersed in a 2T solenoidal magnetic field [1]. As the charged particles pass through the different layers of the inner detector, they will interact with the material there as shown in figure 10, but the interaction between the particle and the material here is very small, so small amount of energy is being absorb. As the result of interaction with material, electron-hole pairs will be created as shown in figure 11. These electrical signals known as a hits, by determining a group of hits belong to one charged particle as shown in figure 11, the direction, momentum, and charge of electrically-charged particles produced in each proton-proton collision can be determined.

The inner detector has three components as shown in figure 12 [11]:

- i. Pixel Detector, which is based on silicon as crystalline semiconductor material. A charged particle traversing a semiconductor loses small amount of energy (almost zero) in the crystal generating electron-hole pairs along its path [12]. The energy transfer of

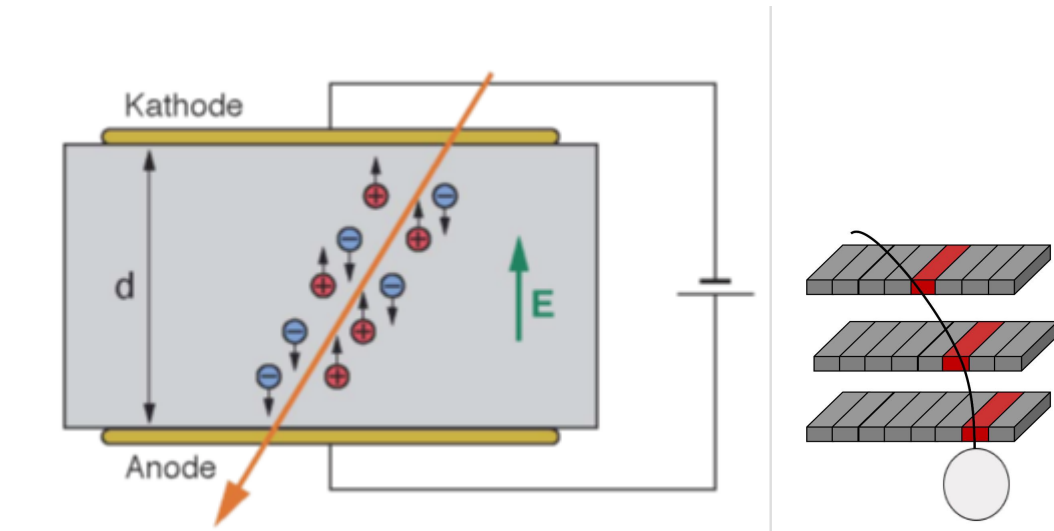


Figure 11: Left: Electron-hole pair formation in the inner detector of ATLAS. Right: Trajectory of a charged particle leaving hits through different layers of the inner detector.

a charged particle in matter is known as the amount of energy loss per unit length $(dE/dx)^4$, this measurement technique is used for a particle identification. dE/dx depends on the particle charge and velocity and atomic properties of the medium. For a known medium, from dE/dx we can calculate the velocity and the momentum, knowing both of them lead us to identify the mass of particle. A detailed description of pixel detector will be presented in section 2.3.4.

- ii. Four layers of Semiconductor Tracker (SCT), help to identify the position of a charged particle.
- iii. Transition Radiation Tracker (TRT), provides additional information helping in particle identification by using transition radiation technique, which provides discrimination between electrons and pions over the energy range of 1 GeV to 200 GeV.

⁴Bethe–Bloch formula

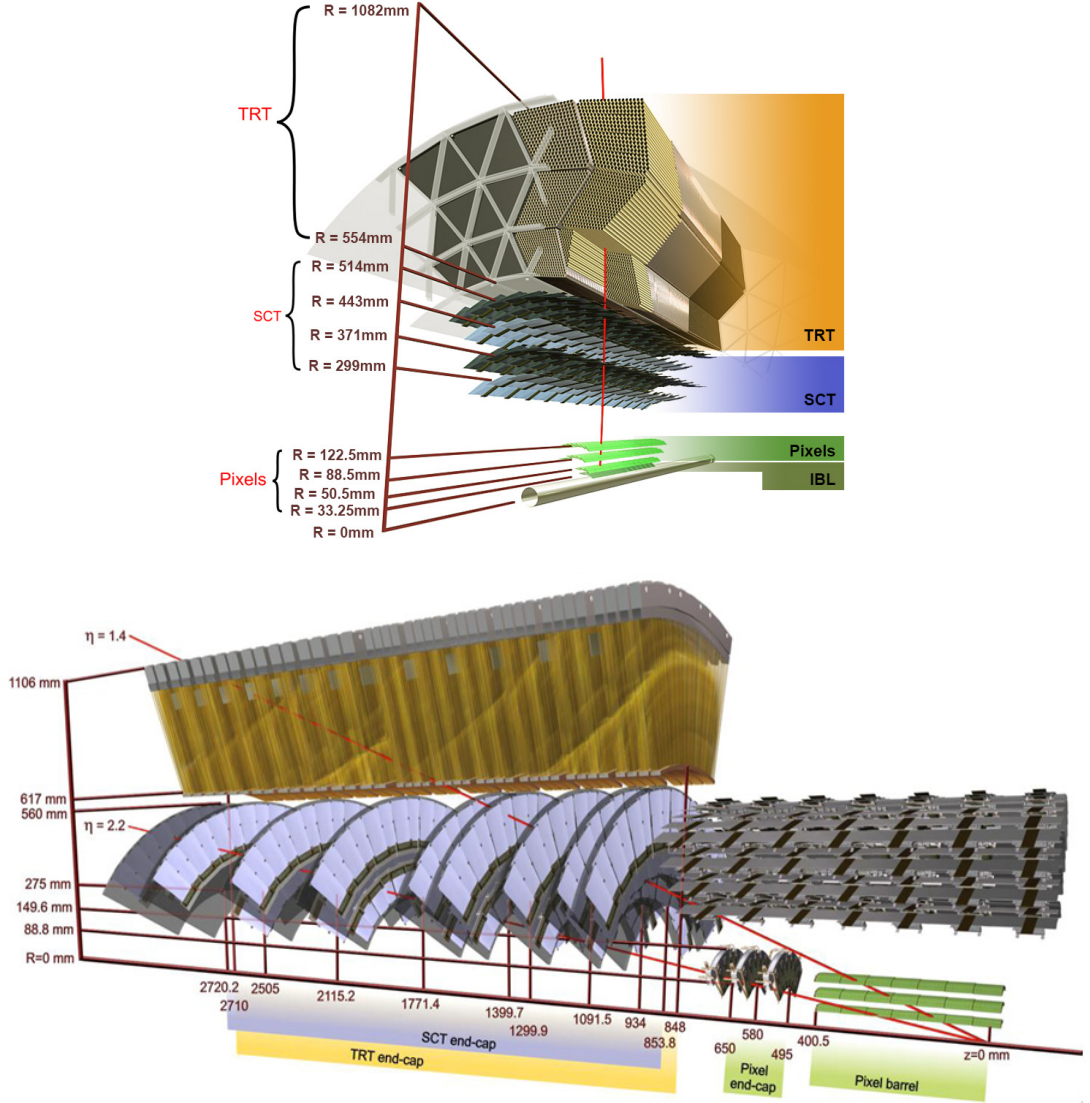


Figure 12: The inner detector of ATLAS.

The inner detector covers pseudorapidity η up to 2.5 as shown in figure 12, where $\eta = -\log(\tan(\frac{\theta}{2}))$, $\tan(\frac{\theta}{2}) = 0.082$ and $\frac{\theta}{2}$ is equal to 4.7° and as a result θ takes the values of 9.4° as a minimum value [11]. The current inner detector can cover θ from 9.4° to 170.6° .

2.3.4 Pixel Detector in The Current ID (after adding the Insertable B Layer (IBL))

The pixel detector is the innermost sub-detector in ATLAS. Due to its position, pixel detector must be made with a material that have special properties: low material budget, excellent radiation hardness, mechanical and thermal strength. These requirement are satisfied by choosing silicon to make up the pixel detector [13].

The pixel detector in the current inner detector consists of 1744 silicon pixel modules [14], each silicon module consists of 47000 pixel sensors with size $2 \times 6 \text{ cm}^{-2}$. In total there are 80 million pixel sensors with size $50 \times 400 \mu\text{m}^{-2}$ [15]. The pixel detector as shown in figure 13, consists of[16]:

- a. 3 parallel layers at radii 5, 9 and 12 cm with 1.3 m in length.
- b. 3 disks in each side. Particles that hit the detector with small incident angle θ can not cross the parallel layer but can still cross the disks.

After first long shutdown (LS1) 2013/2014 in phase 0 upgrade, IBL was added as a fourth layer to the pixel detector in the innermost region to the center of ATLAS, with expected life time 5 years [17], as shown in figure 12.

The sensitive location for IBL between pixel detector and a new beam pipe was a challenge for IBL project, the solution was in reducing the beam pipe radius from 29 mm to 25 mm [18]. Another challenge comes from this location is that IBL was exposed to the increased damaged ra-

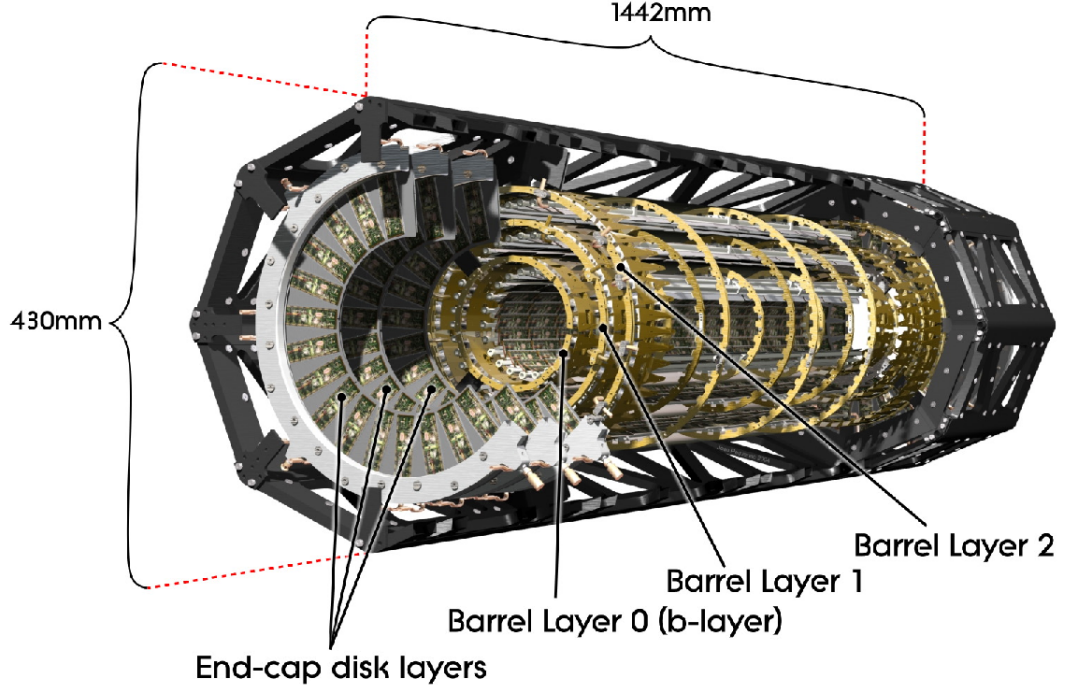


Figure 13: Schematic diagram for pixel detector.

diation and higher particle density [17]. This has been taken into account for the design of the components of IBL.

IBL has the ability to deal with hard radiation in better way than before. Hard radiation caused ATLAS to lose tracking efficiency especially in b-tagging analysis. At the moment, IBL is used to improve tracking, vertexing, b-hadron tagging performance and sensitivity improvement [19].

In table 2, a comparison between previous pixel detector and pixel detector with IBL, this comparison shown the improvement in pixel detector after addition of the IBL [20, 21]:

IBL comes in 14 staves, it has 12 million pixels with a length of 64 cm

$$5 \cdot 10^{15} n_{eq} \cdot s^{-2} = 50 Mrad$$

Table 2: Difference between pixel without IBL and pixel with IBL [22, 23].

The difference phase	Previous pixel detector	Current pixel detector
Pixel size	$50 \times 400 \mu m^{-2}$	$50 \times 250 \mu m^{-2}$
Beam pipe rad	$29 nm$	$25 nm$
Innermost layer rad	$5.05 cm$	$3.3 cm$
Pixel sensors number	80 million	92 million
Radiation hard	$10^{15} n_{eq}.s^{-2} 5$	$5 \times 10^{15} n_{eq}.s^{-2}$

and has been inserted at radius of 3.3 cm as shown in the right panel of figure 14.

After addition the IBL, the range of η that the inner detector can cover was increased. From the values in figure 14, the minimum θ that IBL covers can be calculated, $\theta_{min} = \tan^{-1}(\frac{3.3}{32}) = 5.9^\circ$, so IBL covers up to $\eta = |2.9|$ [20].

The increasing high dose of radiation day after day damages the pixel

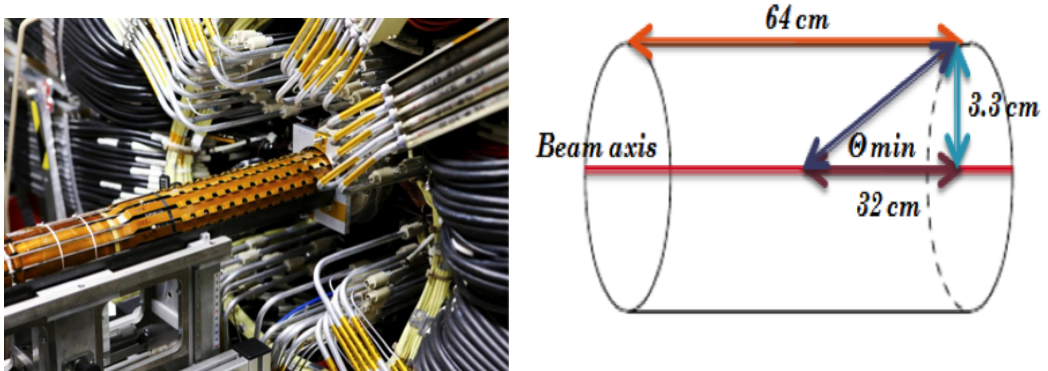


Figure 14: Left: The ATLAS IBL detector prior to the insertion [23]. Right: Schematic diagram for θ calculations that IBL covers, depending on the geometry of the IBL.

detector and the inner detector in general. Moreover, the world is still

looking forward for more contributions from LHC in the advancement of science, such as better understanding of the Higgs boson properties. Thus, the replacement of the inner detector by the Inner TracKer (ITK) is a crucial and needed upgrade in Phase *II* (2023 – 2025). My contribution to the ITK in the thesis is discussed in chapters 3 and 4.

Chapter Three

Inner Tracker (ITK)

3.1 Overview

The current tracking system of the ATLAS detector will be replaced in Phase *II* (*LS3*) 2023 – 2025 by a new all-silicon inner tracker (ITK). This upgrade will improve the tracking performance, b-tagging and lepton identification. Which would allow to study rare process with more accurate results.

Moreover, ITK has the ability to deal with HL-LHC environment, that results from increasing the luminosity five times ($5 - 7 \times 10^{34} \text{ cm}^{-2}\text{s}^{-1}$) more than it nowadays, it will reach 3000 fb^{-1} for integrated luminosity by 2035. The increase in luminosity means high particle densities, high pile-up as μ will increase from 40 (nowadays) up to 200 in HL-LHC. The current inner detector deals with hard radiation up to $5 \times 10^{15} \text{ n}_{eq}.\text{s}^{-2}$, but ITK is expected to deal with $10^{16} \text{ n}_{eq}.\text{s}^{-2}$ hard radiation, so ITK has also the ability to cope with hard radiation environment.

ITK is also a full silicon detector but without TRT, which is immersed in a 2 T solenoidal field like the current inner detector. ITK will contain two main components [24]:

- i. Pixel detector: it is much like the current pixel detector. It consists from 5 pixel parallel layers with 4 end-cap rings on each side instead of discs in the current inner detector as shown in figure 15.

ii. Silicon micro-strip system (strip): as shown in figure 15, it consists of:

- a. 4 parallel layers surrounding the pixel detector with radii from 400 mm to 1000 mm.
- b. 6 end-cap disks on each side with normal length arranged from 1400 mm to 3000 mm.

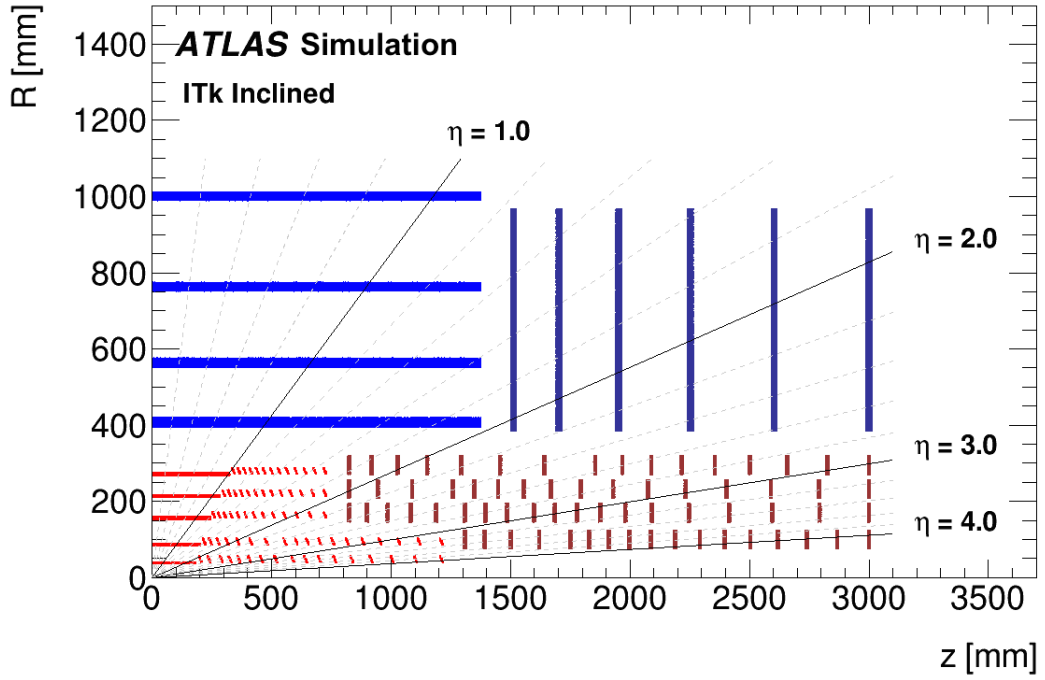


Figure 15: ATLAS Inner Tracker (ITK) layout, red lines are strips and blue lines are pixels.

As shown in figure 15, silicon micro-strip system covers pseudorapidity up to $|\eta| = 2.5$, but ITK will cover up to $|\eta| = 4$ [25]. Where $|\eta| = 2.5 - 4$ is called the forward region, it is the new region covered by the ITK as shown in figure 16. This improvement in coverage creates many benefits, it will improve b-jet identification and pile-up jet identification,

better identification of the hard scatter vertex beyond to increasing the range of lepton construction.

From the formula of pseudorapidity, θ can be calculated, as $|\eta| = 4$,

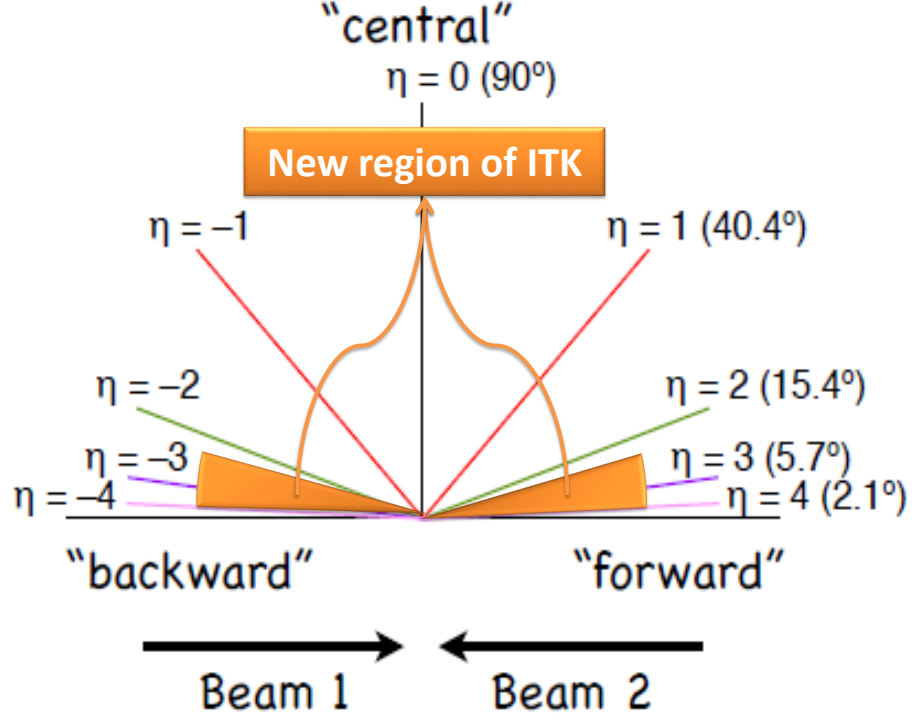


Figure 16: New reach in pseudorapidity η of ITK.

$\theta = 2.1^\circ$. In general ITK can cover θ from 2.1° to 177.9° .

3.2 Tracking Performance

As the charged particle enters a superconducting magnetic field region in the tracking system of ATLAS, it will be affected by a Lorentz force (magnetic force only), which can be represented by the motion of relativistic charged particle in a magnetic field equation:

$$F = q(\vec{v} \times \vec{B}) \rightarrow \frac{d\vec{P}}{dt} = q(\vec{v} \times \vec{B}) \quad (4)$$

$$P = mv = qB(T)R(m) \quad (5)$$

by changing the units from Joule and kg into GeV and using the charge of proton which is $1.6 \times 10^{-19}c$, we can get:

$$P(GeV/c) = 0.3B(T)R(m) \quad (6)$$

The transversed component of the momentum (P_T) is given by the equation:

$$P_T(GeV/c) = P(GeV/c) \sin(\theta) \quad (7)$$

where B is the magnetic field in Tesla, the purpose of the solenoid magnetic field is to bend the charged particles and as a result will be moved in a circular path. R is the radius of curvature that results from bending the charged particles by the magnetic field, it depends on the momentum of the charged particle as shown in figure 17. Particles with different momentum moves in trajectories with different radius of curvature, thus one can distinguish particles from each other based on the trajectory.

In order to calculate the momentum (p), R is needed to be calculated first. As shown in figure 17, R can be calculated from :

$$R^2 = (R - s)^2 + \left(\frac{L}{2}\right)^2$$

$$R^2 = R^2 + s^2 - 2Rs + \frac{L^2}{4}$$

$$2Rs = s^2 + \frac{L^2}{4}$$

$$R = \frac{s}{2} + \frac{L^2}{8s}$$

Since s is too small compared to L , then $R = \frac{L^2}{8s}$, where:

- i. L is the longest path length [26] (between the first hit and the last

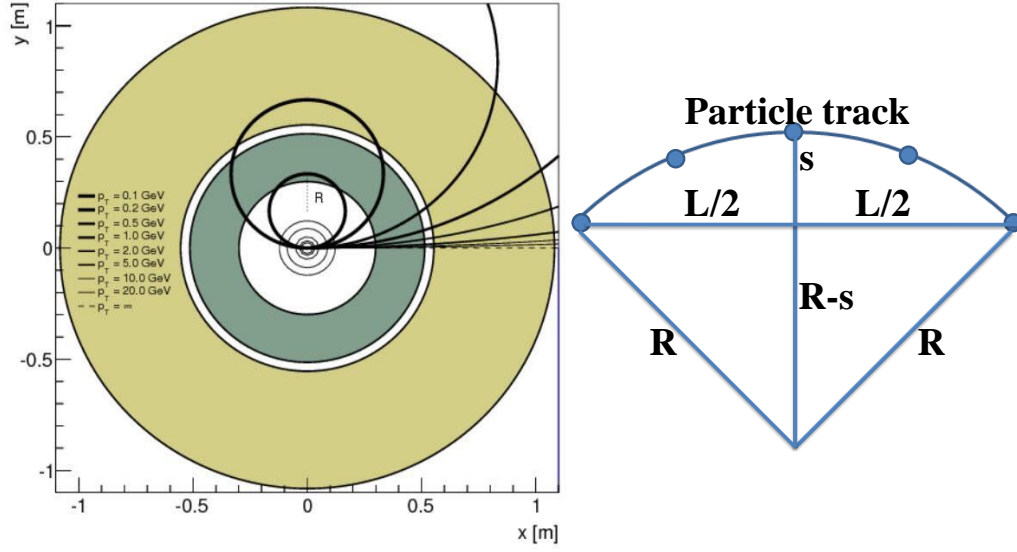


Figure 17: The trajectory of charged particles in a magnetic field, left plot indicates that the radius is increasing with momentum while the right figure shows how R can be calculated.

hit).

- ii. s is the least perpendicular distance between the half of the longest path length and the charged particle trajectory.

From equation 4, large mass particle carries high momentum causes increasing in the radius of curvature. Particle in ATLAS run clockwise if it has a negative charge and counter clockwise if it has a positive charge. The aim of tracking system is to determine the position, direction and momentum of a particle given hits associated to it.

A significantly large number of particles are produced due to collisions that take place in LHC. These particles will cause hits on several layers of the inner detector. The produced particles are not identical and they must be distinguished. The track reconstruction is used to distinguish the hits according to the type of particle that caused it. It will also find the

best trajectory that matches a group of hits. These trajectories are called reconstructed tracks as shown in figure 18.

From the tracking of a charged particle in the inner detector, a life time

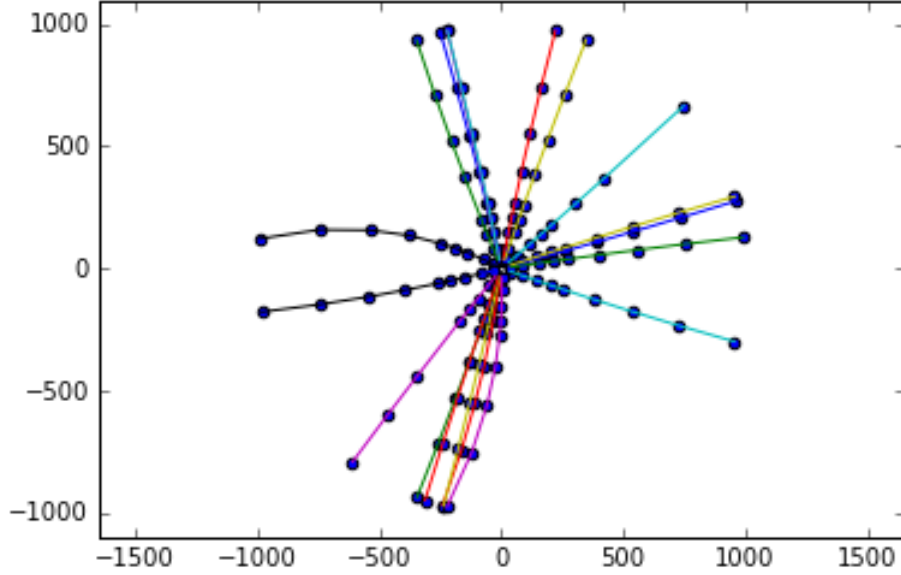


Figure 18: Reconstructed tracks associated to groups of hits.

tag also can be determined, in order to determine the primary vertices and secondary vertices in order to reconstruct them. The Primary vertices stems from the hard inelastic collision among many low p_T proton-proton interactions so called minimum bias events, while the secondary vertices are the resultant from decaying of primary vertices as shown in figure 19, which they are long-lived particles. So τ leptons and b jets are the most common light jets can be identified from each others [27].

The track reconstruction process can be divided into two stages: pattern recognition and track fitting. In pattern recognition, which hits belong to which tracks can be determined, in order to estimate the parameters for each one [28]. In track fitting the best possible estimation for the track

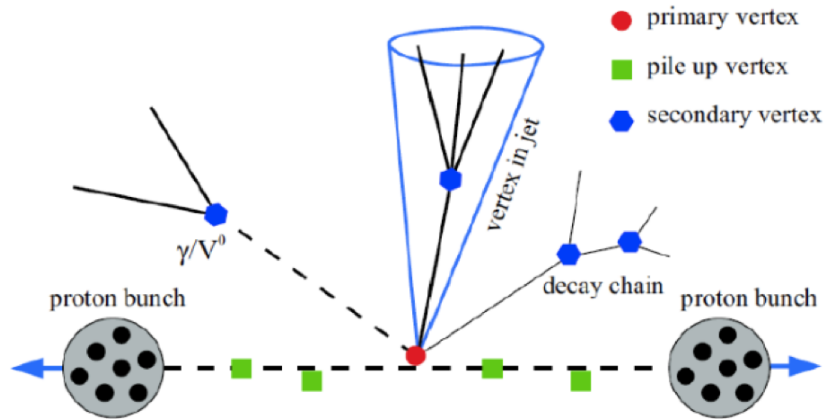


Figure 19: Types of vertices.

parameters can be determined in order to identify the particle trajectory. As shown in figure 20, some of reconstructed tracks can be matched completely or partially to truth particles tracks and there is some of reconstructed tracks that do not match to truth particles tracks [9].

There is many criteria to check the tracking detector performance. The

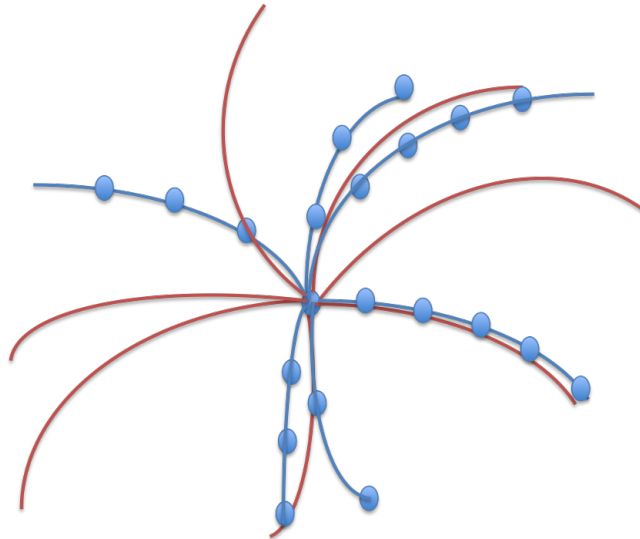


Figure 20: Blue circles are the hits in the ITK, blue lines associated to the reconstructed tracks while the red lines associated to the truth particles tracks.

first one is the tracking efficiency (ϵ), which is defined as the number of

reconstructed tracks match a truth particles with matching probability in general more than 50% over the total number of truth particles, as shown in equation 8 [29].

$$\epsilon_{track} = \frac{N_{reco}(selected, matched)}{N_{truth}(selected)} \quad (8)$$

Where the matching probability (P_{match}) is defined as the fraction of hits that was caused by the same true tracks[30]:

$$P_{match} = \frac{2N(pixel, common) + N(strip, common)}{2N(pixel, track) + N(strip, track)} \quad (9)$$

Where:

- i. $N(pixel, common)$ is the number of pixel hits common between the reconstructed track and truth track, the factor 2 due to the fact that the pixel detector provides a 2D measurement since we have a double sided silicon layer in each pixel layer.
- ii. $N(strip, common)$ is the number of strip hits common between the reconstructed track and truth track.
- iii. $N(pixel, track)$ is the total number of pixel hits in the reconstructed track.
- iv. $N(strip, track)$ is the total number of strip hits in the reconstructed track.

The other criteria is to check the performance of the detector is the fake rate, which can be defined the fraction of reconstructed tracks that do not

match to a truth particle (the matching probability is less than 50%) over the total number of truth particles [29].

$$fake\ rate = \frac{N_{reco}(selected, not\ matched)}{N_{truth}(selected)} \quad (10)$$

If the probability of matching more than 50% and less than 80%, then we call it poorly matched or bad matched. These particles are reconstructed, but the measurement will be poor because many hits on the reconstructed track do not come from the truth particle.

Many things affect the charged particle tracking efficiency and the fake rates. First of them is the type of particle, since they are highly sensitive to the interaction process between the particle and the detector material. For example muons have small interactions so it will have a very high tracking efficiency but in opposite case like pions and protons they have a lower tracking efficiency. The second parameter is the momentum; lower momentum particles suffer from high interaction rates and high multiple scattering which make the process of finding the track very difficult. Finally the amount of material traversed by a particle determines the probability of having a nuclear interaction, which reduces the tracking efficiency [31].

3.3 Tracking In Dense Environment (TIDE) in ITK

Increasing the luminosity in HL-LHC increases the number of large-mass particles, that are decaying through the ATLAS ITK. At high momentum, these particles decay to products that have trajectories very

much close to each other, these groups of particle's tracks form jets. Moreover, increasing μ up to 200 will increase the density of environment. Thus, ITK must have the ability to cope with this environment and to reconstruct the tracks of the produced particles [32].

The track reconstruction efficiency and the fake rate for Tracking In Dense Environment (TIDE) of the pixel detector in the ITK is evaluated in this section. Hypothetical gauge boson Z' is a massive electrically neutral, colorless boson which couples to showers of charged quarks and leptons as shown in the interaction 11. In core of jets, it is an excellent performance indicator for TIDE in ITK, and this allows to apply the study on b-jets⁶ and light jets⁷, which they are very important in ATLAS analysis. Many theories predict the existence of Z' with a mass in TeV scale, the results of Z' decaying will carry high energy, up to 2 TeV. Thus, many studies focus on Z' in order to find it, which leads to better understanding the universe around us [32].

$$pp \rightarrow Z' \rightarrow e^+e^-, jj, t\bar{t}, \tau^+\tau^-, e\mu, \mu^+\mu^- \quad (11)$$

A $5\text{TeV } Z' \rightarrow jj$ sample with $\mu = 200$ is used for the baseline variables studies, these variables are the key to assess ITK performance and they are :

- i. Truth jet transverse momentum (p_T), as in section 3.3.1.
- ii. Truth jet pseudorapidity(η), as in section 3.3.2.

⁶Light jet contains b quark.

⁷Light jet contains only u and d quarks.

iii. Truth jet angular distance (ΔR), as in section 3.3.3.

iv. Displaced vertices, as in section 3.3.4.

p_T is mostly related to the energy of the jet, and one wants to see the performance in the full energy spectra. η , ΔR and displaced vertices are mostly connected to the detector resolution, geometry, and overall performance. We thus want to see how the detector performs by looking at these observables.

All the tracks are selected in a cone around the jet axis that has ΔR less than 0.4 mm and p_T is more than 2 GeV.

3.3.1 Jet Transverse Momentum (p_T) Study

First of all, the track reconstruction efficiency for pixel detector in the ITK within all jets as function of truth jet transverse momentum (p_T) is shown in figure 21. The overall tracking efficiency is around 90%, while the error bars come from statistical uncertainty. The efficiency is increased with truth jet p_T , it reaches a maximum around 500 GeV, with increasing the value of p_T more than 500 GeV, the track reconstruction efficiency stays very much constant up to 3 TeV, since the particles with low momentum are difficult to reconstruct and particles with higher p_T gets further through the detector. More hits can be gotten and one has greater chance to get them reconstructed properly. The higher p_T means higher tracks collimation. Thus, from the good values of efficiency at this region, one can conclude that ITK layout performs very good in dense environment.

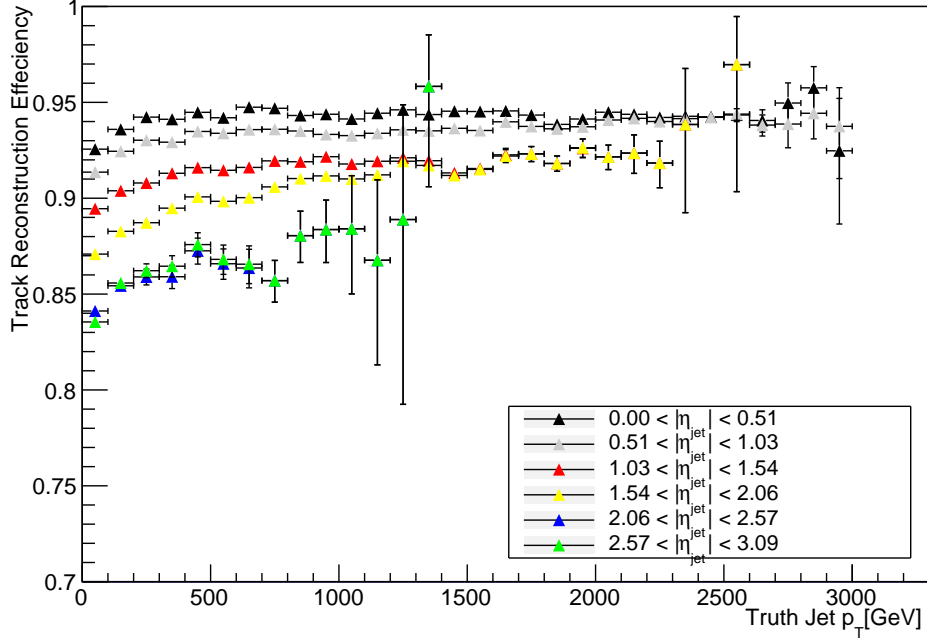


Figure 21: The track reconstruction efficiency as a function of truth jet p_T within all jets in the ITK for different ranges of truth jet η .

As shown in figure 21, the tracking efficiency reaches 95% in the central region as p_T is more than 700 GeV. While it is around 86% in the forward region. One can conclude that when η is increased the efficiency is decreased since the particles must pass through larger amount of material. Thus particle loses energy or is scattered, making it harder to reconstruct it properly [33].

By having a look on some ATLAS official results similar to what we do, a 5 TeV $Z' \rightarrow t\bar{t}$ sample is used in the study in order to study the track reconstruction efficiency as a function of truth jet p_T within all jets in the ITK as shown in figure 22, truth jet $\eta < |4|$, $\Delta R < 0.4$ mm and truth jet $p_T > 1$ GeV [34]. The tracking efficiency as a function of truth jet p_T in two figures show similar behaviour and much close results. Thus, our

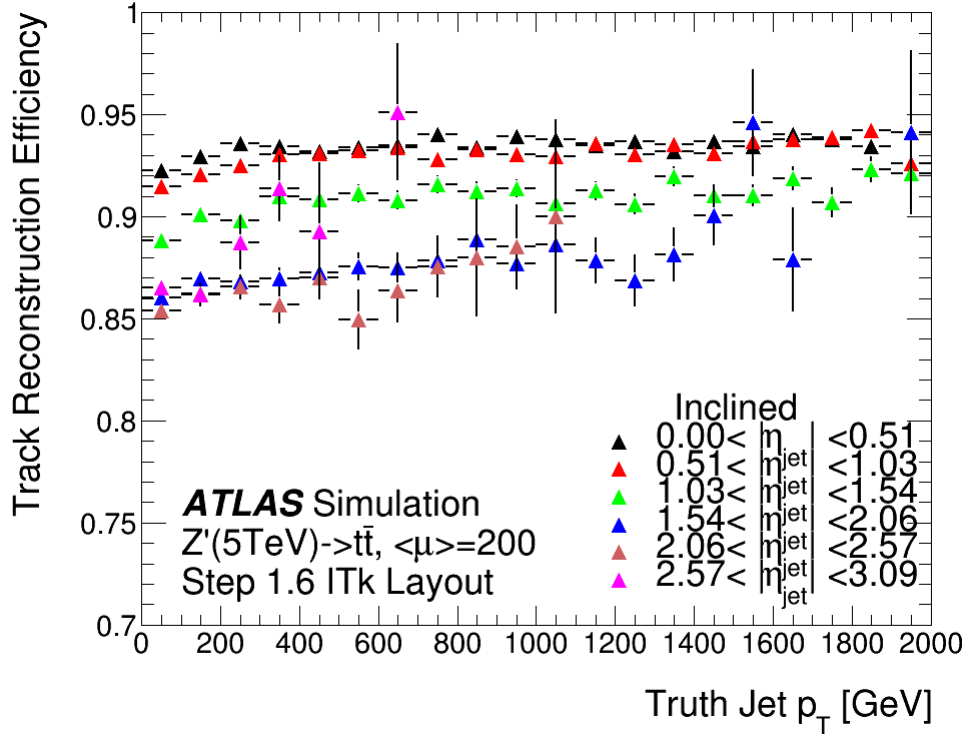


Figure 22: The track reconstruction efficiency as a function of truth jet p_T within all jets in the ITK for different ranges of truth jet η (ATLAS simulation, 2016) [34].

study confirms a very good performance of ITK layout.

The rate of reconstructed tracks with a poor truth matching probability $50\% < P_{match} < 80\%$, which is known as a Bad Match rate is shown in figure 23 as a function of truth jet p_T for different ranges of truth jet η in the ITK within all jets. Since Z' is an excellent example to study the performance of ITK, jets that are coming only from Z' is studied as a special case. Thus, the bad match rate within jets are only coming from Z' as a function of truth jet p_T for different ranges of truth jet η is shown in figure 24.

Both figures show similar behavior, which means that most of jets are coming from Z' . The bad match rate is increased with truth jet p_T and

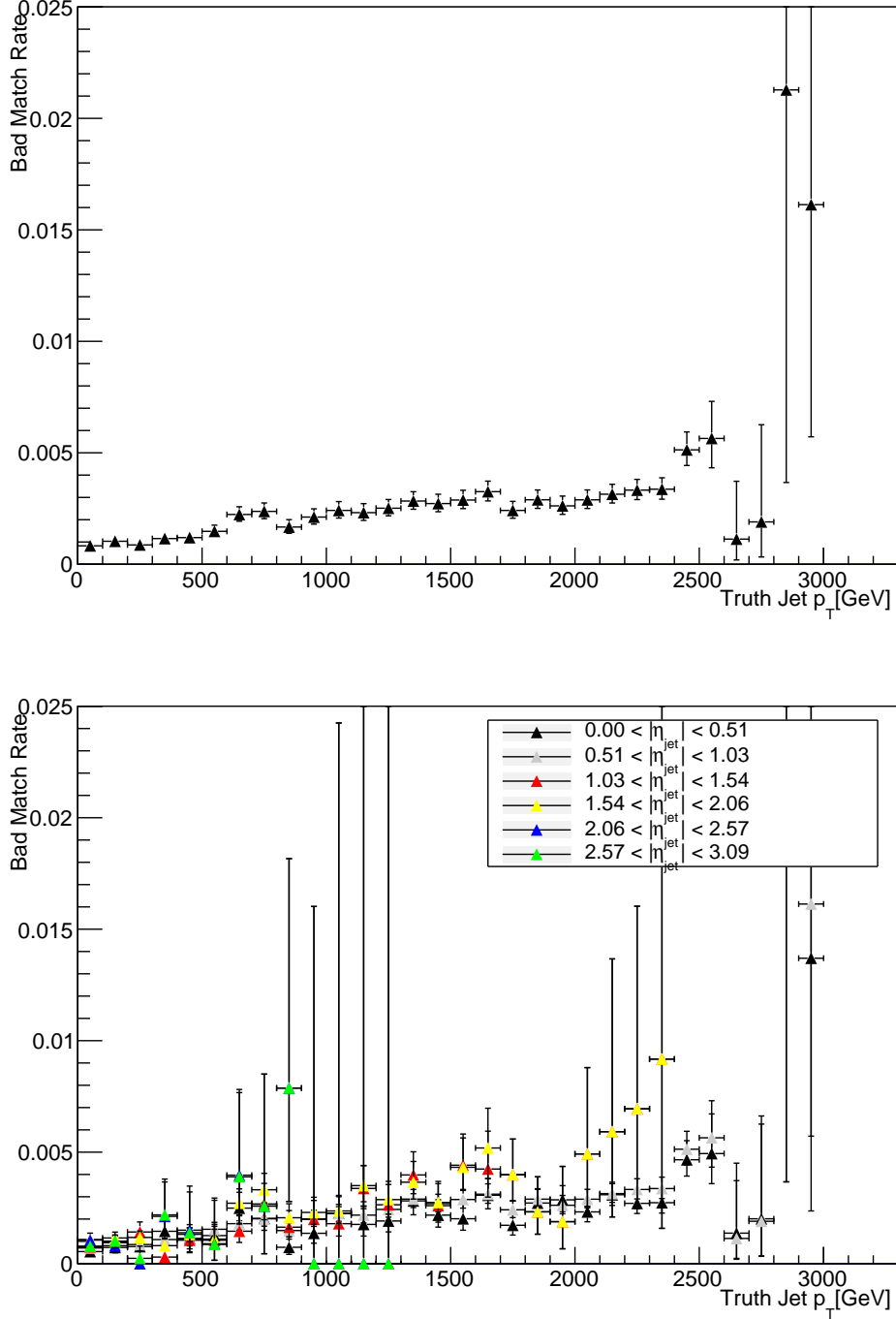


Figure 23: The bad match rate as a function of truth jet p_T within all jets in the ITK.

Top: all η are included.

Bottom: different ranges of truth jet η are taken.

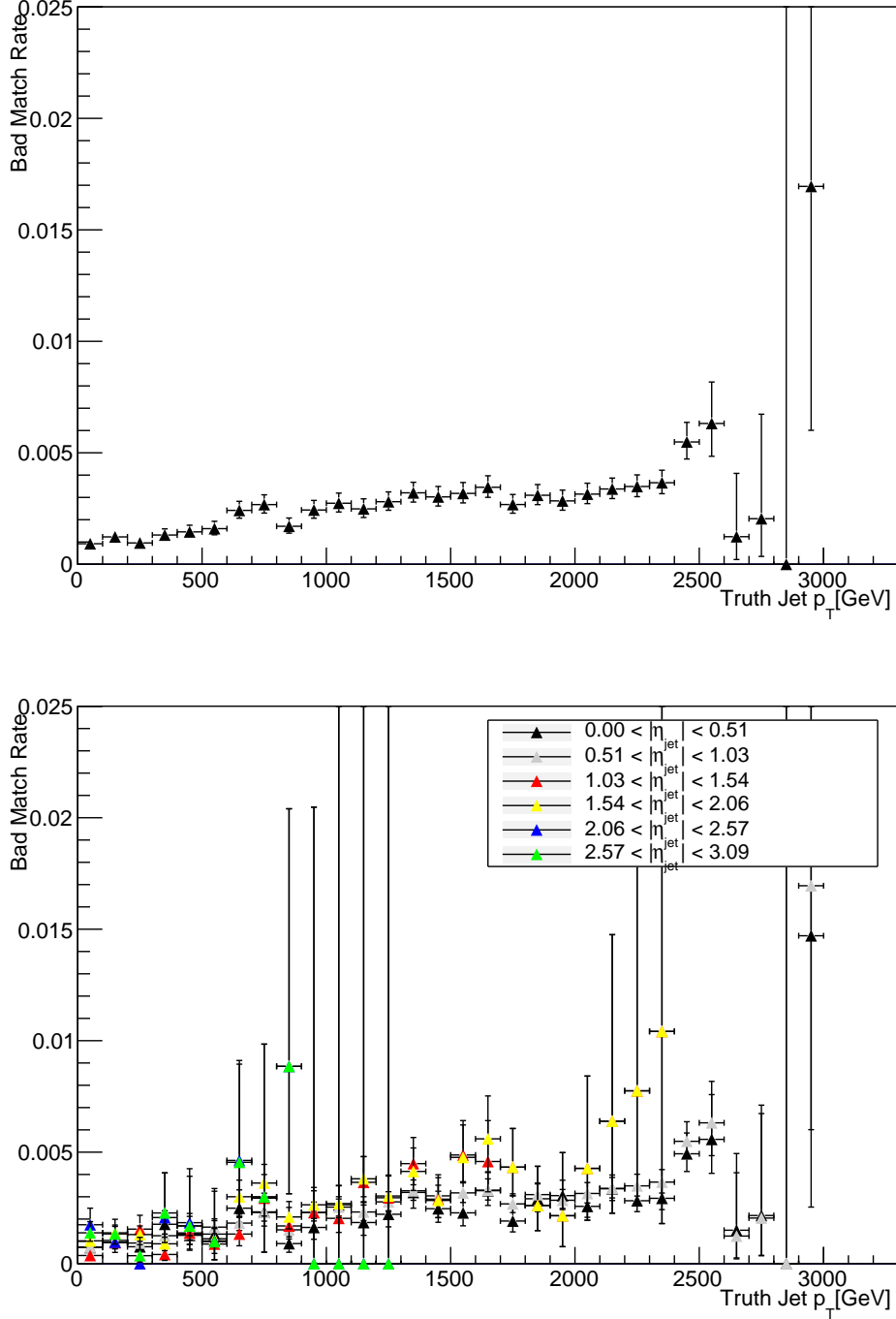


Figure 24: The bad match rate as a function of truth jet p_T within jets coming only from Z' in the ITK.
Top: all η are included.
Bottom: different ranges of truth jet η are taken.

increased with different ranges of truth jet p_T . The maximum bad match rate is 2%, but in general the bad match rate is around 0.3% in both cases. The fake rate, that consists a reconstructed tracks with a very poor truth matching probability $P_{match} < 50\%$ has not been studied because it is very small and the samples studied do not have enough events to measure it properly.

3.3.2 Jet Pseudorapidity (η) Study

The track reconstruction efficiency in the pixel detector of ITK within all jets as function of truth jet η for different ranges of p_T is shown in figure 25. The maximum tracking efficiency in the central region is around 94%, but in the forward region, the minimum is around 80%.

In conclusion, the efficiency is increased with truth jet p_T since particles with higher p_T gets further through the detector. More hits can be gotten and one has greater chance to get them reconstructed properly. But the efficiency is decreased with transverse jet η , since the particles must pass through larger amount of material. Thus particle loses energy or is scattered, making it harder to reconstruct it properly [33]. In general the efficiency here has a value around 90%. These results also shown in the truth jet p_T study, so one can confirm the good performance of ITK layout.

By comparing the results in figure 25 and the results in figure 26, the tracking efficiency for $Z' \rightarrow jj$ sample is slightly lower by 3% than the tracking efficiency for $Z' \rightarrow t\bar{t}$ in the forward region, while in the cen-

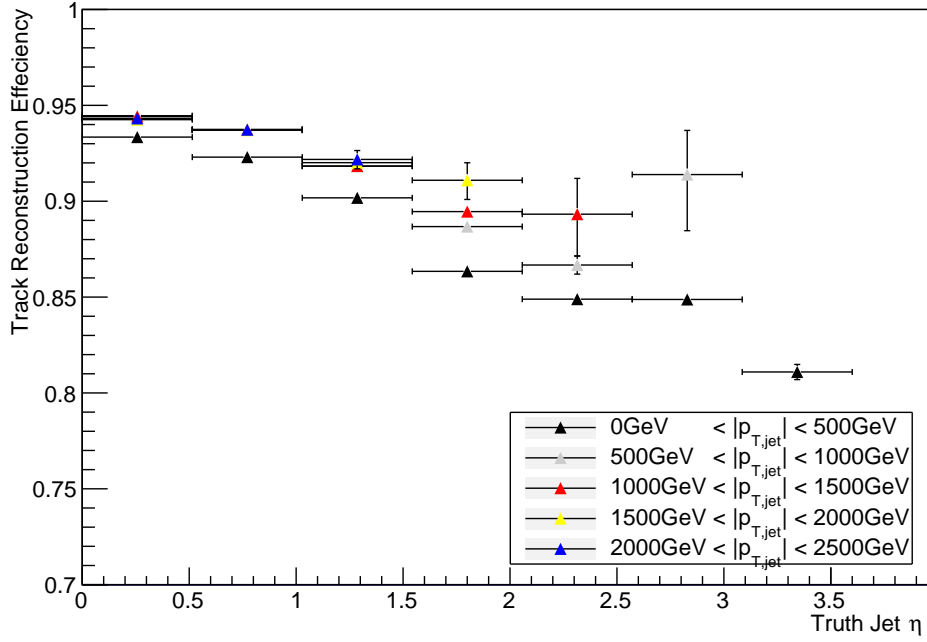


Figure 25: The track reconstruction efficiency as a function of truth jet η within jets in the ITK for different ranges of truth jet p_T .

tral region both figures show similar behaviour and much close results. Thus, both results indicate the good performance of ITK.

The bad match rate as a function of truth jet η for different ranges of truth jet p_T of the ITK is shown in figure 27 for all jets. Due to the importance of Z' , the bad match rate for jets that are coming only from Z' is shown in figure 28. The two figures show similar behavior, which means that most of jets are coming from Z' . In general, the bad match rate is around 0.2% in both cases, while the highest value is 0.5% when p_T is the highest. One can conclude that the bad match rate is increased as truth jet p_T increased. While for specific range of truth jet p_T , the bad match rate stays very much constant for different truth jet η .

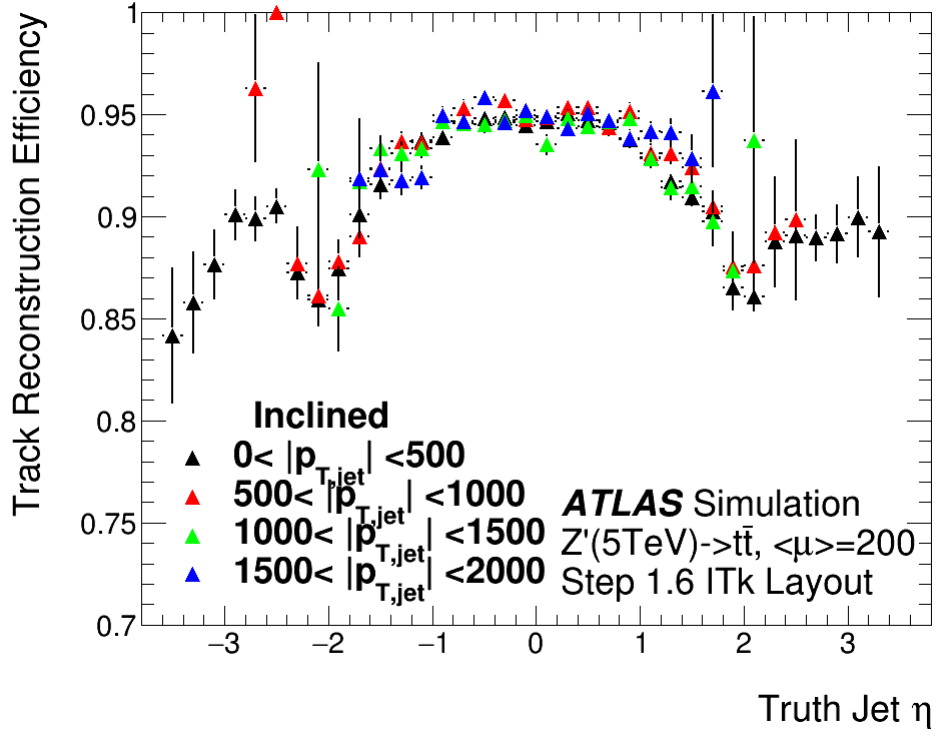


Figure 26: The track reconstruction efficiency as a function of truth jet η within jets in the ITK for different ranges of truth jet p_T (ATLAS simulation, 2016) [34].

3.3.3 Jet Angular Distance (ΔR) Study

In ΔR study, a 5 TeV $Z' \rightarrow jj$ sample is used to study the track reconstruction efficiency and bad match rate for pixel detector of the ITK as function of the ΔR of each truth particle from the jet axis, within ΔR is less than 0.4 mm. Jets will be divided into two groups depending on the contents of a jet. if the jet contains bottom quark (b), it has a name of b jet. If it does not, it will be considered as a light jet⁸. These studies are a good indicator of the performance in the jet substructure.

b quark is the heaviest mass among quarks beyond to t quark, it has a mass of 4.180 GeV/ c^2 [35], it comes from the decay of massive particles,

⁸Light jet contains only u and d quarks.

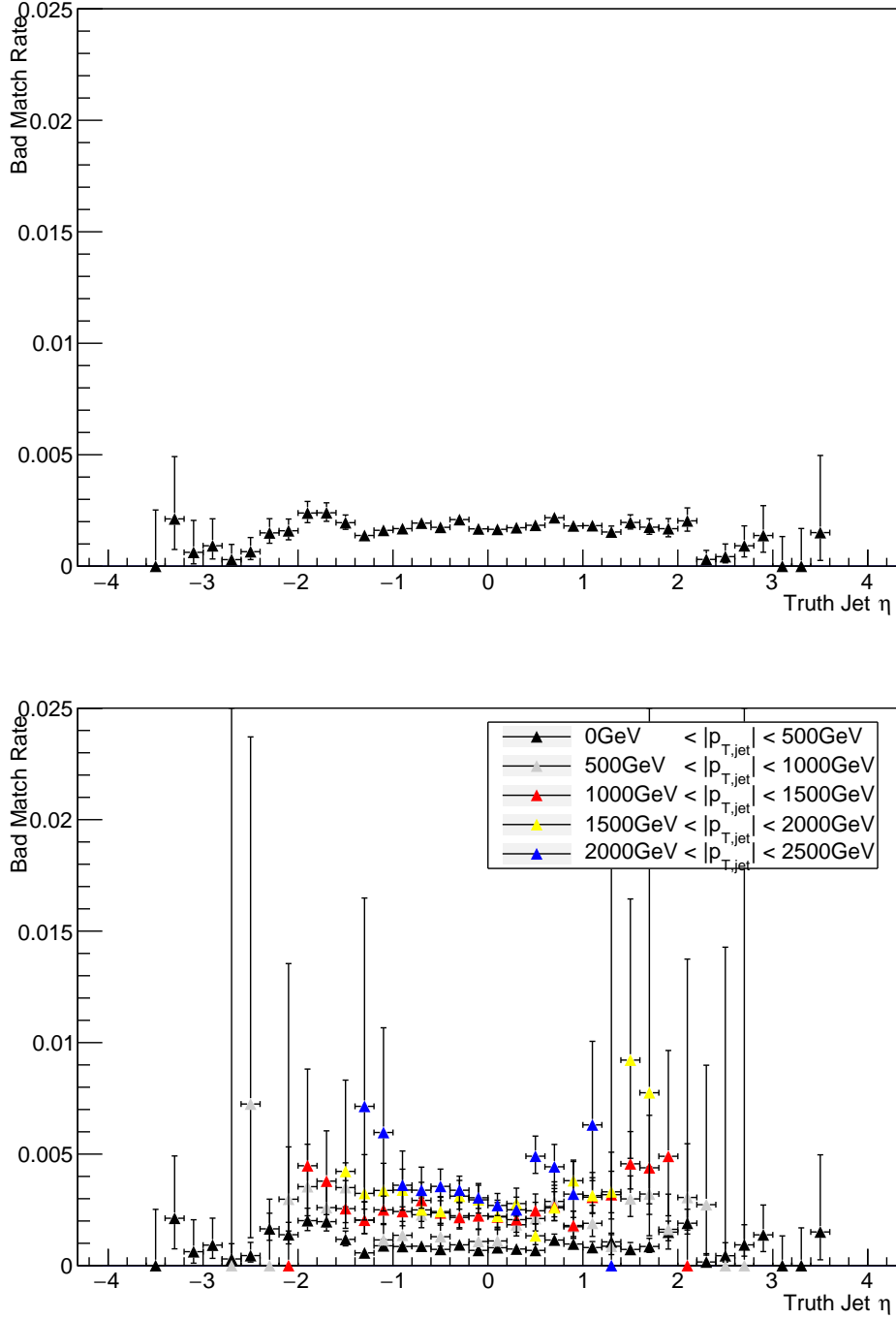


Figure 27: The bad match rate as a function of truth jet η within all jets in the ITK.

Top: all p_T are included.

Bottom: different ranges of truth jet p_T are taken.

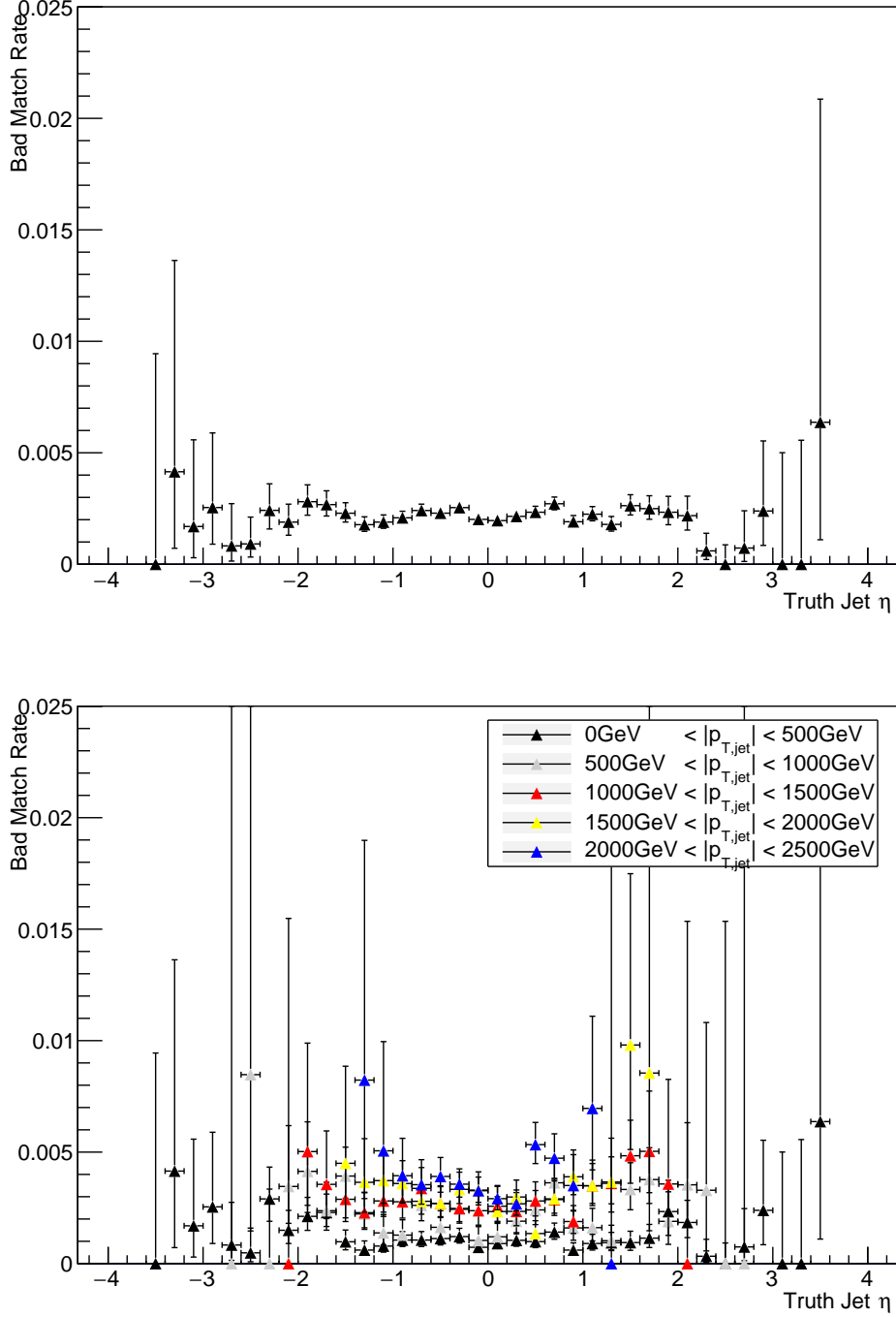


Figure 28: The bad match rate as a function of truth jet η within jets coming only from Z' in the ITK.

Top: all p_T are included.

Bottom: different ranges of truth jet p_T are taken.

like Z' . It is preferred since it has a life time 10^{-12} sec [36], thus, it travels some distance before decaying through the ITk.

The track reconstruction efficiency in the ITK as function of the ΔR of each truth particle from the jet axis is shown in figure 29 for b jets and figure 30 for light jets. For different ranges of truth jet η is studied in top figures, and for different ranges of truth jet p_T is studied in the bottom figures. The efficiency is increased with truth jet p_T , while it decreased with truth jet η .

For the b jets, the tracking reconstruction efficiency is increasing slightly with the ΔR , since at small ΔR the density of the particles is the highest. 80% is the minimum efficiency, it happens in the forward region, however, the efficiency is more than 90% and it reaches 95%. By comparing these results with the efficiency for $Z' \rightarrow t\bar{t}$ sample, that shown in figure 31. The tracking efficiency for $Z' \rightarrow jj$ sample is slightly better than the tracking efficiency for $Z' \rightarrow t\bar{t}$ sample except at high range of η [$2.06 < |\eta| < 2.57$].

For the light jets, the tracking efficiency stays very much constant with the ΔR for specific range of truth jet η or truth jet p_T . 80% is the minimum efficiency, it happens in the forward region, however, the efficiency is more than 90% and it reaches 98%. By comparing the values of efficiency for each range of η between $Z' \rightarrow jj$ sample results and $Z' \rightarrow t\bar{t}$ sample results that are shown in figure 32, both samples have nearly the same values of efficiency, which is very good for both.

B-tagging and light jets are very important for many ATLAS searches,

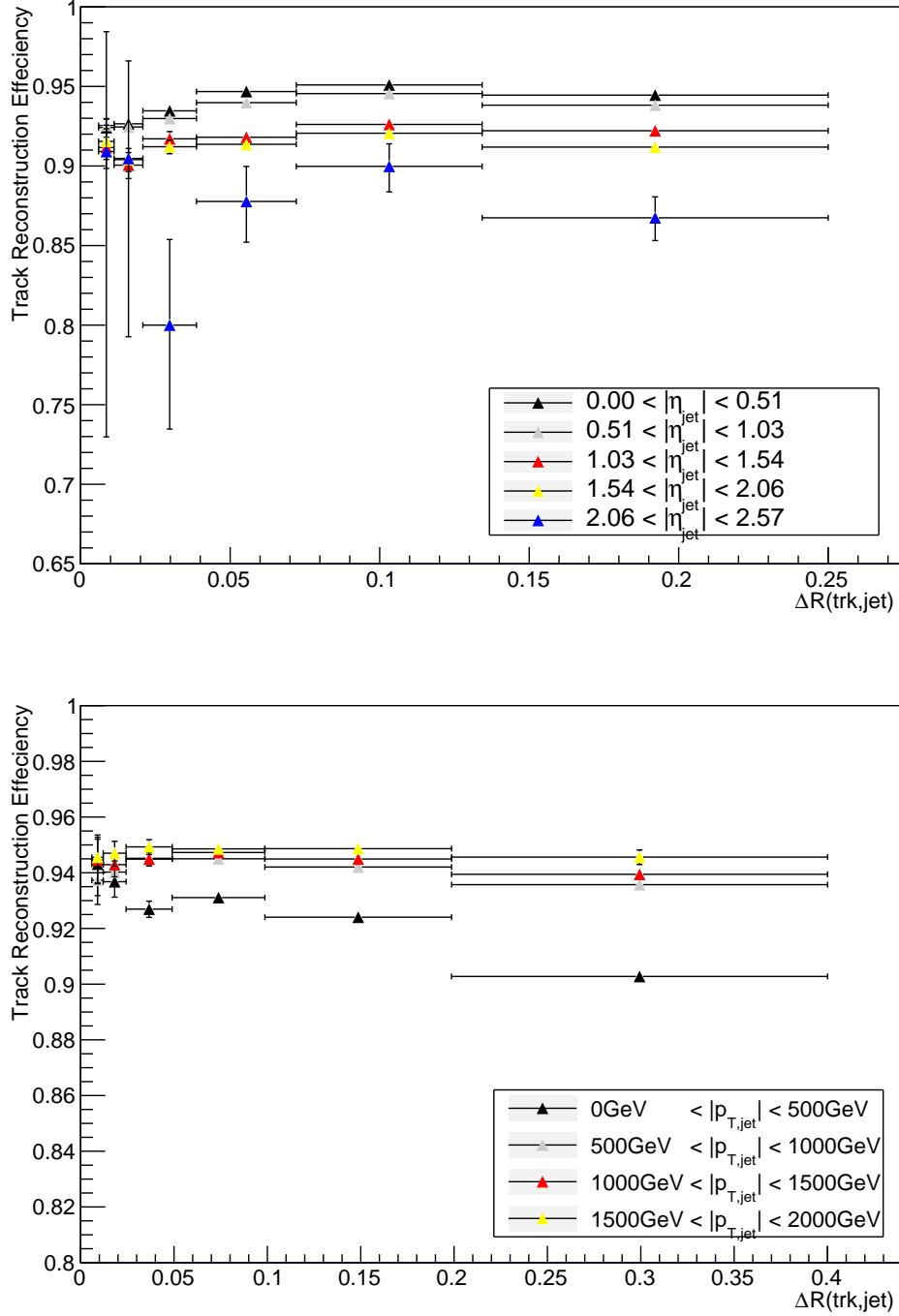


Figure 29: The track reconstruction efficiency as a function of truth jet ΔR for b-jets in the ITK.

Top: different ranges of truth jet η are taken.

Bottom: different ranges of truth jet p_T are taken.

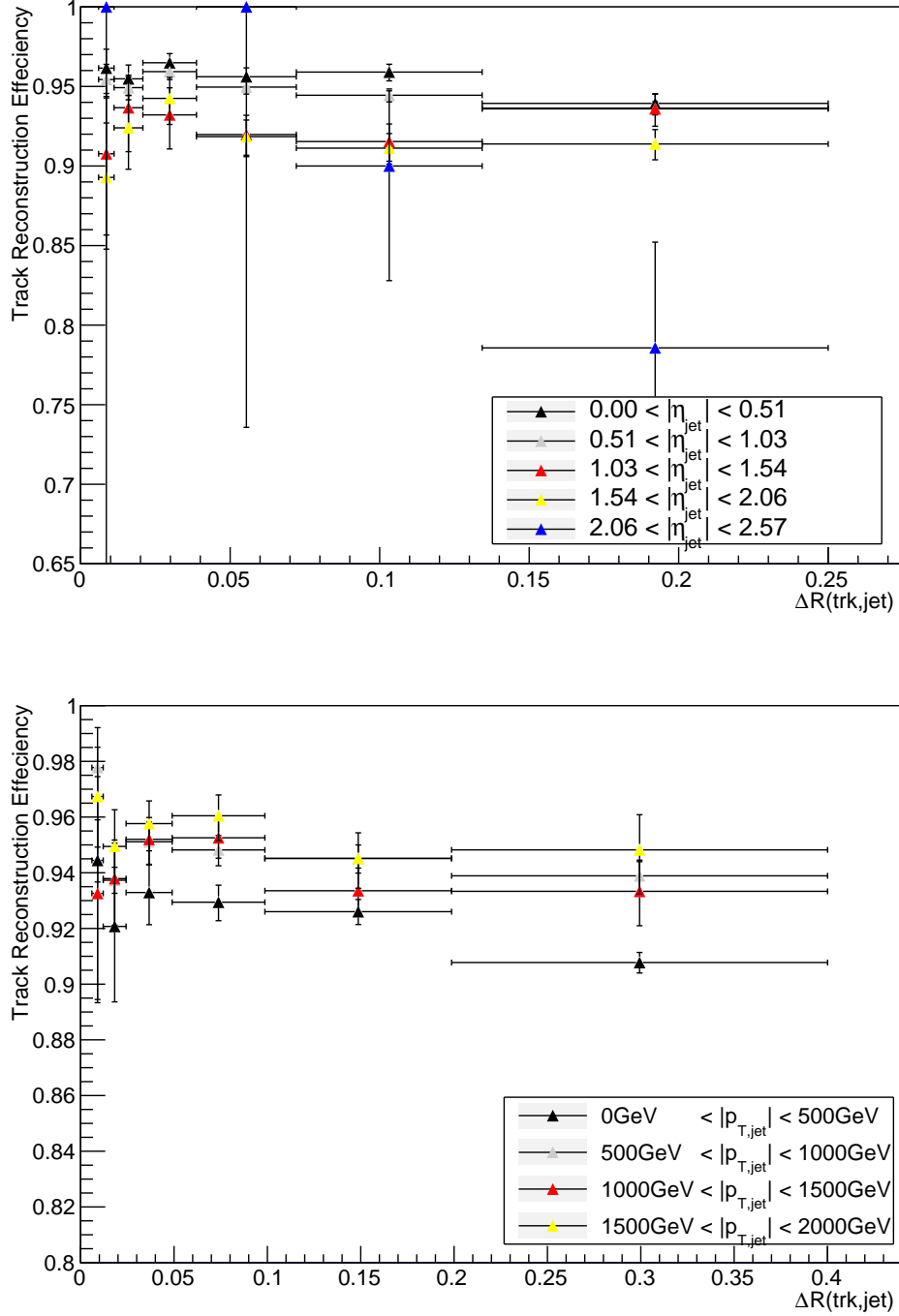


Figure 30: The track reconstruction efficiency as a function of truth jet ΔR for light jets in the ITK.

Top: different ranges of truth jet η are taken.

Bottom: different ranges of truth jet p_T are taken.

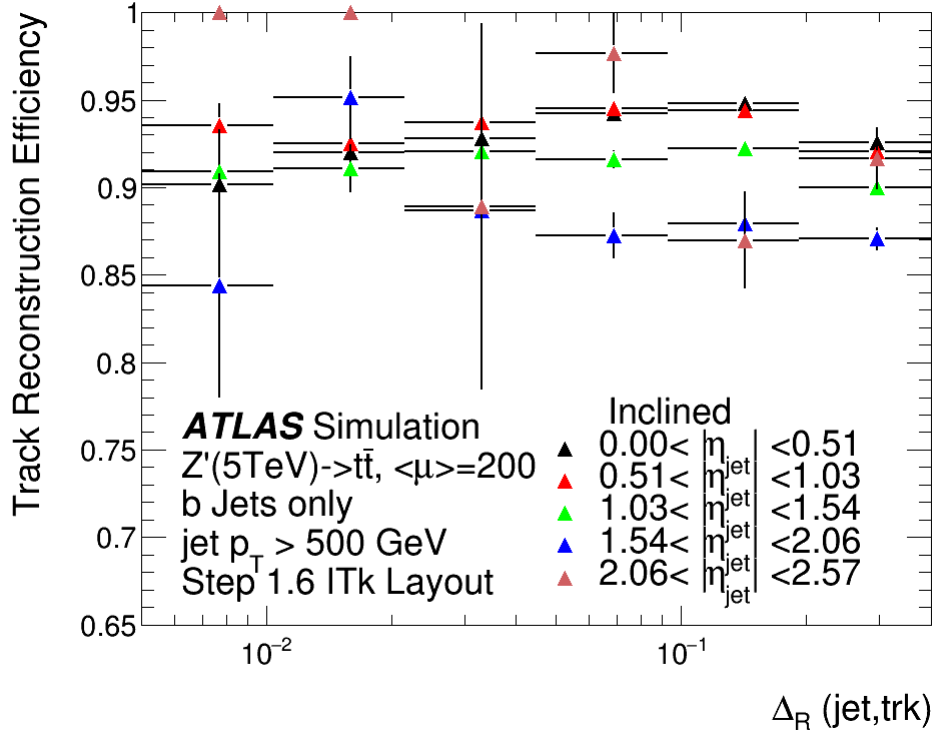


Figure 31: The track reconstruction efficiency as a function of truth jet ΔR for different ranges of truth jet η , for b-jets in the ITK (ATLAS simulation, 2016) [34].

and in core of jets, studying the efficiency as a function of the ΔR and getting a good results confirm the ITK good performance.

The bad match rate for b jets as a function of the ΔR in the ITK for different ranges of truth jet η is shown in figure 33 within all jets. Figure 34, for different ranges of truth jet p_T , within all jets. And for different ranges of truth jet η , within jets that are coming only from Z' is shown in figure 35.

All figures reflect similar behavior. The bad match rate is decreased significantly with ΔR , it has a values between 0% and 0.9%. The bad match rate is lower in the central region than the forward region, it is increased with η . Figures 33 and 35 are exactly the same, which means most of

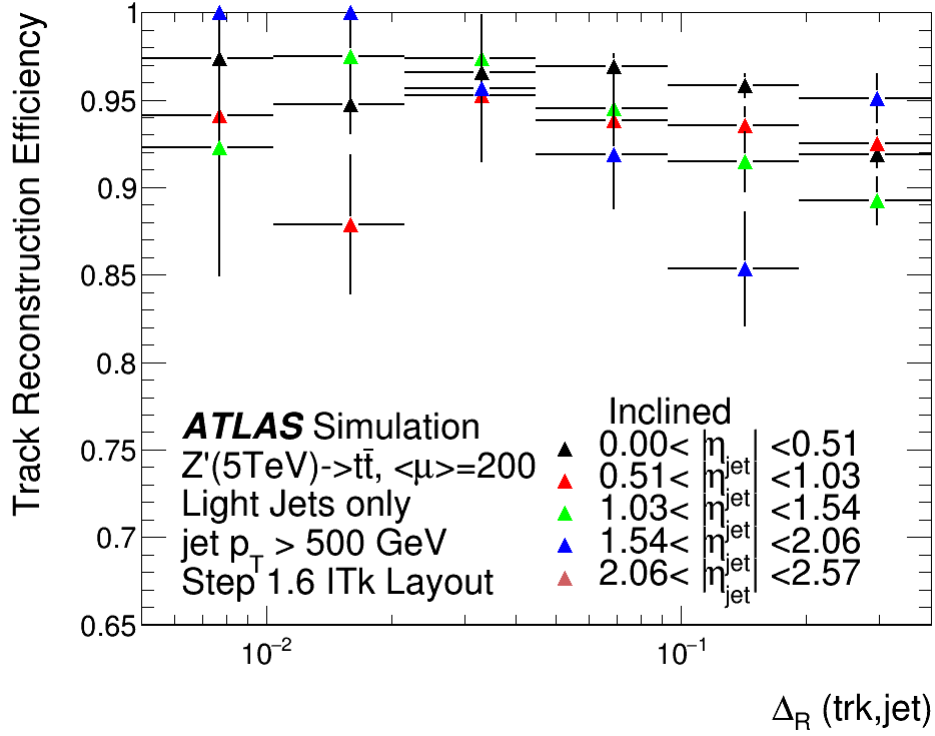


Figure 32: The track reconstruction efficiency as a function of truth jet ΔR for different ranges of truth jet η , for light jets in the ITK (ATLAS simulation, 2016) [34].

jets are coming only from Z' .

3.3.4 Displaced Vertices Study

A 5 TeV $Z' \rightarrow jj$ sample is used in displaced vertices study. Displaced vertices are points of interactions of at least two or more tracks take place far from the primary interaction point, as shown in figure 36. In most cases they are coming from massive particles and their decay products tracks form dense environment. Thus, they are very important in ATLAS searches.

The truth particles that result from b-hadron decay are taken in this study, and they are separated into hadrons and leptons [37], and the b-

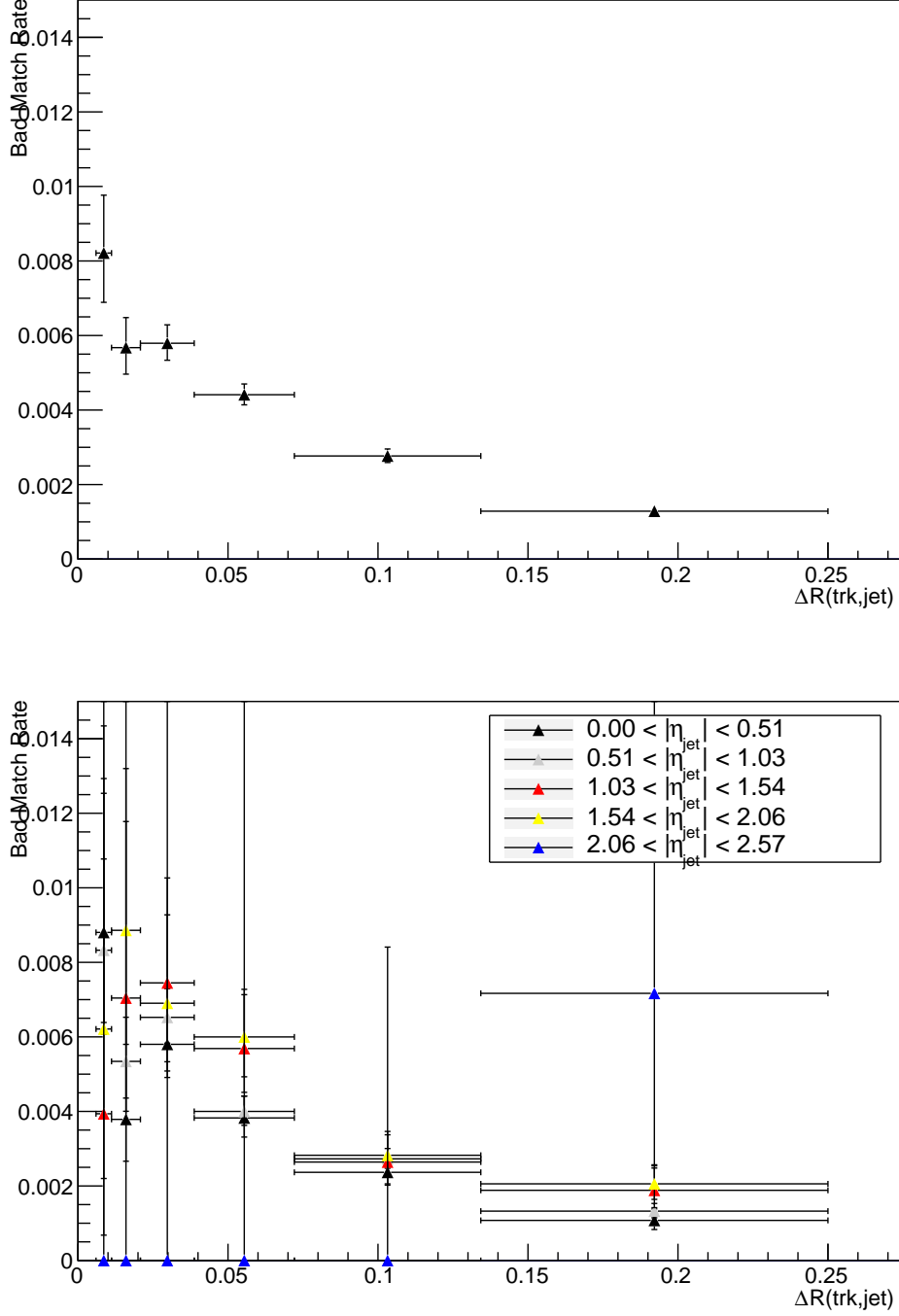


Figure 33: The bad match rate for b jet as a function of ΔR within jets in the ITK.

Top: all η are included.

Bottom: different ranges of truth jet η are taken.

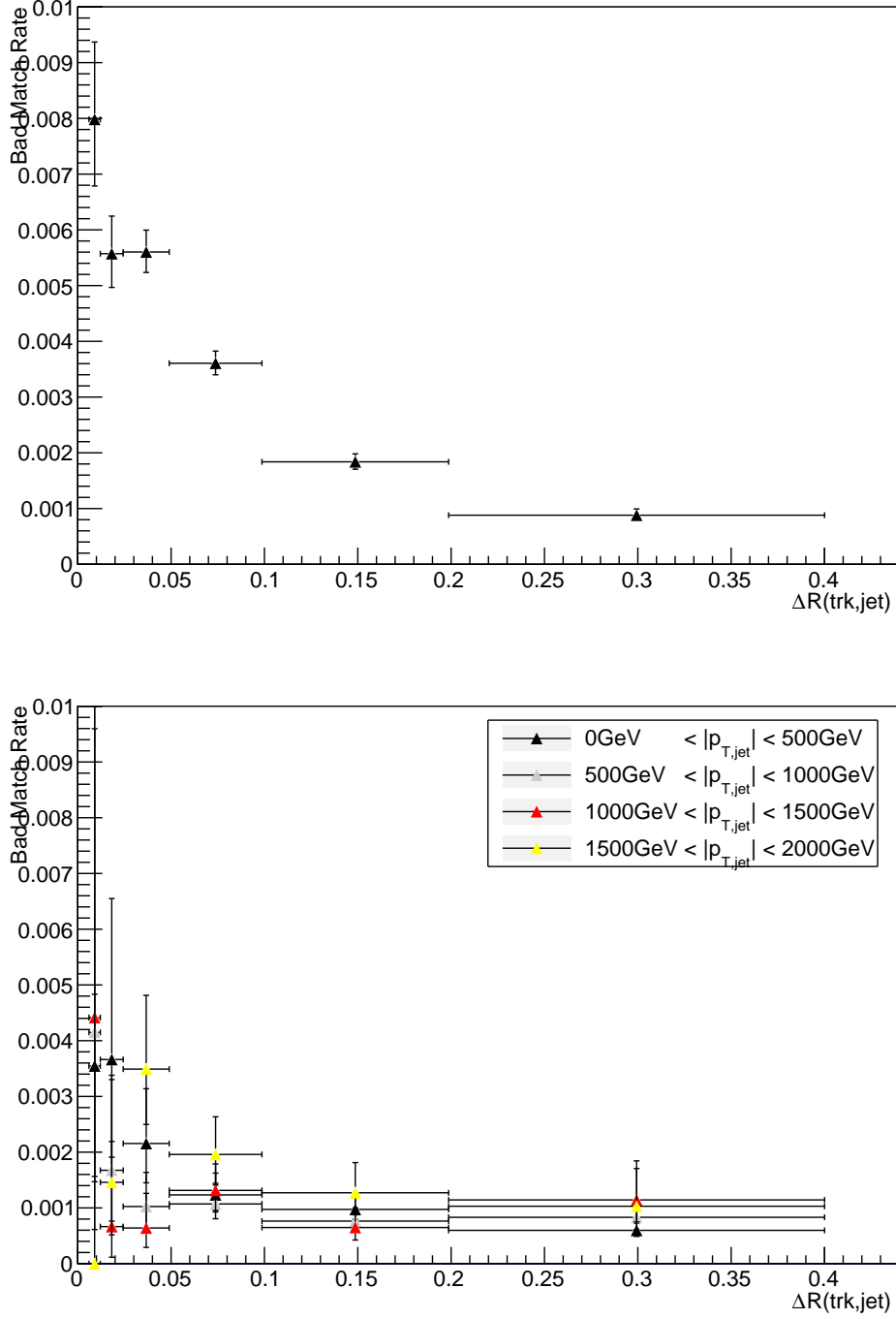


Figure 34: The bad match rate for b jet as a function of ΔR within jets in the ITK.

Top: all p_T are included.

Bottom: different ranges of truth jet p_T are taken.

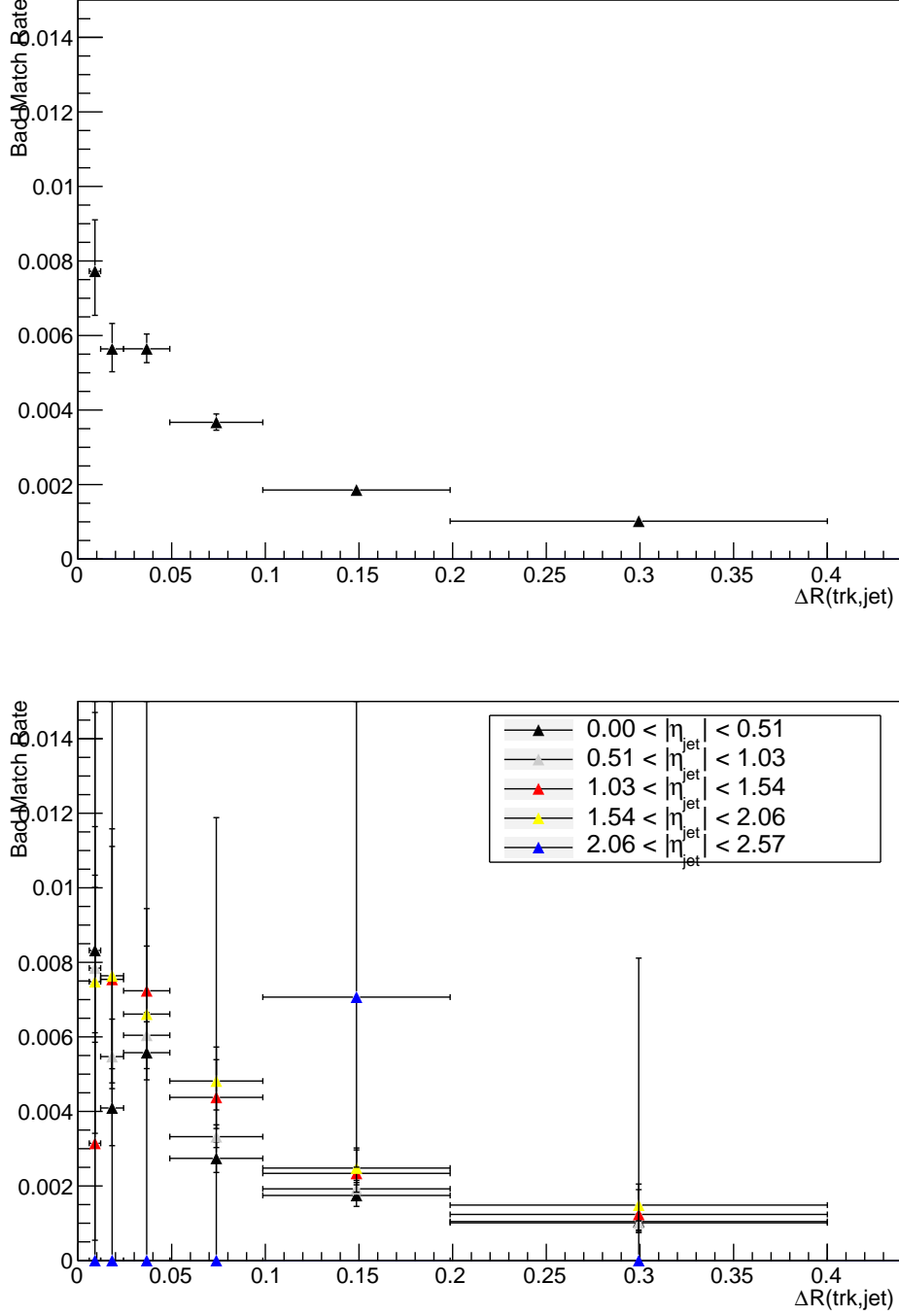


Figure 35: The bad match rate for b jet as a function of ΔR within jets that are coming only from Z' in the ITK.

Top: all η are included.

Bottom: different ranges of truth jet η are taken.

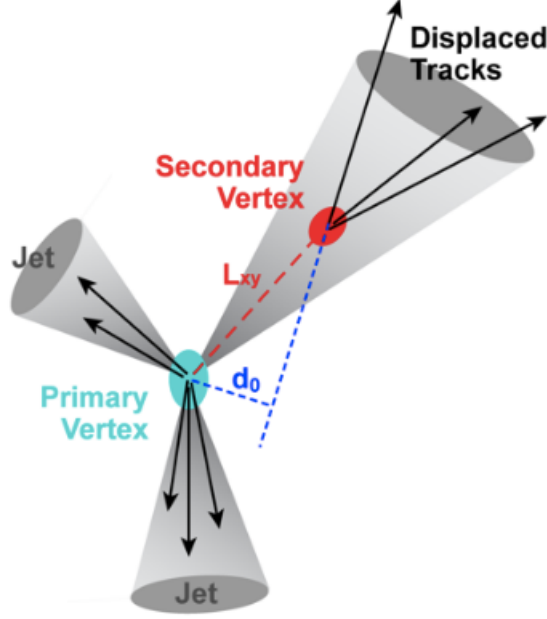


Figure 36: Schematic diagram of Displaced tracks.

hadron decay radius is determined. In order to study the effect of displaced vertices on the track reconstruction efficiency and bad match rate as a function of truth production radius.

The tracking efficiency for different ranges of truth jet η within all jets in the ITK as a function of the decay radius of the b-hadron for leptons decaying from b-hadron is shown in figure 37, and for hadrons decaying from b-hadron is shown in figure 38. The efficiency is decreased with truth jet η . While it is increased with truth production radius. Since at small radius the particles are very close to each other. The tracking efficiency takes a value between 75% and less than 100%.

By comparing the values of efficiency for each range of η between $Z' \rightarrow jj$ sample results and $Z' \rightarrow t\bar{t}$ sample results that shown in figures 39 for leptons and 40 for hadrons. For both hadrons and leptons, samples

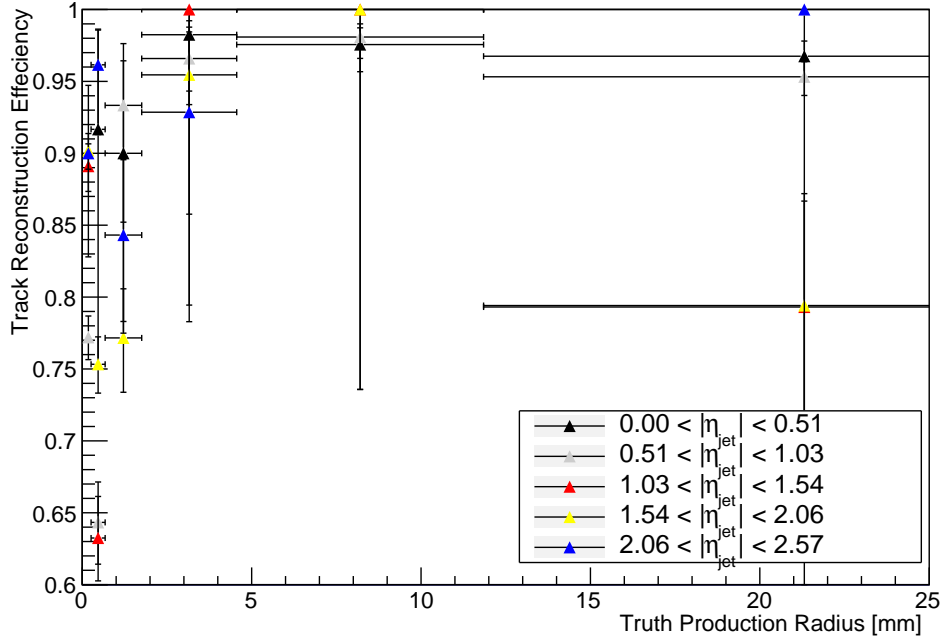


Figure 37: Track reconstruction efficiency for leptons decaying from b-hadron as a function of truth production radius of the b-hadron within jets in the ITK for different ranges of truth jet η .

have nearly the same values of efficiency, which is very good for both.

The bad match rate for different ranges of truth jet η within all jets in the ITK as a function of the b hadron decay radius, for hadrons decaying from b-hadron, is shown in figure 41. The bad match rate is decreased with the radius. In general the bad match rate takes a value between 0% – 3%.

After studying the tracking performance of the ITK, in different base line variables studies: truth jet transverse momentum (p_T), truth jet pseudorapidity(η), truth jet angular distance (ΔR) and displaced vertices, by using a $5TeV$ $Z' \rightarrow jj$ sample with $\mu = 200$. And comparing them with other studies from ATLAS simulation, one can conclude that we have obtained good results, thus, confirms that our methodology in studying the performance

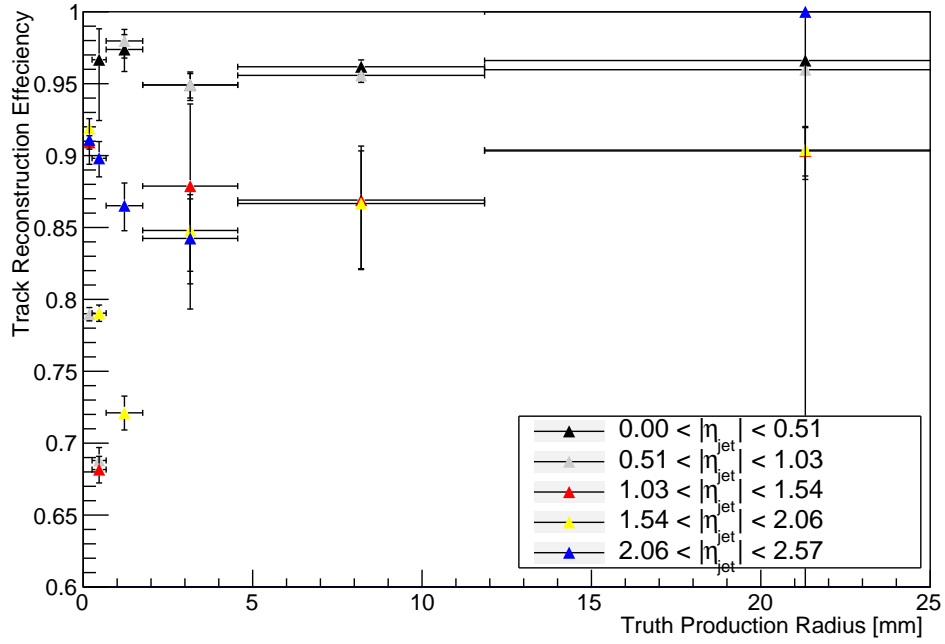


Figure 38: Track reconstruction efficiency for hadrons decaying from b-hadron as a function of truth production radius of the b-hadron within jets in the ITK for different ranges of truth jet η .

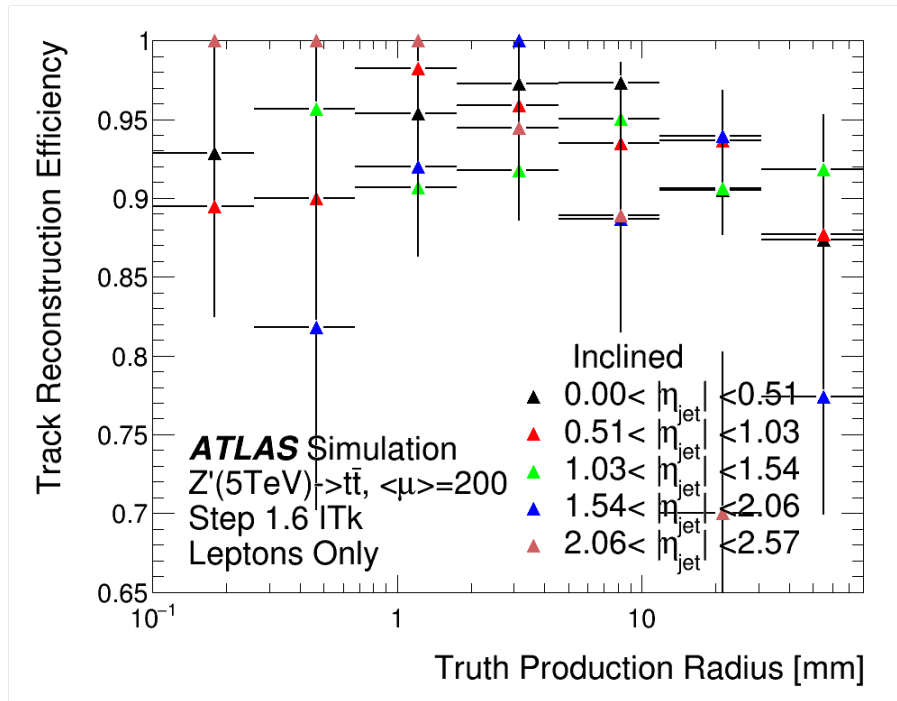


Figure 39: Track reconstruction efficiency for leptons decaying from b-hadron as a function of truth production radius of the b-hadron within jets in the ITK for different ranges of truth jet η (ATLAS simulation, 2016) [34].

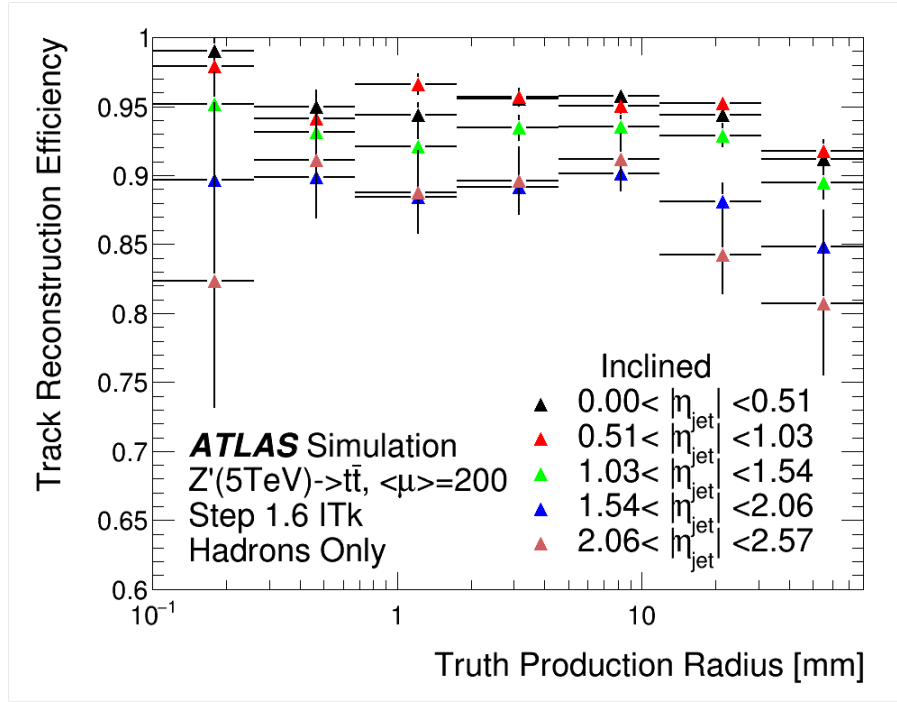


Figure 40: Track reconstruction efficiency for hadrons decaying from b-hadron as a function of truth production radius of the b-hadron within jets in the ITK for different ranges of truth jet η (ATLAS simulation, 2016) [34].

of ITK is validated, and it was used in the coming studies.

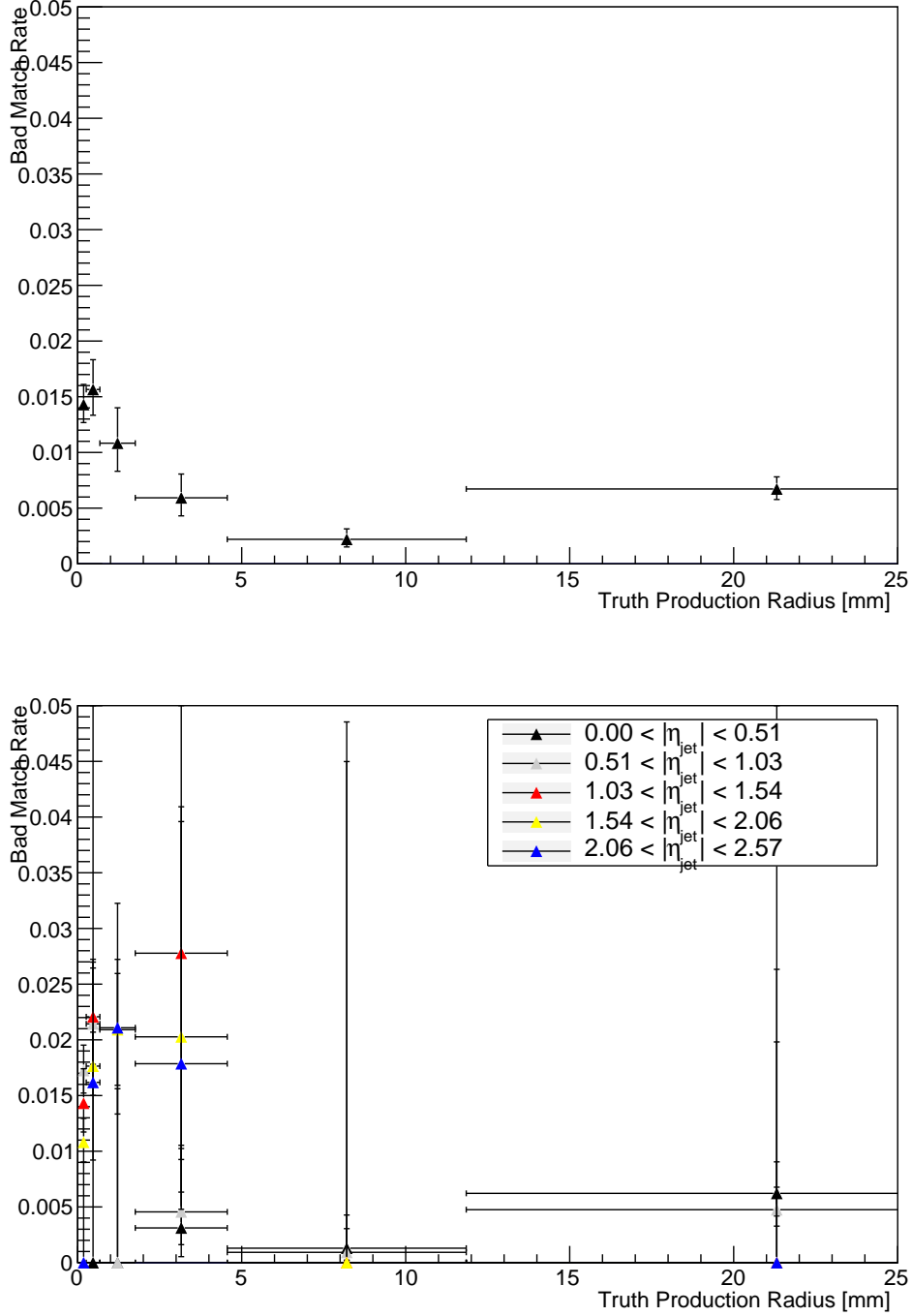


Figure 41: The bad match rate for hadrons decaying from b-hadron as a function of truth production radius of b-hadron within jets in the ITK.

Top: all η are included.

Bottom: different ranges of truth jet η are taken.

Chapter Four

ITK Pixel Modules

4.1 Overview

The electrical module is the basic unit in pixel detector building. ITK needs around 10000 hybrid pixel modules while the number of modules now just 1744 modules, each module as shown in figure 42 basically contains: sensor and new read out chip (front end chip (FE-chip)) with high data rate and electrical transmission, beyond to flex hybrid for interconnection of data power line to the local support services. The connection between three components is done by wire bond [38].

As shown in figure 43, there was two proposed designs for the pixel

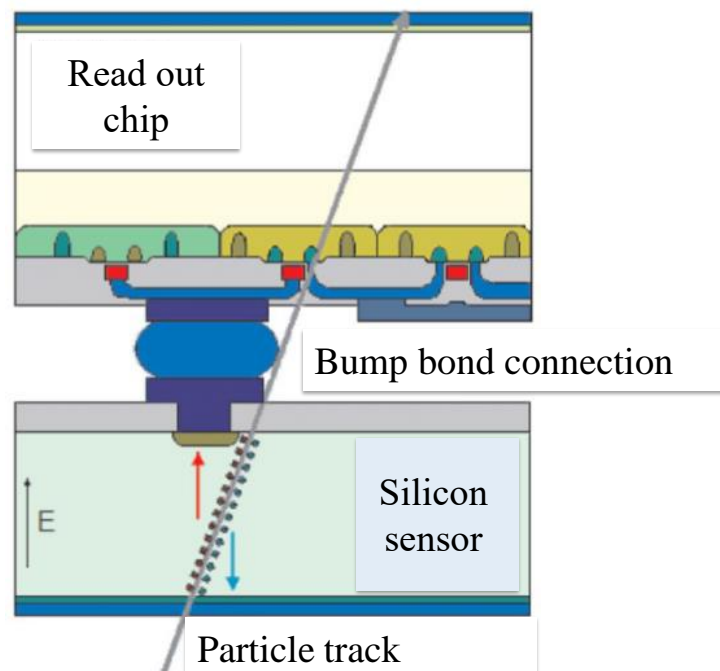


Figure 42: ITK pixel module.

detector in the ITK (at the time of this work):

- i. Extended ITK: parallel pixel modules to the beam line, it is like the traditional current pixel detector, so it is well-tested support structure. Long pixel clusters are expected to be measured at low incident angle, which can improve the tracking efficiency and reduce the fake rate [39].
- ii. Inclined ITK: angled pixel modules to the beam line in the forward region of the parallel layers, which make them more perpendicular to the tracks directions in order to minimize the transversed material and the cluster size. More hits on the modules per one layer can be obtained in the inclined ITK at large η as shown in figure 44.

The end caps are same in both types.

ATLAS collaboration decided to use an inclined modules.

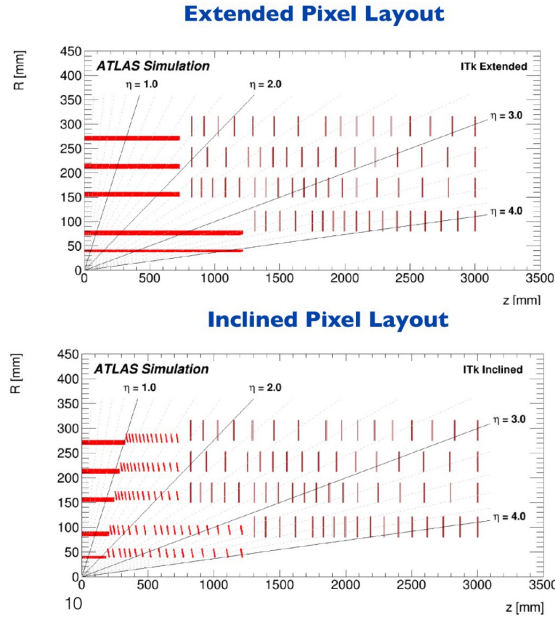


Figure 43: Extended and inclined ITK.

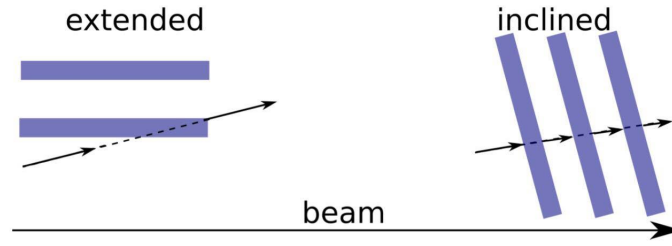


Figure 44: More hit modules can be obtained in the inclined ITK at low incident angle.

4.2 Sensors

There are two technologies of sensors that will be used in the ITK: planar sensors and 3D sensors, they are shown in figure 45. Planar sensor is suitable to be used in the outer layers due to its high efficiency and low cost, they are under development. The main difference between the planar sensors in the current inner detector and the planar sensor in the ITK is in the electrode arrangement, the current sensors used n-in-p technology while the planar sensor in the ITK will use n-in-n technology. Moreover, the planar sensor thickness will be more reduced than it now, since thinner sensor means high efficiency and low cost, it will be $100 - 150 \mu\text{m}$, $100 \mu\text{m}$ for layers 0 and 1, $150 \mu\text{m}$ for layers 2, 3 and 4, while it is now $200 \mu\text{m}$ in the IBL and $285 \mu\text{m}$ in the other three pixel layers [40].

3D sensors are suitable to be used in the inner layers and some of the inner end-cap rings because of their advantages in power consumption and radiation tolerance, it was used successfully in the innermost layer IBL in the current inner detector.

The pixel size of each sensor was reduced from $50 \times 400 \mu\text{m}^2$ to 50×250

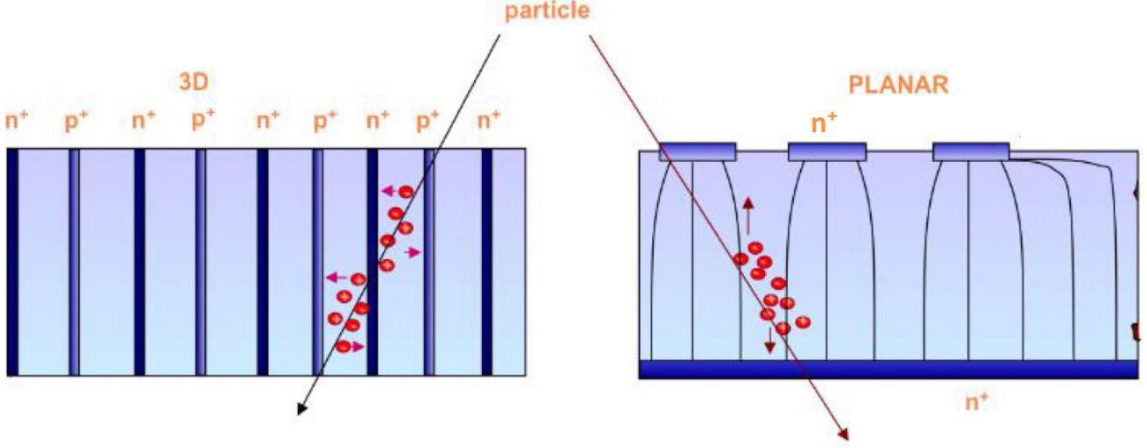


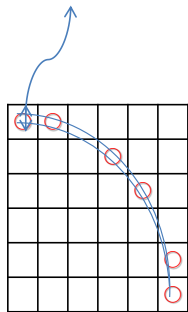
Figure 45: Sketch of the two hybrid pixel technologies, that will be used in the ITK of ATLAS [40].

μm^2 after adding the IBL, it will also be more reduced in the ITK, it will be $25 \times 100 \mu\text{m}^2$ or $50 \times 50 \mu\text{m}^2$, reducing the pixel module size will improve the tracking resolution, by optimizing signals and hits per track as shown in figure 46. These two choices must be compared based on the tracking performance so that one of them can be integrated into the system[38]. This study will give a hint to the collaboration which one will use.

In this study, two $t\bar{t}$ samples with two different pixel size are used, in order to compare the tracking performance between both as a function of: p_T , η , ΔR and production radius of b-hadron decay, in order to give an indication which is better to use a modules with $25 \times 100 \mu\text{m}^2$ pixel size or $50 \times 50 \mu\text{m}^2$ pixel size.

These two samples are:

χ^2 is very small



χ^2 is larger

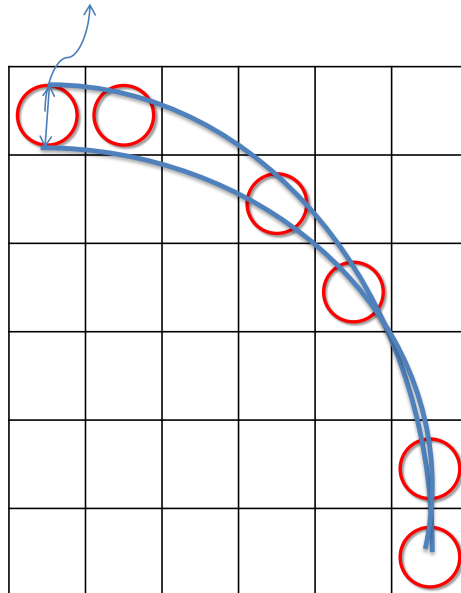


Figure 46: The pixel module size is $50 \times 50 \mu\text{m}^2$ in the left figure while it is $50 \times 250 \mu\text{m}^2$ in the right figure, χ^2 is smaller in the left one, which means that the resolution is better when the pixel size is smaller.

- i. *mc15_14TeV117050.PowhegPythia_P2011C_ttbar.recon.*
AOD.e2176_s2988_s3000_r9071

For a sample with pixel size $25 \times 100 \mu\text{m}^2$ and $\mu = 200$.

- ii. *mc15_14TeV117050.PowhegPythia_P2011C_ttbar.recon.*
AOD.e2176_s2988_s3000_r9060

For a sample with pixel size $50 \times 50 \mu\text{m}^2$ and $\mu = 200$.

Always, same selections are used.

The track reconstruction efficiency within jets as a function of truth jet p_T in the ITK for two different samples are different in pixel size is shown in figure 47. The efficiency is increased with p_T , it has a value of 89% when the p_T is 50 GeV and it reaches 96% when p_T is around 1400 GeV. The efficiency for a sample with $50 \times 50 \mu\text{m}^2$ pixel size is slightly better than the efficiency for a sample with $25 \times 100 \mu\text{m}^2$ pixel size.

The bad match rate within jets as a function of truth jet p_T in the ITK is shown in figure 48. The bad match rate is increased with p_T , it has a value from 0 at low p_T , then it increases until 1% when p_T is around 1500 GeV. The bad match rate for a sample with $25 \times 100 \mu\text{m}^2$ pixel size is better at some points and worse at other points than the bad match rate for a sample with $50 \times 50 \mu\text{m}^2$ pixel size. It is hard to conclude something, due to small statistics used.

The track reconstruction efficiency within jets also is studied as a function of truth jet η in the ITK as shown in figure 49. The efficiency is decreased with $|\eta|$, it has a value around 80% in the forward region, while it reaches 93% in the central region. The efficiency is nearly same

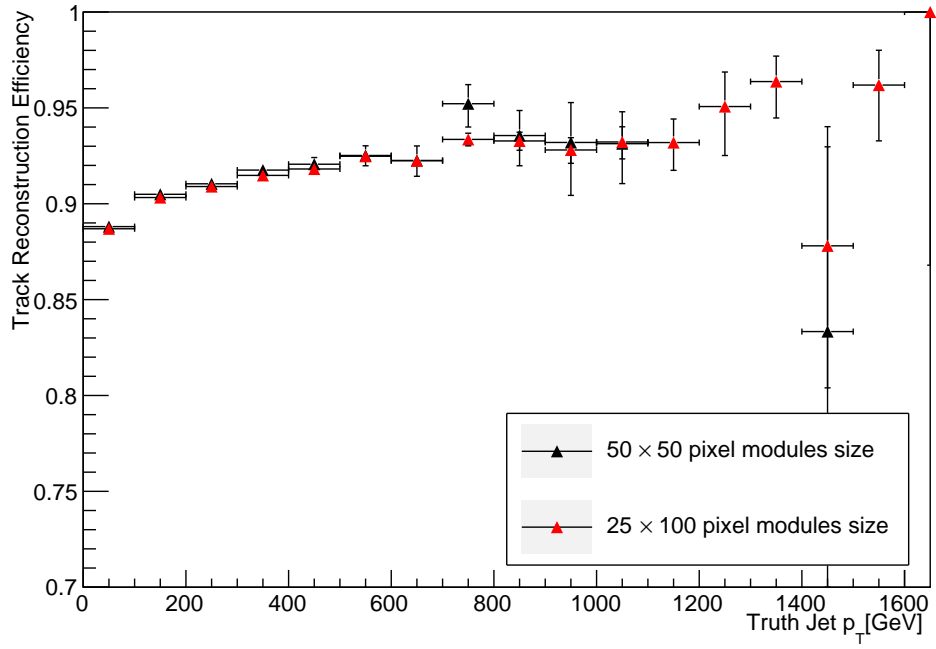


Figure 47: The track reconstruction efficiency within jets as a function of truth jet p_T in the ITK for two samples with $50 \times 50 \mu\text{m}^2$ pixel size and $25 \times 100 \mu\text{m}^2$ pixel size.

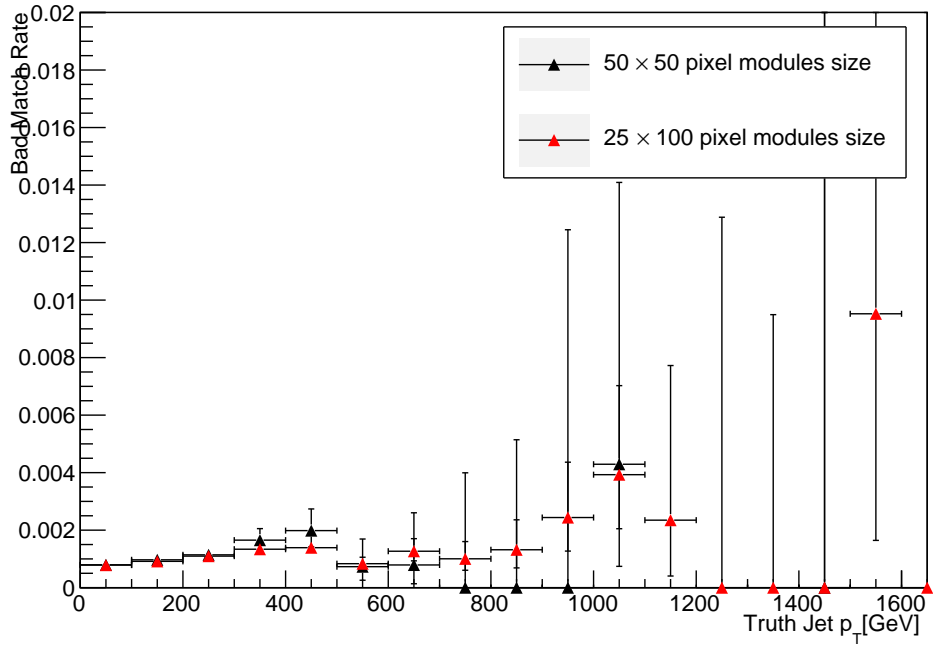


Figure 48: The bad match rate within jets as a function of truth jet p_T in the ITK for two samples with $50 \times 50 \mu\text{m}^2$ pixel size and $25 \times 100 \mu\text{m}^2$ pixel size.

for a sample with $50 \times 50 \mu\text{m}^2$ pixel size and sample with $25 \times 100 \mu\text{m}^2$ pixel size.

The bad match rate within jets also is studied as a function of truth jet η

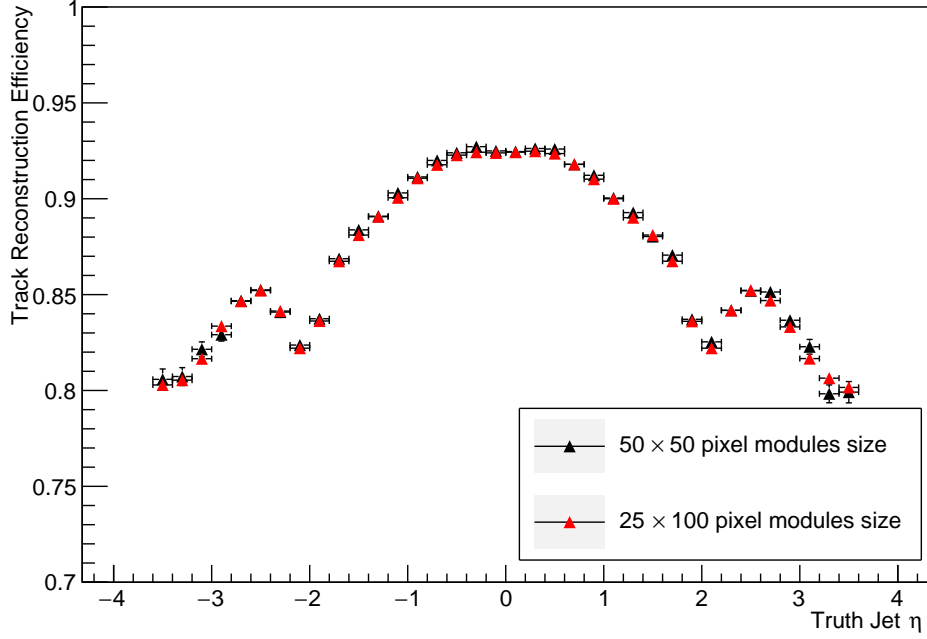


Figure 49: The track reconstruction efficiency within jets as a function of truth jet η in the ITK for two samples with $50 \times 50 \mu\text{m}^2$ pixel size and $25 \times 100 \mu\text{m}^2$ pixel size.

in the ITK as shown in figure 50. The bad match rate is less than 0.2%. The bad match rate for a sample with $25 \times 100 \mu\text{m}^2$ pixel size and for a sample with $50 \times 50 \mu\text{m}^2$ pixel size are nearly same.

The track reconstruction efficiency within jets as a function of the angular distance (ΔR) of each truth particle from the jet in the ITK is shown in figure 51 for b jets and figure 52 for light jets within ΔR is less than 0.4 mm. The study here is done with respect to truth jet η in the top figures and with respect to truth jet p_T in the bottom figures. For both samples, the b jets tracking efficiency and the light jets tracking effi-

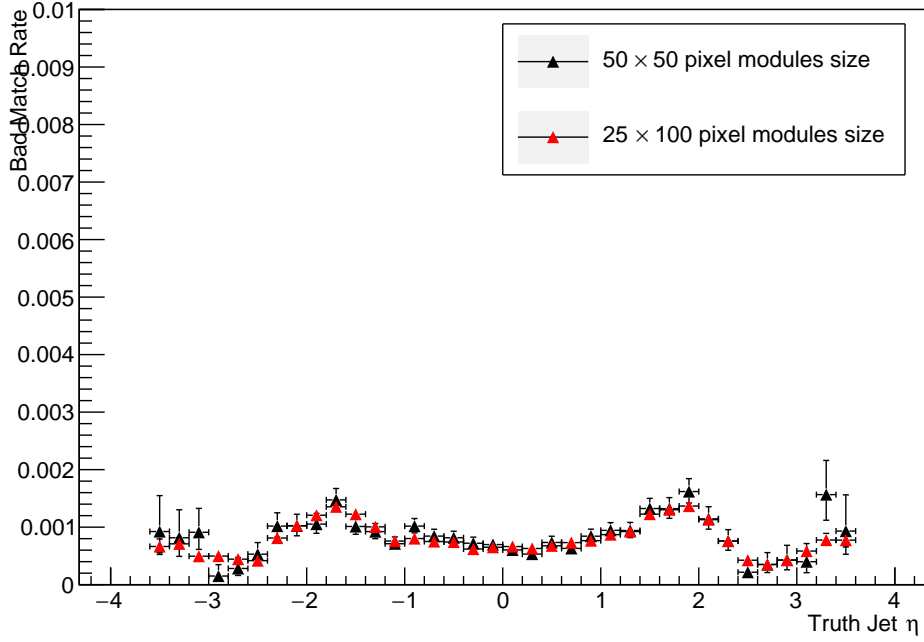


Figure 50: The bad match rate within jets as a function of truth jet η in the ITK for two samples with $50 \times 50 \mu\text{m}^2$ pixel size and $25 \times 100 \mu\text{m}^2$ pixel size.

ciency are more than 90%, which is very good for both.

As shown in figure 51, the efficiency of b jets for a sample with $50 \times 50 \mu\text{m}^2$ pixel size is a little bit better than the efficiency for a sample with 25×100 pixel size. For light jets the case is different, the efficiency for both samples are nearly same, thus, it is hard to determine from the ΔR study for light jets which pixel size is preferred to use.

The track reconstruction efficiency within jets in ITK as a function of the decay radius of the b-hadron for hadrons decaying from b-hadron is shown in figure 53 and for leptons decaying from b-hadron is shown in figure 54. The efficiency is increased with b-hadron decay radius. The tracking efficiency takes a value between 90% and 100%, which is good for both samples. For both leptons and hadrons, the efficiency for a sam-

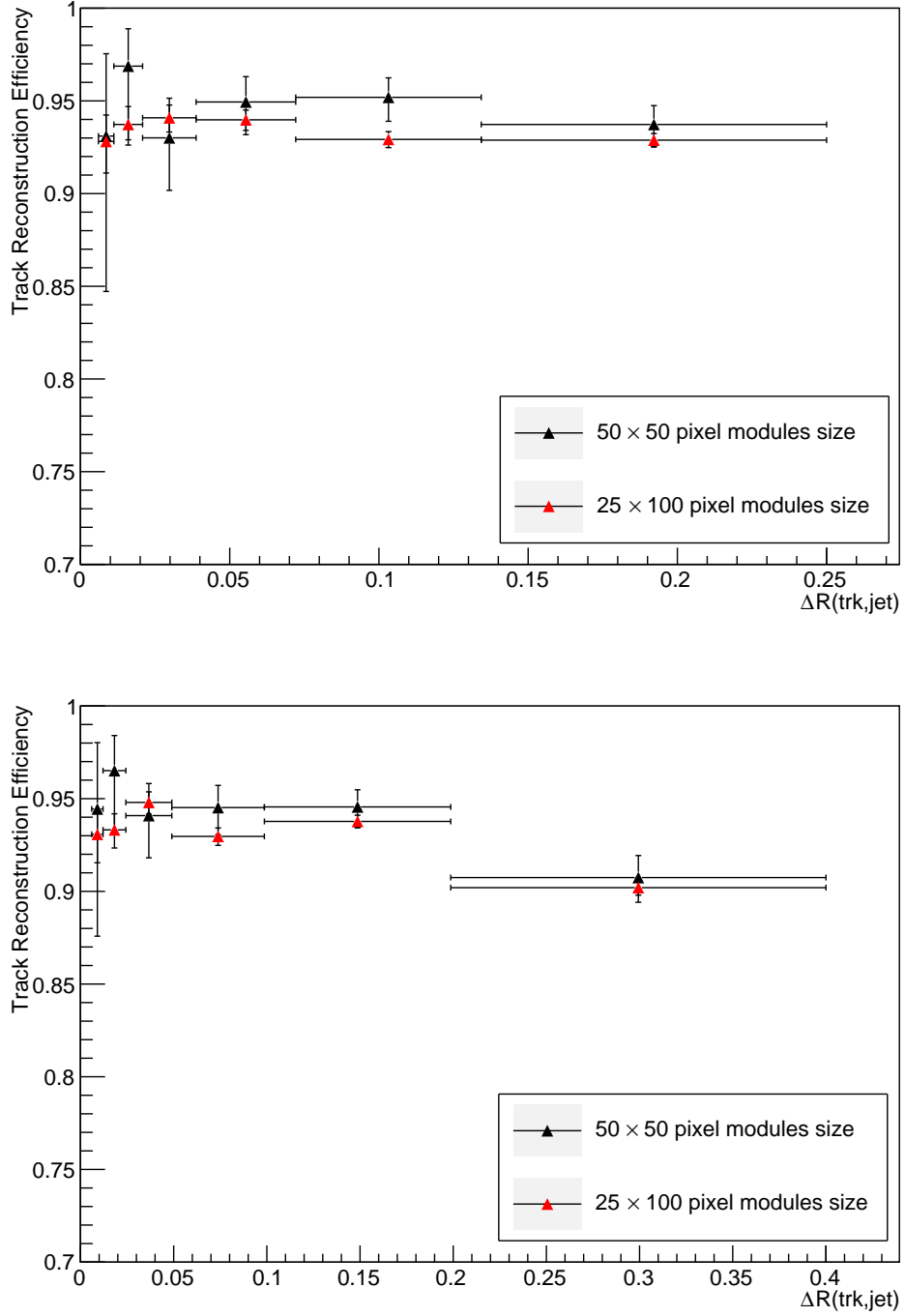


Figure 51: The track reconstruction efficiency within jets as a function of the ΔR for b jets in the ITK for two samples with $50 \times 50 \mu\text{m}^2$ pixel size and $25 \times 100 \mu\text{m}^2$ pixel size.

Top: truth jet η study.

Bottom: truth jet p_T study.

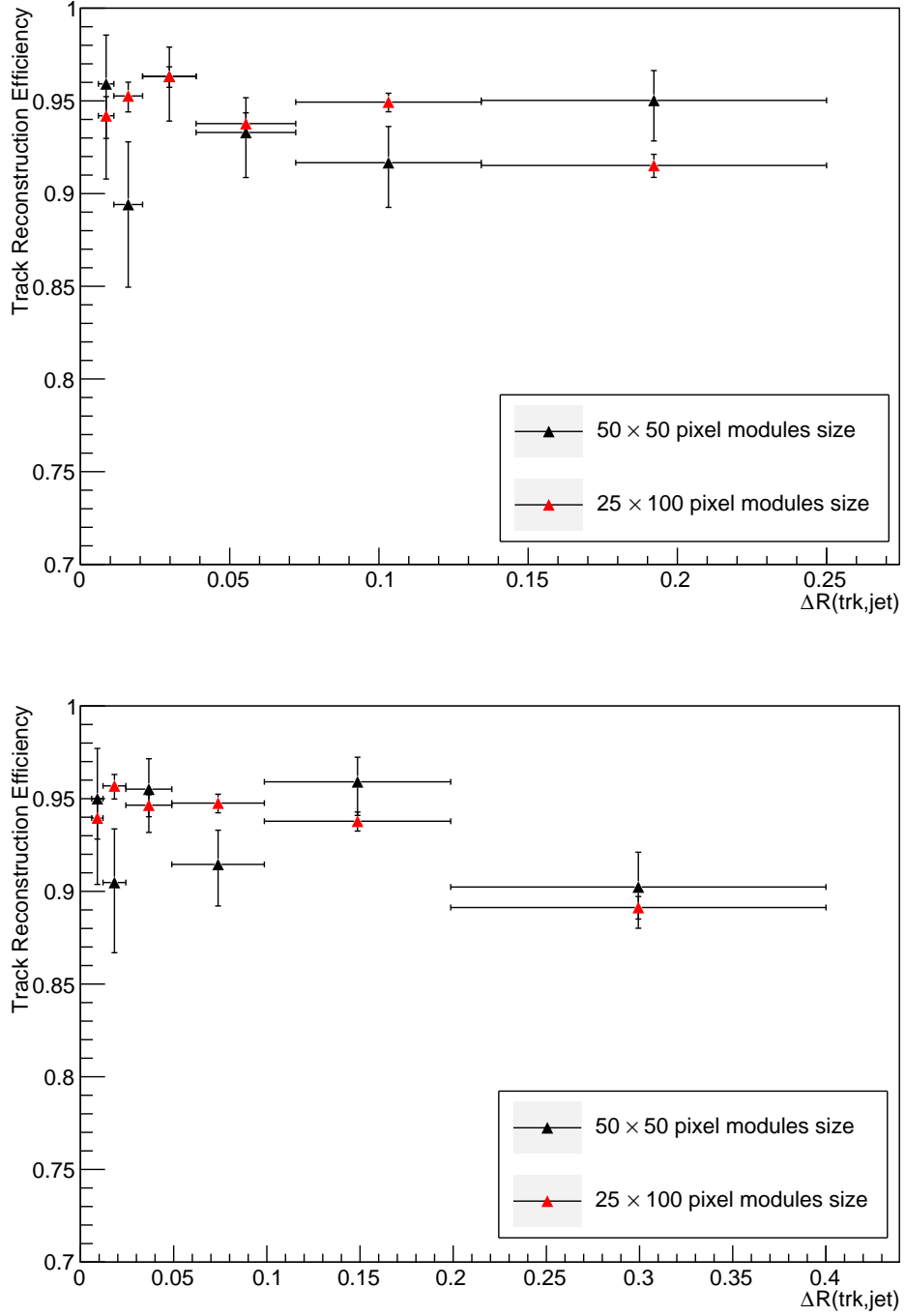


Figure 52: The track reconstruction efficiency within jets as a function of the ΔR for light jets in the ITK for two samples with $50 \times 50 \mu\text{m}^2$ pixel size and $25 \times 100 \mu\text{m}^2$ pixel size.

Top: truth jet η study.

Bottom: truth jet p_T study.

ple with $25 \times 100 \mu\text{m}^2$ pixel size is better at some points and worst at other points than the efficiency for a sample with $50 \times 50 \mu\text{m}^2$ pixel size, Thus, from this study, it is difficult to determine which pixel size is preferred to use.

In general, for two samples with $50 \times 50 \mu\text{m}^2$ pixel size and 25×100

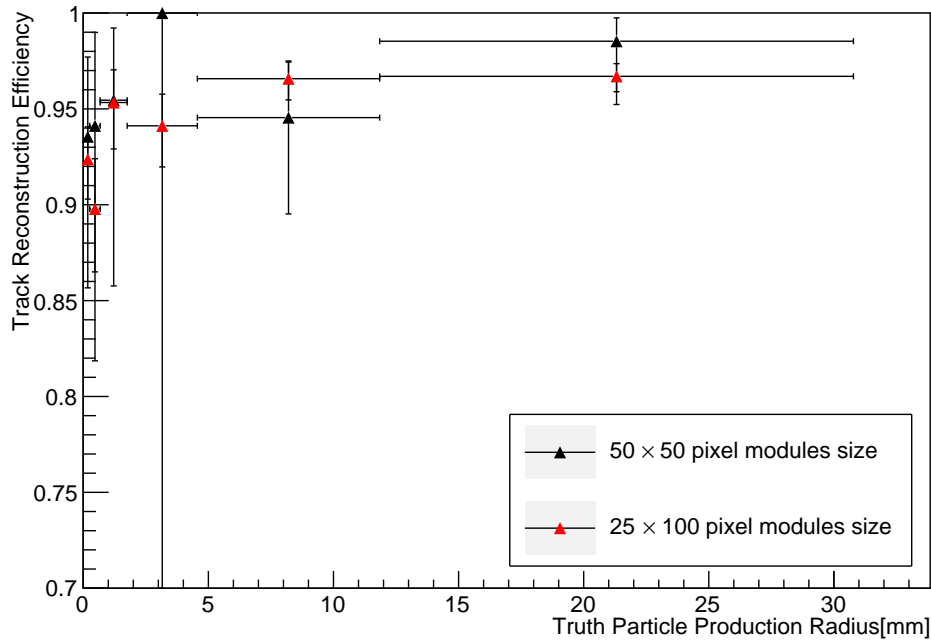


Figure 53: The track reconstruction efficiency within jets as a function of truth production radius for hadron in the ITK for $50 \times 50 \mu\text{m}^2$ and $25 \times 100 \mu\text{m}^2$ sensors samples.

μm^2 pixel size, the tracking efficiency is nearly similar in some studies. But in other, like, the tracking reconstruction efficiency in truth jet p_T study and ΔR study for b jets, results show that using a sensors with pixel size $50 \times 50 \mu\text{m}^2$ is preferred.

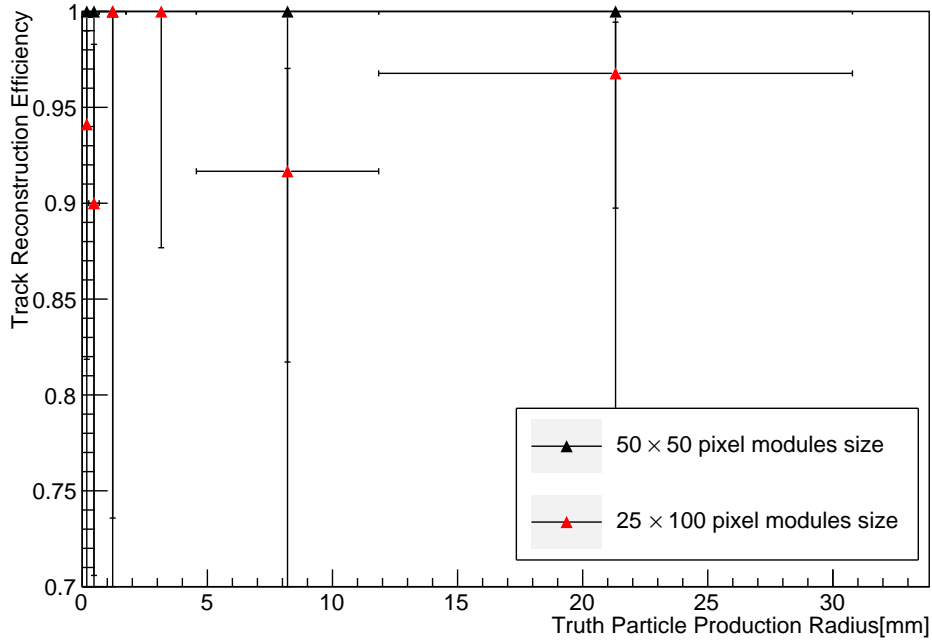


Figure 54: The track reconstruction efficiency within jets as a function of truth production radius for lepton in the ITK for two samples with $50 \times 50 \mu\text{m}^2$ pixel size and $25 \times 100 \mu\text{m}^2$ pixel size.

4.3 Pile-up Study

In LHC, two beams of hadrons are being accelerated then they are collided at four main positions. Each beam contains around 2808 bunches and bunch crossing occurs every 25 nanosecond. The number of p-p interaction per bunch crossing (pile up or μ) is around 40 nowadays (run 2). μ is expected to be around 140 in HL-LHC and the maximum μ will be 200.

In this section the effect of increasing μ is studied, by taken four $t\bar{t}$ samples that have a pixel size $50 \times 50 \mu\text{m}^2$, but with different values of μ ; 0, 80, 140 and 200, in order to compare the tracking performance between them as a function of: truth jet p_T , truth jet η , ΔR of each truth

particle from the jet axis and production radius of b-hadron decay in order to study the robustness of the track reconstruction efficiency with respect to high pile-up. Same selections are used.

The four samples are:

- i. *mc15_14TeV117050.PowhegPythia_P2011C_ttbar.recon.*
AOD.e2176_s2988_s3000_r9060

For a sample with pixel size $50 \times 50 \mu\text{m}^2$ and $\mu = 200$.

- ii. *mc15_14TeV117050.PowhegPythia_P2011C_ttbar.recon.*
AOD.e2176_s2988_s3000_r9052

For a sample with pixel size $50 \times 50 \mu\text{m}^2$ and $\mu = 140$.

- iii. *mc15_14TeV117050.PowhegPythia_P2011C_ttbar.recon.*
AOD.e2176_s2988_s3000_r9054

For a sample with pixel size $50 \times 50 \mu\text{m}^2$ and $\mu = 80$.

- iv. *mc15_14TeV117050.PowhegPythia_P2011C_ttbar.recon.*
AOD.e2176_s2988_s3000_r9052

For a sample with pixel size $50 \times 50 \mu\text{m}^2$ and $\mu = 0$.

The track reconstruction efficiency within jets as a function of truth jet p_T in the pixel detector of the ITK for four different samples is shown in figure 55. The four samples have a pixel size $50 \times 50 \mu\text{m}^2$ but μ is different for each. As $\mu = 0$, the values of efficiency are between 91% and 95%. For a sample that has $\mu = 80$, it has values of efficiency between 89% and 97%. The third sample with $\mu = 140$ has values of efficiency between 89% and 93%. Finally, the fourth sample with $\mu = 200$ has

values of efficiency between 89% and 95%.

The efficiency is increased with p_T , it has a value of 89% when the p_T is 50 GeV and it reaches 97% when p_T is around 1000 GeV. The efficiency is decreased slightly with μ which is expected, but the good thing that the efficiency is decreased slightly and still has high values as $\mu = 200$ in comparison with efficiency values as $\mu = 0$, one has conclude that the ITK layout has the ability to cope with HL-LHC environment.

The bad match rate within jets as a function of truth jet p_T in the ITK is

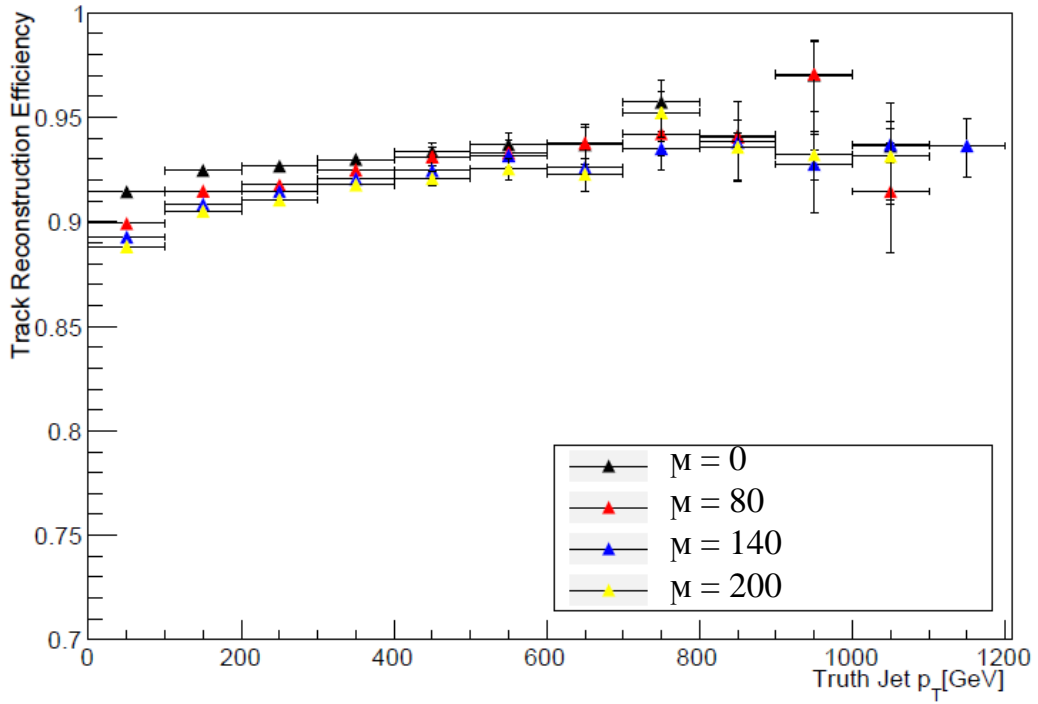


Figure 55: The track reconstruction efficiency within jets as a function of truth jet p_T in the ITK for four different samples that have a pixel size $50 \times 50 \mu\text{m}^2$ with four different values of μ .

shown in figure 56. The bad match rate is increased with p_T , it has values from 0.05% at low p_T , then it increases until 1% when p_T is around 950 GeV. The bad match rate is decreased with μ , as $\mu = 200$ the maximum,

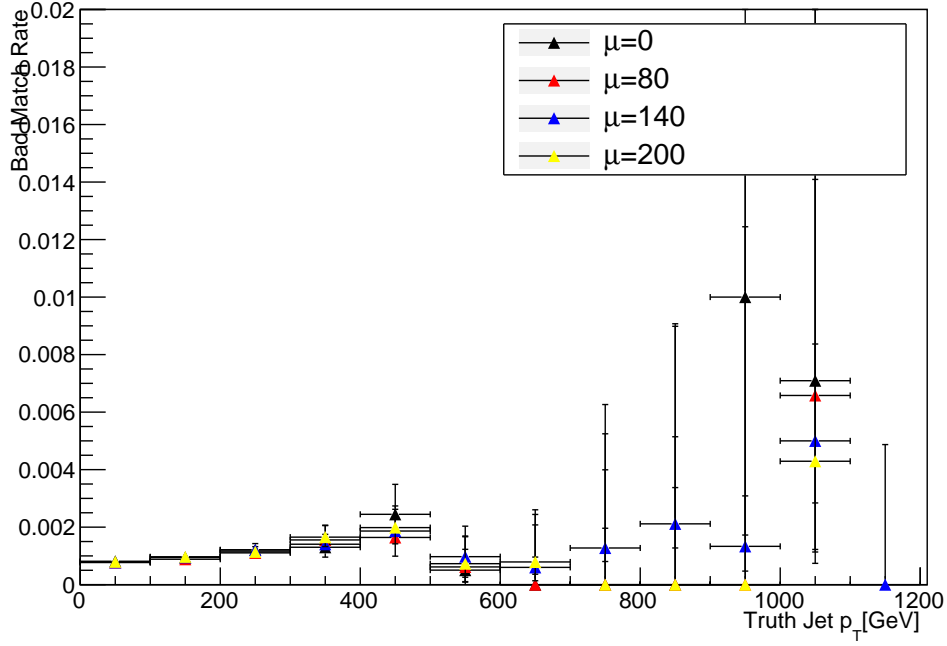


Figure 56: The bad match rate within jets as a function of truth jet p_T in the ITK for four different samples that have a pixel size $50 \times 50 \mu\text{m}^2$ with four different values of μ .

the bad match rate is 0.45%, which is a very good indicator of ITK performance in HL-LHC environment.

The track reconstruction efficiency within jets also is studied as a function of truth jet η in the ITK as shown in figure 57. The efficiency is decreased with $|\eta|$, it has values between 80% and 90% in the forward region, while it reaches 95% in the central region. The efficiency is decreased very slightly with μ , it has 84% – 95% efficiency as $\mu = 0$, 79% – 93% efficiency as $\mu = 200$ and between them as $\mu = 80$ and 140. The values of efficiency with different μ are very close, thus, one can conclude that truth jet η study confirms the good performance of ITK in HL-LHC.

The bad match rate within jets also is studied as a function of truth jet η

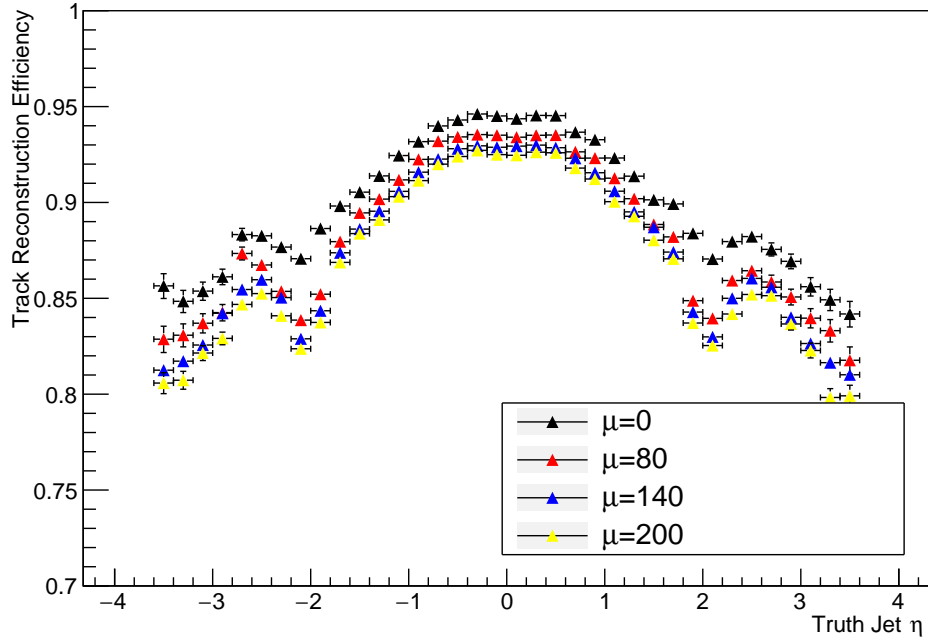


Figure 57: The track reconstruction efficiency within jets as a function of truth jet η in the ITK for four different samples that have a pixel size $50 \times 50 \mu\text{m}^2$ with four different values of μ .

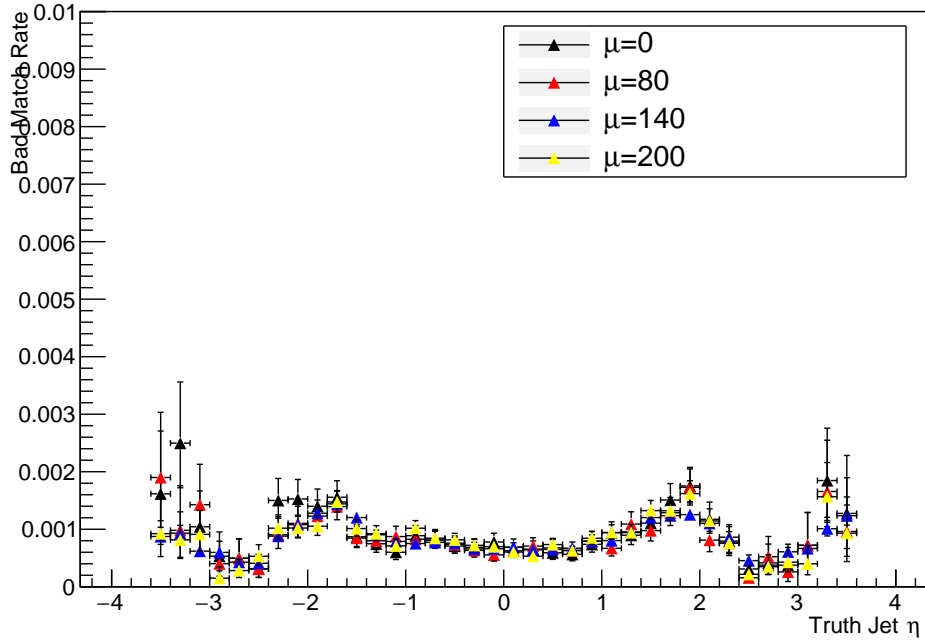


Figure 58: The bad match rate within jets as a function of truth jet η in the ITK for four different samples that have a pixel size $50 \times 50 \mu\text{m}^2$ with four different values of μ .

in the ITK as shown in figure 58. The bad match rate is less than 0.25%. For samples with different μ , the bad match rates are very close, thus, one can conclude that the bad match rate is not affected by changing the value of μ .

The track reconstruction efficiency within jets as a function of the angular distance (ΔR) of each truth particle from the jet axis in the ITK is shown in figure 59 for b jets and figure 60 for light jets within ΔR is less than 0.4 mm. The study here is done with respect to truth jet η in the top figures and with respect to truth jet p_T in the bottom figures. For both samples, the b jet tracking efficiency and the light jet tracking efficiency are more than 90% whatever the value of μ , which is very good for both. It is hard to determine how the tracking efficiency behaves with μ . Thus, one can conclude that ITK layout performance is a very good especially with $\mu = 200$, thus, it can cope with harsh environment in HL-LHC.

The track reconstruction efficiency within jets in ITK as a function of the decay radius of the b-hadron for hadrons decaying from b-hadron is shown in figure 61, and for leptons decaying from b-hadron is shown in figure 62. The efficiency is increased with b-hadron decay radius. In general the tracking efficiency takes a value between 89% and less than 100%, which is good for leptons and hadrons, while it is hard to determine at which value of μ we can get the best efficiency, due to small statistics used.

In general, after comparing the tracking efficiency between four different samples that have a pixel size $50 \times 50 \mu\text{m}^2$ with four different values

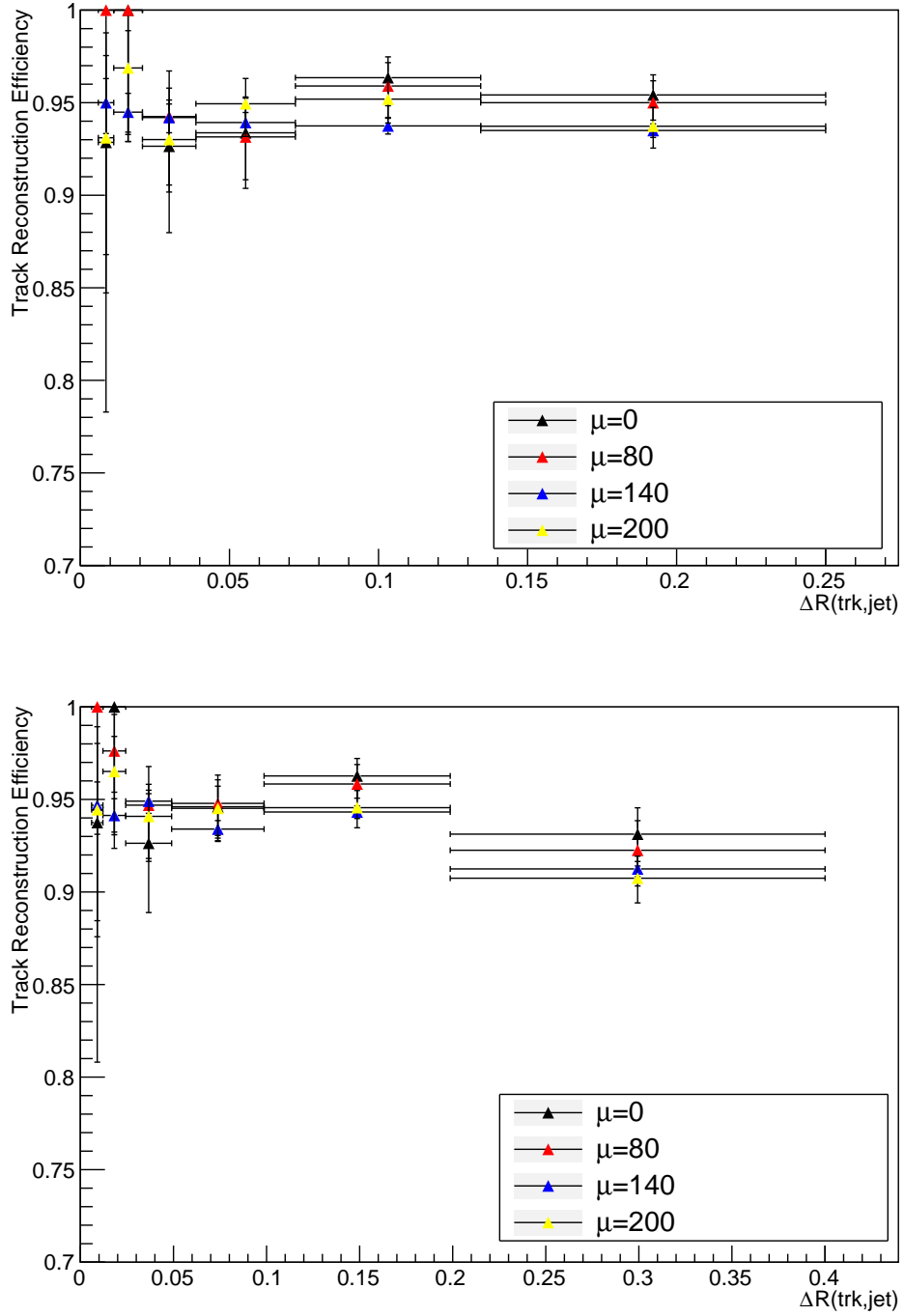


Figure 59: The track reconstruction efficiency within jets as a function of the ΔR for b jets in the ITK for four different samples that have a pixel size $50 \times 50 \mu\text{m}^2$ with four different values of μ .

Top: truth jet η study.

Bottom: truth jet p_T study.

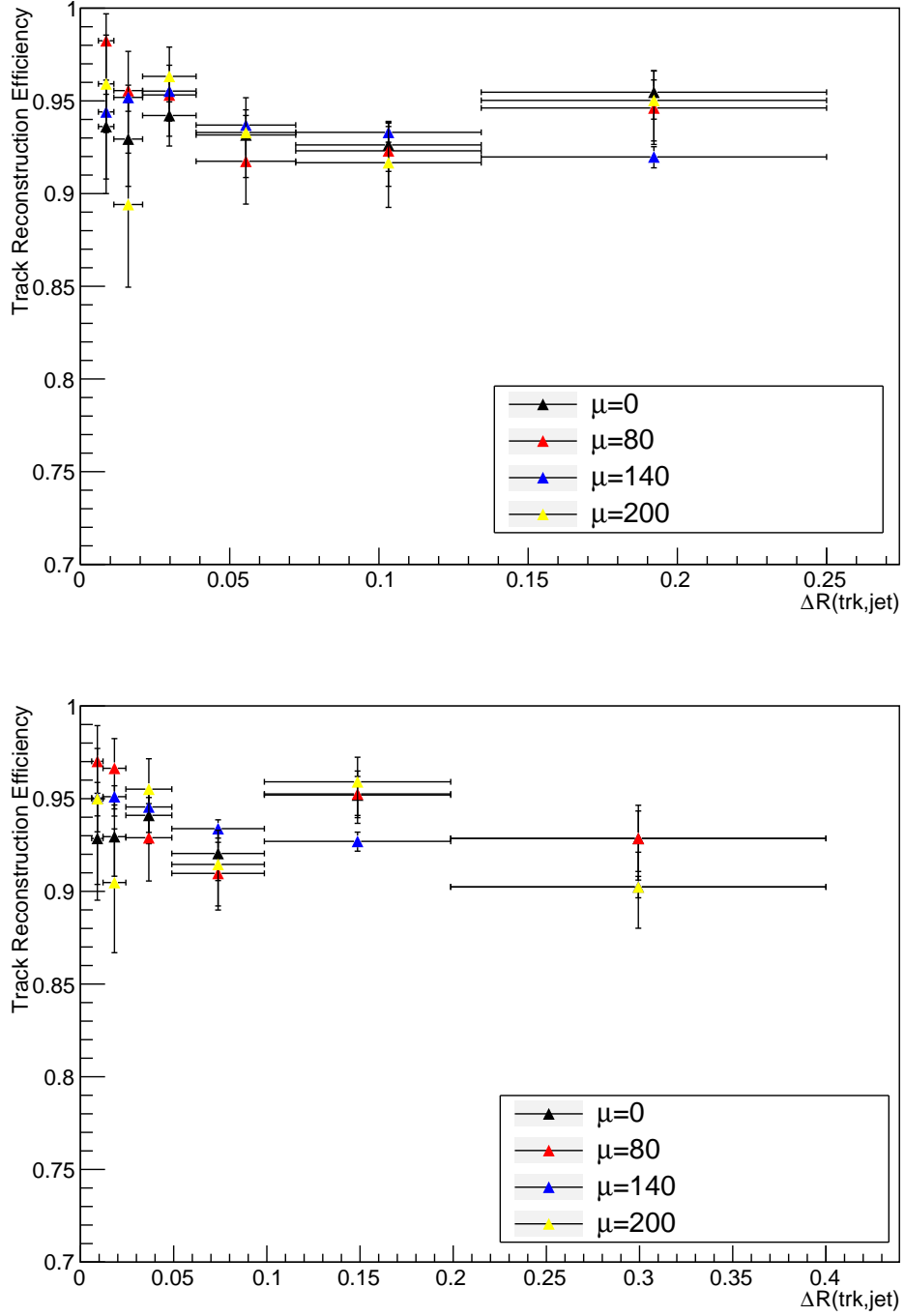


Figure 60: The track reconstruction efficiency within jets as a function of the ΔR for light jets in the ITK for four different samples that have a pixel size $50 \times 50 \mu\text{m}^2$ with four different values of μ .

Top: truth jet η study.

Bottom: truth jet p_T study.

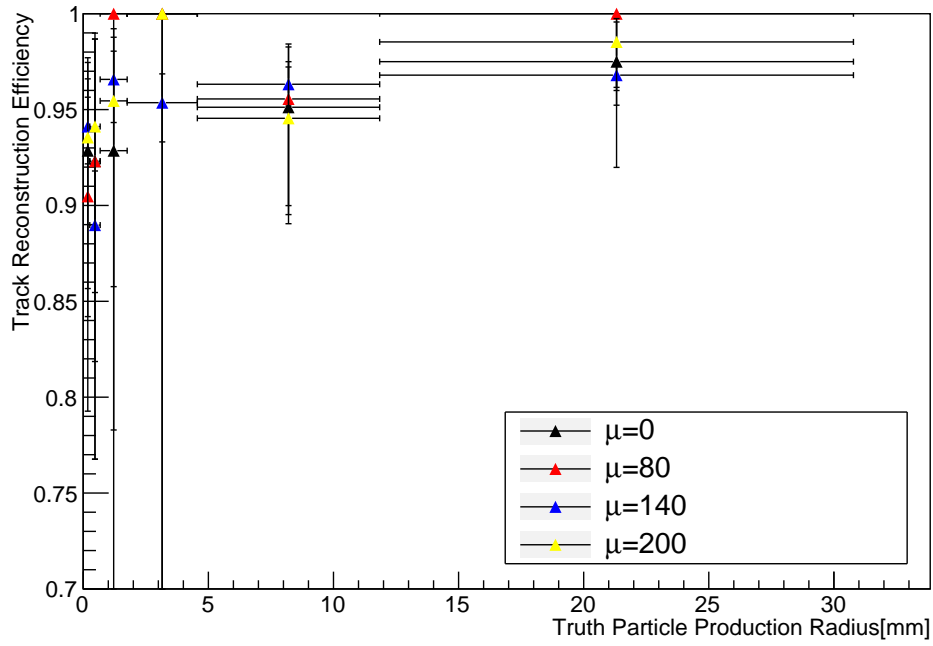


Figure 61: The track reconstruction efficiency within jets as a function of truth production radius for hadron in the ITK for four different samples that have a pixel size $50 \times 50 \mu\text{m}^2$ with four different values of μ .

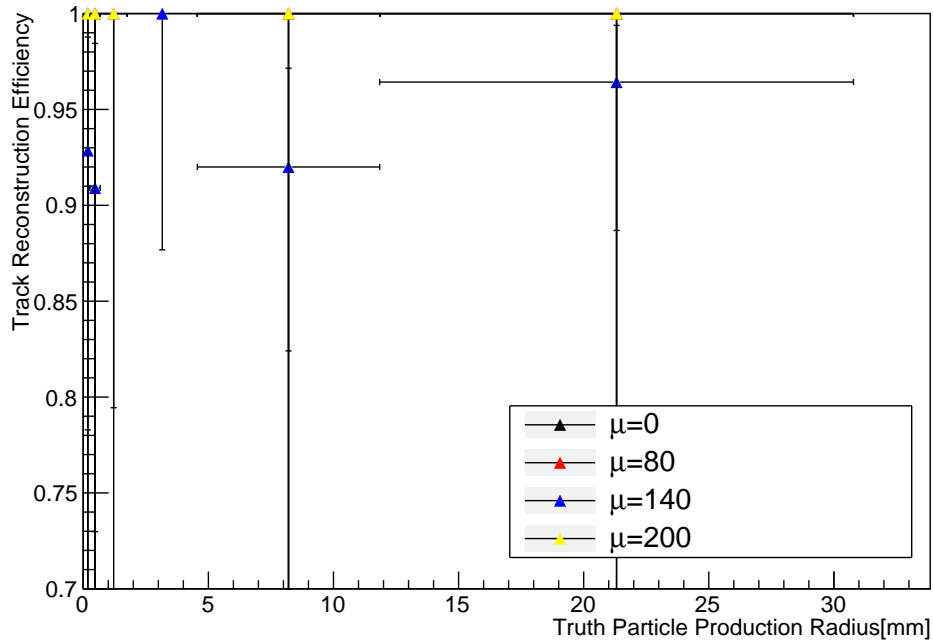


Figure 62: The track reconstruction efficiency within jets as a function of truth production radius for lepton in the ITK for four different samples that have a pixel size $50 \times 50 \mu\text{m}^2$ with four different values of μ .

of μ : 0 ,80 ,140 and 200. Different studies show that the ITK layout is designed to cope well with HL-LHC environment since the tracking efficiency for a sample with $\mu = 200$ has a similar or slightly less values than the others. Thus, the robustness of the track reconstruction efficiency with respect to high pile-up is confirmed in this study.

Chapter Five

Conclusion

ATLAS is one of the main general-purpose detector in LHC, it will be upgraded in 2023-2025 (which is called phase II). The major upgrade will be for the inner detector, it will be replaced by the new inner tracker (ITK). At that time the stage of high luminosity LHC (HL-LHC) will start with luminosity five times more than the luminosity in run 2 (nowadays), which creates a hope for a substantial advancement in the understanding of physics phenomena related to high-energy physics. The layout of ITK will cover a pseudorapidity up to $|\eta| = 4$, while the current inner detector covers a pseudorapidity up to $|\eta| = 2.5$.

In this thesis the performanc of the new ITK of ATLAS is studied, by studying the track recostruction efficiency and the bad match rate, by using a 5 TeV $Z' \rightarrow jj$ sample with $\mu = 200$. The tracking performance is done as a function of different variables; truth jet p_T , truth jet η , truth jet ΔR and displaced vertices, including particles travel in the forward region with a values of $2.5 < |\eta| < 4$. After comparing them with other studies from ATLAS simulation, one can conclude that we have obtained good results, confirming that our methodology in studying the performance of ITK is valid, and can be used for further studies.

The pixel size of ITK module will be reduced, the pixel size in the current inner detector is $50 \times 400 \mu\text{m}^2$ and $50 \times 50 \mu\text{m}^2$ in the IBL. There are two proposed pixel size to use in the ITK, as follows:

- i. $50 \times 50 \mu\text{m}^2$ pixel size.

- ii. $25 \times 100 \mu\text{m}^2$ pixel size.

The tracking performance as a function of different baseline variables for two $t\bar{t}$ samples that are different in pixel size is studied and compared, the study here is done with high pile-up, $\mu = 200$ for both. In general, for two samples the tracking efficiency is almost similar in some studies. But in other, like, the tracking reconstruction efficiency in truth jet p_T study (figure 47) and ΔR study for b jets (figure 51), results show that using a sensors with pixel size $50 \times 50 \mu\text{m}^2$ is preferred. Thus, it could be considered as a hint to ATLAS collaboration that is better to use modules with $50 \times 50 \mu\text{m}^2$ pixel size.

The tracking performance of the new ITK of ATLAS as the value of μ increases is also studied as a function of different variables, in order to see the effect of changing μ on the tracking performance of it. This allows to study the robustness of the track reconstruction efficiency with respect to high pile-up.

In this study, four different $t\bar{t}$ samples that have a pixel size $50 \times 50 \mu\text{m}^2$ with four different values of μ : 0 ,80 ,140 and 200 is used to study the tracking reconstruction efficiency and bad match rate for them.

In general, after comparing the tracking efficiency between four different samples. Different studies show that the ITK layout is designed to cope well with HL-LHC environment since the tracking efficiency for a sample with $\mu = 200$ has a similar or slightly less values than the others. Thus, the robustness of the track reconstruction efficiency with respect to high pile-up is confirmed in this study.

References

- [1] ATLAS Collaboration, **ATLAS central solenoid: Technical Design Report**. Technical Design Report ATLAS. CERN, Geneva, 1997. <https://cdsweb.cern.ch/record/331067>.
- [2] ATLAS Collaboration, **ATLAS inner detector: Technical Design Report 1**. Technical Design Report ATLAS. CERN, Geneva, 1997. <https://cdsweb.cern.ch/record/331063>.
- [3] ATLAS Collaboration, **ATLAS inner detector: Technical Design Report, 2**. Technical Design Report ATLAS. CERN, Geneva, 1997. <https://cdsweb.cern.ch/record/331064>.
- [4] Cian O’Luanaigh, **The High-Luminosity LHC**, November, 2015, <http://cds.cern.ch/record/2114693>.
- [5] arXiv:1409.5002v1 [**physics.ins-det**] 17 Sep 2014.
- [6] Wells, Pippa S., **Philosophical Transactions of the Royal Society of London A: Mathematical, Physical and Engineering Sciences**, volume 373 (2023), 2014.
- [7] B T Huffman, Journal of Instrumentation, **9, 02, C02033, 2014**.
- [8] **ATL-PHYS-PROC-2013-324** 06, December 2013.
- [9] **Track and vertex reconstruction in the ATLAS inner detector**, Maaïke Limper, Ph.D thesis.

- [10] **Fundamental Physical Constants from NIST**. The NIST Reference on Constants, Units, and Uncertainty. US National Institute of Standards and Technology. June 2015. Retrieved 2016-10-31.
- [11] Atlas collaboration, **journal of instrumentation**, volume 3, august 2008.
- [12] Flick, Tobias, **Studies on the Optical Readout for the ATLAS Pixel Detector**, 2006, WUB-DIS-2006-05, <https://cds.cern.ch/record/1498117>.
- [13] F. Hugging, **IEEE Transactions on Nuclear Science**, Volume: 53, Issue: 3, Pages:1732-1736, June 2006.
- [14] Timon Heim, **Nuclear Instruments and Methods in Physics Research A** 765 (2014) 227-231.
- [15] Ewa Stanecka, Pos (vertex 2013) 001, 22nd **International Workshop on Vertex Detectors**, 15-20 September 2013, Lake Starnberg, Germany.
- [16] J. Jimnez Pe, on behalf of the ATLAS collaboration, **J. Phys.: Conf. Ser.** 664072025 (2015).
- [17] Fabian Hgging, On behalf of the ATLAS Collaboration, **Nuclear Instruments and Methods in Physics Research Section A: Accelerators, Spectrometers, Detectors and Associated Equipment**, vol 650 (1), pages 45 - 49, (2011). International Workshop on Semiconductor Pixel Detectors for Particles and Imaging 2010A.

- [18] vorgelegt von, **Development and operation of a testbeam setup for qualification studies of ATLAS Pixel Sensors**, thesis.
- [19] ATLAS IBL Community, **CERN-LHCC- 2010-013/ATLAS TDR** 19, September 2010.
- [20] Miucci, **Journal of Instrumentation, Volume 9**, February 2014.
- [21] Jennifer Jentzsch, **Pixel detector modules performance for ATLAS IBL and future pixel detectors**, Ph.D dissertation.
- [22] **A Miucci 2014 JINST 9 C02018.**
- [23] **arXiv:1610.01994v3 [physics.ins-det]**, 22 Nov 2016.
- [24] Richard L. Bates, **Proceeding of science, 24th International Workshop on Vertex Detector -VERTEX2015- 1-5, June 2015.**
- [25] Simon Vieletal, **ATL-INDET- PROC-2015- 011, submitted to Nuclear Instruments and Methods in Physics Research, Section A.**
- [26] **Particle Physics Experiments at High Energy Colliders**, John Hauptman, Wiley publishing.
- [27] **ATL-INDET-PUB-2009-001.**
- [28] **Track fitting in the ATLAS experiment**, Thijs Gerrit Cornelissen. PhD thesis.
- [29] **ATL-PHYS-PUB-2016-025.**

- [30] **ATL-UPGRADE-PUB-2013-001.**
- [31] **arXiv:1405.6569v2 [physics.ins-det] 28 Oct 2014.**
- [32] **Technical Design Report for the ATLAS ITk - Strips Detector (2016).**
- [33] **Cern-Thesis-2015-243.**
- [34] Talk by Felix Cormier, **Upgrade Tracking TIDE Jet update - Step 1.6**, internal use, Nov 16th 2016.
- [35] J. Beringer (Particle Data Group); et al. (2012). **PDGLive Particle Summary Quarks (u, d, s, c, b, t, b?, t?, Free) (PDF)**. Particle Data Group. Retrieved 2012-12-18.
- [36] Nave, C. R. **Transformation of Quark Flavors by the Weak Interaction**. HyperPhysics.
- [37] G. Aad et al. (ATLAS Collaboration)**Phys. Rev. D 92, 012010, 2015.**
- [38] **ATL-ITK-PROC-2016-006** 29, November 2016.
- [39] **Atl-itk-proc2016-002.**
- [40] **ATL-ITK-PROC-2016-010**, 10 December 2016.

List of Symbols and Abbreviations

CERN	: Conseil European pour la Recherche Nuclaire (European Organization for Nuclear Research)
LAL	: Linear Accelerator Laboratory
LHC	: Large Hadron Collider
HL-LHC	: High Luminosity LHC
ATLAS	: A Toroidal LHC Apparatus experiment
CMS	: Compact Muon Solenoid experiment
LHCb	: LHC-beauty experiment
ALICE	: A Large Ion Collider Experiment
ITK	: Inner Tracker
ID	: Inner Detector
SCT	: Semiconductor Tracker
TRT	: Transition Radiation Tracker
Strip	: Silicon micro-strip system
η	: Pseudorapidity
p	: Momentum
p_T	: Transverse Momentum
q	: Charge
ΔR	: Angular distance
IBL	: Inserted B-Layer
θ	: Polar angle
ϕ	: Azimuthal angle
d_0	: Transverse impact parameter

z_0	: Longitudinal impact parameter
p_x	: x-component for the momentum
p_y	: y-component for the momentum
μ	: Pile-up
ns	: nanosecond
B	: Magnetic field
R	: Radius of curvature
ϵ	: Efficiency
BM	: Bad Match rate
P_{match}	: Probability of matching
$TIDE$: Tracking In Dense Environment
Z'	: Hypothetical gauge boson
j	: Jet
b	: Bottom quark
$b\text{ jet}$: Jet contains b quark
light jet	: Jet does not contain b quark
t	: Top quark
\bar{t}	: Top quark with negative charge
u	: Up quark
d	: Down quark
c	: Charm quark
s	: Strange quark
e	: Electron
μ	: Muon

τ	: Tau
ν_e	: Electron neutrino
ν_μ	: Muon neutrino
ν_τ	: Tau neutrino
H	: Higgs boson
g	: Gluon
γ	: Photon
SUSY	: Supersymmetry
LS1	: First Long Shutdown (2013-2015)
LS3	: Third Long Shutdown (2023-2025)
GEANT4	: full monte-carlo simulation
N_{reco}	: Number of reconstructed tracks
N_{truth}	: Number of truth particles
2D	: Two dimension
N(pixel, common)	: The number of pixel hits common between the reconstructed track and truth track
N(strip, common)	: The number of strip hits common between the reconstructed track and truth track
N(pixel, track)	: The total number of pixel hits in the reconstructed track
N(strip, track)	: The total number of strip hits in the reconstructed track

جامعة النجاح الوطنية
كلية الدراسات العليا

دراسة أداء المتتبع الداخلي للكاشف أطلس الموجود في مصادم
الهدرونات الكبير التابع للمنظمة الأوروبية للأبحاث النووية

إعداد
تسليم باسم عبدالكريم عبدالله

إشراف
د. أحمد بصلات

قدمت هذه الأطروحة استكمالاً لمتطلبات الحصول على درجة الماجستير في الفيزياء
بكلية الدراسات العليا في جامعة النجاح الوطنية، نابلس، فلسطين.

2018

ب

دراسة أداء المتعقب الداخلي للكاشف أطلس الموجود في مصادم الهدرونات الكبير التابع للمنظمة الأوروبية للأبحاث النووية

إعداد

تسليم عبد الله

إشراف

د. أحمد بصلات

الملخص

تجربة أطلس في الفيزياء هو مكشاف جسيمات أولية صُمم مع ثلاثة تجارب رئيسية أخرى في مصادم الهدرونات الكبير لقياس كتل وطاقات و شحنات الجسيمات الأولية والإشعاعات. ويعد أهمها نظرا لتعدد الأبحاث و الدراسات التي تتم من خلال البيانات التي يتم تجميعها بواسطته. وفي داخله جهاز يدعى المتعقب الداخلي الذي يرصد ويحلل كمية تحرك الجسيمات التي تمر عبر أطلس، سيتم في المستقبل ما بين عامي 2023-2025 استبدال المتعقب الداخلي بمتعقب أكثر حداثة قادر على تعقب عدد تصادمات أكبر من الوقت الحالي. بالإضافة لذلك ستكون لديه القدرة على تغطية الجسيمات التي تتحرك بزوايا صغيرة بالنسبة لمحور التصادم. في هذه الرسالة يتم دراسة فعالية إعادة بناء تركيب المسارات ونسب التطابق غير الجيد بين المسارات الحقيقية والمسارات المعاد بناؤها بالنسبة لعدة متغيرات مثل كمية الزخم الخطي وغيرها. وقمنا أيضا بالتركيز على الجسيمات التي تتحرك بزوايا صغيرة، وهو الأمر الذي يعد إضافة جديدة على المتعقب الداخلي الجديد. قمنا أيضا بدراسة فعالية إعادة بناء مسار الجسيمات داخل عينتين مختلفتين الأبعاد من المجسات المقترح استخدامهم داخل المتعقب الداخلي الجديد، الأولى ذات أبعاد 25×100 ميكرومتر مربع والثانية 50×50 ميكرومتر مربع. هذه الدراسة تمت في وسط تبلغ فيه عدد التصادمات 200 تصادم كل 25 نانوثانية، وقد وجدنا أن استخدام النوع الثاني أكثر فعالية نوعا ما. في النهاية، تم دراسة أثر زيادة عدد التصادمات وملاحظة مدى نقصان فعالية إعادة بناء المسارات بفعل زيادة عدد التصادمات على عينات تحتوي مجسات ذات بعد 50×50 ميكرومتر مربع، وقد وجدنا أن الفعالية ما زالت عالية و أنها تصل قيم أكثر من 90%.